TE
662
.A3
no.
FHWA-
RD-
75-
121

rt No. FHWA-RD-75-121

YMER-IMPREGNATED PRECAST STRUCTURAL CRETE BRIDGE DECK PANELS

Dept. of Transportation
MAY 4 1978
Library

October 1975

Final Report

This document is available to the public through the National Technical Information Service, Springfield, Virginia 22161

Prepared for

FEDERAL HIGHWAY ADMINISTRATION
Offices of Research & Development
Washington, D.C. 20590

NOTICE

This document is disseminated under the sponsorship of the Department of Transportation in the interest of information exchange. The United States Government assumes no liability for its contents or use.

The contents of this report reflect the views of the U. S. Department of the Interior, Bureau of Reclamation, which is responsible for the facts and the accuracy of the data presented herein. The contents do not necessarily reflect the official views or policy of the Department of Transportation. This report does not constitute a standard, specification, or regulation.

The United States Government does not endorse products or manufacturers. Trade or manufacturers' names appear herein only because they are considered essential to the object of this document.

FHWA DISTRIBUTION

Sufficient copies of this report are being distributed by FHWA Bulletin to provide two copies to each regional office, one copy to each division office, and two copies to each State highway department. Direct distribution is being made to the division offices.

Technical Report Documentation Page

1. Report No.	2. Government Accession No.	3. Recipient's Catalog No.
FHWA-RD-75-121		

4. Title and Subtitle	5. Report Date
POLYMER-IMPREGNATED PRECAST STRUCTURAL CONCRETE BRIDGE DECK PANELS	October 1975
	6. Performing Organization Code
	8. Performing Organization Report No.

7. Author(s)	
William T. Lockman and William C. Cowan	

9. Performing Organization Name and Address	10. Work Unit No. (TRAIS)
Department of the Interior, Bureau of Reclamation, Division of General Research, Engineering and Research Center, P.O. Box 25007, Denver Federal Center, Denver Colorado 80225	FCP 35F3-032
	11. Contract or Grant No. FHWA P.O. 2-1-2398
	13. Type of Report and Period Covered

12. Sponsoring Agency Name and Address	14. Sponsoring Agency Code
Department of Transportation Federal Highway Administration Office of Research Washington, DC 20590	S0714

15. Supplementary Notes
This program was a cooperative program cosponsored by Federal Highway Administration and the Bureau of Reclamation with support by the Prestressed Concrete Institute.
FHWA Contract Manager: Craig A. Ballinger, HRS-11

16. Abstract

This report contains the results of a research program that shows how the inherent structural and durability properties of polymer-impregnated concrete (PIC) can be incorporated into a precast panel system to provide an excellent bridge deck. Panels were designed and tested under both static and fatigue loading. The tests verified the design procedures and load carrying capabilities. Extensive physical property testing in compression, tension, flexure, and fatigue was performed on specimens to verify the quality of the initial concrete and PIC used in the panels. An investigation into prestress losses was performed. Also, various nondestructive tests were evaluated to determine a method for quality control for PIC.

Dept. of Transportation
MAY 4 1978
Library

17. Key Words	18. Distribution Statement
polymer concrete, precast decks, concrete fatigue, prestress loss	No restrictions. This document is available to the public through the National Technical Information Service, Springfield, Virginia 22161.

19. Security Classif. (of this report)	20. Security Classif. (of this page)	21. No. of Pages	22. Price
Unclassified	Unclassified	181	

TABLE OF CONTENTS

	Page
List of Tables	iv
List of Figures	vi
Definition of Terms Pertaining to Polymer Impregnation	xii
Introduction	1
Background	2
Scope of Study	3
Panel Design	5
Material Properties	6
Panel Thickness	7
Loading Conditions	7
Panel Design Using AASHTO Specifications	7
Panel Design Using Elastic Analysis	8
Bond Development in Ends of Panel	11
Panel and Girder Fabrication	12
Panel Fabrication	12
Girder Fabrication	13
Impregnation Facility	14
Test Program	16
Physical Properties Tests	17
Deck Panel Concrete	17
Low Temperature Tests	17
Simple Span Tests of Small Panels	19
Fatigue Tests of Beams	19
Prestress Loss Tests	22
Prestress Loss Due to Elastic Shortening	23
Investigation of High Temperature on Stress Relaxation in Prestressing Strands	23
Laboratory Investigation of Prestress Loss Due to Creep in Concrete	24
Laboratory Investigation of Prestress Loss Due to Concrete Shrinkage	25

TABLE OF CONTENTS - Continued

	Page
Panel Tests	27
Assembly of Test Configurations	28
Unimpregnated Single-panel Static Test	30
PIC Single-panel Static Tests	31
PIC Three-panel Static Tests	33
PIC Single-panel Fatigue Test	36
PIC Three-panel Fatigue Test	37
Panel-to-girder Connection Shear Test	39
Nondestructive Test Evaluation	40
Ultrasonic Pulse Velocity	40
Microwave Transmission	41
Neutron and Gamma Ray	42
Other Nondestructive Tests	42
Ultrasonic Resonant Frequency	42
Acoustic Impact	42
Neutron Radiography	43
Infrared Radiography	43
Acoustic Emission	43
Electrical Resistivity and Dialectric Constant	43
Impact Hammer	43
Summation	44
Conclusions	45
Recommendations	47
References	48
Appendix A	139

LIST OF TABLES

Page

1. Summary of structural and durability properties of MMA impregnated concrete 49

2. Summary of strength and elastic modulus of unimpregnated 6- by 12-inch cylinders 50

3. Summary of polymer loadings of panels and companion 6- by 12-inch cylinders impregnated with the panels and average strength and elastic modulus of the cylinders 51

4. Summary of flexural tests on unimpregnated 4- by 4- by 30-inch bars 52

5. Summary of flexural tests on impregnated 4- by 4- by 30-inch bars 52

6. Low temperature compressive tests of plain concrete and PIC 6- by 12-inch cylinders 53

7. Low temperature flexural tests of plain concrete and PIC 4- by 4- by 30-inch bars 53

8. Low temperature tensile tests of plain concrete and PIC 3- by 6-inch cylinders 54

9. Simple span flexural tests of small panels 54

10. Summary of data from fatigue tests of 3- by 6- by 54-inch unimpregnated concrete and PIC beams 55

11. Measured values of panel shortening at prestress strand release 56

12. Prestress loss due to temperature in unbonded prestress strand 57

13. Measured transverse strains in unimpregnated single-panel with 20-kip load in position 4 58

14. Measured longitudinal strains in unimpregnated single-panel with 20-kip load in position 4 59

15. Measured transverse strains in panel No. 8 with 20-kip load in position 4 60

LIST OF TABLES - Continued

Page

16. Measured transverse strains in panel No. 8 with 20-kip load in position 8 61

17. Measured transverse strains in panel No. 8 with 20-kip load in position 12 62

18. Measured longitudinal strains in panel No. 8 with 20-kip load in position 4 63

19. Comparison of average measured transverse strains in panels No. 2 and 8 with 20-kip load in position 4 64

20. Measured transverse strains along midspan section from three-panel tests with 20-kip load in position 1 65

21. Measured transverse strains along midspan section from three-panel tests with 20-kip load in position 2 66

22. Measured transverse strains along midspan section from three-panel tests with 20-kip load in position 3 67

23. Measured transverse strains along midspan section from three-panel tests with 20-kip load in position 4 68

24. Displacements along midspan section with 20-kip load for first three-panel test 69

25. Displacements along midspan section with 20-kip load for second three-panel test 69

26. Neutron and gamma ray moisture and density determination 70

LIST OF FIGURES

Page

1. Plan and section of a single panel and girder support 71
2. Design layout for panels 72
3. Details of panel-to-panel and panel-to-center girder connections 73
4. Schematic layout for casting panels and test specimens 74
5. Panel casting bed just prior to placing concrete 75
6. Prestressing strand, conduits for post-tensioning cables, and plate for center girder to panel connection 75
7. Panels stacked after removal from the casting bed 76
8. Details for fabrication of the support girders 77
9. Schematic drawings of the impregnation/polymerization tank and panel carrier 78
10. Overall view of the impregnation/polymerization facility 79
11. Calibrating the load cell prior to weighing panels 80
12. Placing a panel in the drying oven 81
13. Carrier containing four panels ready for impregnation 81
14. Beam fatigue testing machine 82
15. Curves from fatigue tests of PIC and unimpregnated concrete 3- by 6- by 54-inch beams 83
16. Change in slope of a curve of stress versus load occurring when the tension stress equals the compressive prestress in a cracked PIC panel 84
17. Loading frame used in tests to determine effects of high temperatures on prestress relaxation 85
18. Percent of prestress loss due to temperature in unbonded prestress strand 86
19. Creep curve for a typical unimpregnated concrete 6- by 12-inch cylinder 87

LIST OF FIGURES - Continued

Page

20. Curves of the average concrete creep from each day of casting 88

21. Shrinkage curve for a typical unimpregnated concrete 4- by 4- by 30-inch bar 89

22. Load positions and identifications for both single-panel and three-panel tests 90

23. Girder support for the end of a panel attached to the test floor 91

24. J-hooks welded to the bottom of a panel for the center girder support to panel connection 92

25. J-hooks welded to the bottom of a panel for an end girder support to panel connection 93

26. Typical strain gage installation where both transverse and longitudinal strains were desired 94

27. Placement of a panel onto the girder supports 94

28. Frame on end girder support used for panel alignment 95

29. Pulling of the south panel to center panel by using the longitudinal post-tensioning strands 96

30. Joint between panel and girder support at center of the panel prior to grouting 96

31. Grouting of the panel to the center girder support 97

32. Single-panel test setup 97

33. Data acquisition system used in single-panel testing 98

34. Three-panel test setup 98

35. Hydraulic ram, load cell, and 5- by 20-inch bearing block used to load the panels 99

36. Strain gage locations and identifications for unimpregnated panel No. 3 and PIC panel No. 8 single-panel static tests 100

Page

37. LVDT locations and identifications for unimpregnated and PIC single-panel tests 101

38. Plot of analytical moments and moments computed from tensile strain on the unimpregnated single-panel, 20-kip load at position 4 102

39. Plot of analytical and measured displacements on unimpregnated single-panel, 20-kip load at position 4 103

40. Bottom of end girder support in unloaded span lifting off the test floor during unimpregnated single-panel test 104

41. Cracks in the stem of the center girder support during failure test of the unimpregnated single-panel 104

42. Failure of unimpregnated single-panel 105

43. Failure of stud between embedded plate and panel at the end of the panel of the unimpregnated single-panel 105

44. Strain gage locations and identifications for PIC single-panel No. 2, which was also used for PIC single-panel fatigue test 106

45. Plot of analytical moments and moments computed from measured tensile strains on PIC single-panels, 20-kip load at position 4 107

46. Plot of analytical moments and moments computed from measured tensile strains on PIC single-panels, 20-kip load at position 8 108

47. Plot of analytical moments and moments computed from measured tensile strains on PIC single-panels, 20-kip load at position 12 109

48. Plot of analytical and measured displacements on panel No. 8, 20-kip load at position 4 110

49. Plot of analytical and measured displacements on panel No. 8, 20-kip load at position 8 111

LIST OF FIGURES - Continued

Page

50. Plot of analytical and measured displacements on panel No. 8, 20-kip load at position 12 112

51. Plot of analytical and measured displacements on panel No. 2, 20-kip load at position 4 113

52. Crack pattern in panel No. 8 after ultimate load of 95 kips in load position 4 114

53. Positive moment cracks in panel No. 8 during single-panel static test; end of rule is midspan 115

54. Intersection of cracks No. 3 and 4 over center girder support in panel No. 8 at ultimate load of 95 kips 115

55. Strain gage locations and identifications for first three-panel static test 116

56. Strain gage locations and identifications for second three-panel static test 117

57. LVDT locations and identifications for the three-panel tests 118

58. Plot of top theoretical and measured transverse stresses along the centerline of the center panel in three-panel tests for 20-kip load in position 1 119

59. Plot of bottom theoretical and measured transverse stresses along the centerline of the center panel in three-panel tests for 20-kip load in positon 1 120

60. Plot of top theoretical and measured transverse stresses along the centerline of the center panel in three-panel tests for 20-kip load in position 4 121

61. Plot of bottom theoretical and measured transverse stresses along the centerline of the center panel in three-panel tests for 20-kip load in position 4 122

62. Plot of top theoretical and measured longitudinal stresses along the midspan section of the three-panel tests for 20-kip load in position 1 123

63. Plot of bottom theoretical and measured longitudinal stresses along the midspan section of the three-panel tests for 20-kip load in position 1 124

Page

64. Plot of top theoretical and measured longitudinal stresses along the midspan section of the three-panel tests for 20-kip load in position 4 125

65. Plot of bottom theoretical and measured longitudinal stresses along the midspan section of the three-panel tests for 20-kip load in position 4 126

66. Crack pattern in first three-panel test after ultimate load of 160 kips in load position 3 127

67. Plot of load versus deflection from the failure loading on the first three-panel test with load in position 3 128

68. Shear crack between south and center panels at the transverse joint; south panel is on the right 129

69. Shear crack between center and north panels at the transverse joint; center panel is on the right 129

70. Plots of transverse and longitudinal stresses versus load obtained during static preloading of second three-panel test; load in position 4 130

71. Failure of bottom prestress strand after fatigue loading for 300,000 cycles with load of 5 to 42 kips in load position 4 131

72. Plot of deflection versus load before and after cyclic load of the three-panel fatigue test 132

73. Crack patterns resulting from static failure loading on each of the three panels in the second three-panel test following 2.1 million cycles of fatigue loading 133

74. Shear test to evaluate the horizontal shear capacity between a panel and center girder support 134

75. Panel movement versus shear load from tests of panel-to-girder connections 135

76. Ultrasonic pulse velocity of unimpregnated and PIC 3- by 6-inch cylinders 136

LIST OF FIGURES - Continued

Page

77. Ultrasonic pulse velocity of prestressed concrete bridge deck panels before and after impregnation 137

78. Microwave test of 6- by 12-inch cylinders 138

DEFINITION OF TERMS PERTAINING TO POLYMER IMPREGNATION

Term	Simple definition
Polymer-impregnated concrete (PIC)	Precast portland cement concrete impregnated with a monomer system that is subsequently polymerized in-situ.
Monomer	The simplest basic molecule of an organic material that can be combined to form large molecules of a stable material (example - methyl methacrylate (MMA), which is in liquid form, is the monomer of poly (methyl methacrylate) polymer).
Polymer	A hardened (polymerized) plastic; the product of a large number of monomeric molecules reacting together.
Methyl methacrylate (MMA)	Monomer system used in this study.
Drying	The removal of free water from concrete by heating.
Impregnation	The process of saturating hardened dried concrete with a monomer.
Polymerization	The reaction of monomer molecules joining together to form a polymer; for this study the change from liquid to solid state with plastics.
Polymer loading	The percent by weight of polymer in PIC, usually 4 to 8 percent.

INTRODUCTION

Bridge decking poses a major problem on highway systems in the United States because of its vulnerability to freeze-thaw damage and its exposure to attack by the salt compounds commonly used in ice control during the winter months. Consequently, concrete bridge decks are subject to rapid deterioration. An estimated $70 million per year is spent on repairing deteriorated bridge decks. That figure does not consider the expense of decreased safety caused by poor road conditions or traffic disruption during maintenance.

Extensive research has been performed by the U.S. Department of Interior, Bureau of Reclamation (USBR) and Brookhaven National Laboratory (BNL) on polymer-impregnated concrete (PIC) during the past several years. As discussed later under background, this research has shown that PIC has strength and durability properties far in excess of those of normal portland cement concrete. It has proven durable under extended freeze-thaw cycling, is inert to most chemicals, has near zero water absorption, and is essentially impermeable. Its strength in both compression and tension is much greater that that of normal concrete.

The Federal Highway Administration (FHWA) of the Department of Transportation in reviewing this research foresaw the use of PIC as a possible solution to the problem of bridge deck deterioration due to deicing salt. It was recognized that the use of PIC would result in a significantly higher initial cost over a conventional membrane and asphalt topped cast-in-place concrete bridge. However, in return for this greater initial investment, a virtually maintenance-free deck for the life of the bridge would be provided. Additional economic and safety benefits would accrue in not having to stop or disrupt traffic for bridge deck repair. When all factors were considered from a long-range standpoint, it appeared the higher initial cost could be returned many times over. Therefore, the FHWA initiated this study with the objective of developing a bridge deck comprised of polymer-impregnated precast prestressed concrete panels which would be resistant to corrosion damage due to deicing salt. The panels were not merely surface treated but were fully impregnated.

The study was a cooperative project involving the FHWA, the USBR, and the Prestressed Concrete Institute (PCI). The FHWA was the principal financial supporter and defined the concepts of the study. The USBR also provided major financial support, and, under contract with FHWA, was responsible for a panel design, impregnation and polymerization of the panels, physical testing, and evaluation of test results. The PCI contributed some financial support and under a separate contract with the USBR submitted an independent panel design and furnished the required test panels and support girders.

BACKGROUND

The Concrete-Polymer Materials Program was initiated in 1967 by the former Atomic Energy Commission (now the Energy Research and Development Administration). This program was initiated as a cooperative research program between the BNL and the USBR. Because of its interest in the potential application of concrete-polymer materials for construction of vessels for water desalinization plants, the former Office of Saline Water (now Office of Water Resources and Technology) contributed to the planning, development, and funding of the program.

The long-range objectives of the program were the investigation and development of concrete-polymer composite materials for use as improved or new materials of construction. The following three types of materials were investigated: (1) polymer-cement concrete, a premixed material of water, portland cement, and aggregate to which monomer is added during mixing and subsequently cured and polymerized in place; (2) polymer-concrete, consisting of an aggregate mixed with a monomer or resin that is subsequently polymerized in place; and (3) polymer-impregnated concrete (PIC) which consists of precast portland cement concrete impregnated with a monomer system that is subsequently polymerized in situ.

The main, and most successful, effort in improving the structural and durability properties of a portland cement concrete was with PIC. Many monomers and combinations of monomers were investigated. Vast quantities of data were accumulated from tests conducted from room temperature to 350° F. 1/, 2/, 3/, 4/, 5/, 6/* Limited data were also collected for tests at temperatures as low as -10° F.

In general, all the monomer systems provided significant improvement in strength and durability properties of concrete. Methyl methacrylate (MMA), used to impregnate the bridge deck panels of this project, was one of the two monomer systems which yielded the best results. Table 1 presents a summary of the structural and durability properties of MMA impregnated concrete compared with those of unimpregnated concrete.

Because of the close proximity of Prestressed Concrete of Colorado, Inc. (PCC) to the USBR laboratory at the Denver Federal Center (DFC), they were selected by the PCI to fabricate the prestressed concrete panels and support girders. To avoid confusion on the abbreviation (PCC), in this report it will refer only to Prestressed Concrete of Colorado, Inc. PCC was also selected by the PCI to provide a panel design and act as their designated representative in the project.

---

* Refers to numbered references on page 48.

SCOPE OF STUDY

This study was conducted to establish the feasibility of using polymer-impregnated precast prestressed concrete panels as bridge decking. The following items were included in the study:

1. Design of panels and decking system
2. Manufacture of precast panels
3. Design and setup of impregnation facilities
4. Impregnation of panels
5. Conduct static tests on panels
6. Conduct fatigue tests of panels
7. Conduct shear tests between panels and support girders
8. Conduct tests to investigate relaxation of prestress strands at elevated temperatures
9. Conduct fatigue tests of PIC specimens
10. Conduct static tests on PIC specimens at subzero temperature
11. Investigate nondestructive tests which might be used to evaluate completeness of impregnation

In order to enhance the input of ideas to solve the panel design problems, two separate and independent designs were made. One was made by the USBR and the other by PCC.

The USBR impregnation facility did not have the capability of impregnating specimens as large as the deck panels. It was, therefore, necessary to design and set up a new facility with this capability.

The test program for the panels planned for static tests to failure of two single panels and one three-panel assemblage. One of the single panels was unimpregnated concrete. Additional static tests, well within the elastic limit of PIC, were planned for the fatigue test setups of both single-panel and three-panel configurations.

Two fatigue tests were planned. The first test was to be on a single-panel with the second test on a three-panel assemblage. Loading was to be cycled until failure occurred or until 1 million cycles was reached. If failure had not occurred in 1 million cycles, the load was to be increased and the test restarted.

Horizontal shear tests of the connection between panels and the girder were planned. The center girder and panel connection section were sawed from previously tested single panels and used for this testing.

Drying concrete prior to impregnation required subjecting prestressing strands to elevated temperatures. Typical drying temperatures in PIC research have been as high as 350° F which could cause excessive relaxation of the prestressing strand. Using a stabilized strand and

not exceeding 212° F as a drying temperature would result in a prestress loss of only around 6 percent according to the strand manufacturer. Since this was an area of concern, tests were planned to evaluate the effect of elevated temperatures on prestress loss in the prestressing strands.

Fatigue tests of PIC and plain concrete specimens were included in the program. The specimens for this testing were to be 3- by 6- by 54-inch beams with no prestressing. The stress levels planned for this program were 70, 80, and 90 percent of ultimate strength. Specimens were to be subjected to a maximum of 10 million cycles.

Information on the effect of subzero temperatures on PIC was limited. Since bridge decks in many areas are exposed to subzero temperatures, additional information of these effects was important. Consequently, compressive, tensile, and flexural strength tests were planned for both plain concrete and PIC at -40° F. Tests of companion specimens were to be made at 70° F to provide a basis of comparison.

Weighing concrete specimens before and after impregnation and polymerization was used in PIC research to determine whether a specimen was fully impregnated and polymerized. Destructive tests of specimens have proven this was a reliable method of obtaining the desired results. However, verification of complete impregnation and polymerization was possible only after a specimen had been destroyed. Since the deck panels were larger than any specimens previously impregnated, a method of verifying the completeness of impregnation and polymerization prior to testing was desirable. Therefore, a study was incorporated into the program to evaluate nondestructive test procedures that might be used to determine the degree and uniformity of impregnation and completeness of polymerization.

PANEL DESIGN

The initial objective of the research was to design a segmental system of panels that could be used to form a bridge deck which made use of the structural and durability properties of PIC.

Certain basic criteria were established to simplify the design parameters which would be encountered if a general design study had been performed. These criteria were the following:

1. Bridge length of 90 feet without skew
2. Concrete girders with a maximum spacing of 8 feet center-to-center
3. Maximum live load of an HS20-44 truck load of the American Association of State Highway and Transportation Officials (AASHTO)

Other secondary criteria were established prior to and during the design to make the design more realistic for actual construction. These criteria were the following:

1. The precasting must follow current acceptable practices of precast manufacturers pertaining to: material, tolerances, and quality control.

2. The completed bridge deck surface must be smooth enough to provide acceptable riding quality without a topping.

3. The completed deck must develop a composite action with the girders.

4. The panel-to-girder connections should provide adjustment for variable girder camber and possible panel warpage. Also, the connection was to be made without the use of holes through the panel.

5. Panel-to-panel connections must provide for shear transfer between adjacent panels.

6. It was desired that the deck be erected without any immediate welding, bolting, or grouting that would possibly detain erection equipment for any job function not directly related to erection.

7. Design the system to eliminate tensile cracking or "working" of the panel-to-panel joints under all service load conditions.

Since dead and live loads on a bridge deck are mainly transferred to the bridge girders in the transverse direction, it was decided that a transverse panel concept would be used. The panel dimensions were

limited by the size of impregnation facility that was built under this research study to treat the panels and the size of the test facility to test the various single- and three-panel configurations. A panel length of 16 feet and a width of 4 feet was established to allow a two-span continuous test of a panel, as shown in figure 1.

Separate and independent panel designs were made by the USBR and PCC. A summary of the designs for the panel is presented in appendix A. Figure 2 shows the panel layout as determined by the design. The approach of using two design teams for the panel design allowed PCC's experience in prestress concrete design, fabrication, and construction to be combined with the USBR's capability in elastic analysis, concrete design, and applied research. While the designs were separate and independent, close coordination was maintained between the design teams so both teams would be using the same basic assumptions for physical properties, dimensions, etc. Figure 3 shows the connection details as dictated from the final design.

The specifications of AASHTO were used to the extent possible. However, AASHTO specifications do not apply to either precast bridge decks or PIC. Other guides were used, foremost being the Building Code Requirements for Reinforced Concrete (ACI 318-71).

Two design approaches were used: AASHTO design and elastic analysis. For the final design of the panels more reliance was given to the use of elastic analysis because, for a research program more exact analytical techniques are desirable to verify test results.

Material Properties

The concrete strength for the panels was established as a 5,500 lb/in^2 mix design with a 24-hour release strength of 4,000 lb/in^2. The 3/8-inch-diameter prestressing steel to be used was ASTM A-416 seven-wire strand with an ultimate strength of 270 $kips/in^2$.

The specified compressive strength, molulus of elasticity, modulus of rupture, and permissible shear stress for PIC were established from previous test data as referenced in the the Background section. These are as follows:

f'_c = 15,000 lb/in^2 (specified compressive strength)

E_c = 6,000,000 lb/in^2 (modulus of elasticity)

f_r = 1,300 lb/in^2 (modulus of rupture)

v_c = 750 lb/in^2 (permissible shear stress)

The above values were selected based on the statistical significance and amount of the referenced test data. A greater amount of data was available on compressive strength and modulus of elasticity than was available for modulus of rupture and permissable shear stress. Hence, it was necessary to have a greater standard deviation criteria for modulus of rupture and permissable shear stress than that required for compressive strength and modulus of elasticity. This was the first time a design had been performed using methyl methacrylate impregnated and thermal-catalytic polymerized concrete. Therefore, it was necessary to establish values that were known to be attainable during the production of the panels.

A material strength and fabrication tolerance reduction factor, ϕ, is applied to the design strengths to predict load carrying capacity of the PIC.

Panel Thickness

Conventional cast-in-place reinforced concrete bridge decks with girder spacing of 8 feet center-to-center have a thickness of 7-1/2 inches or greater because of the minimum cover requirements specified in AASHTO. The increased structural properties of PIC indicate that a thinner panel of PIC would carry the load. The thickness of the test panels was selected to assure an acceptable riding quality based on dynamic response. As presented in appendix A, page 141, a 6-inch-thick PIC deck should have similar, if not better, dynamic response than a 7-1/2-inch conventional reinforced concrete deck. Hence, the 6-inch thickness for the panel design was established.

Loading Conditions

Loading conditions for the design are presented in appendix A, page 142. Maximum wheel load for service load conditions, including impact, is 20,800 pounds over a 5- by 20-inch area. The 20-inch dimension being perpendicular to the direction of traffic.

Panel Design Using AASHTO Specifications

Initially in the program a panel design was performed using Standard Specifications for Highway Bridges adopted by the American Association of State Highway Officials (AASHO), 10th Edition, 1969. However, the computations presented in appendix A, pages 143 through 149, are mainly based on the more current AASHTO, 11th Edition, 1973, and Interim Specifications Bridges, 1974. The AASHTO design of the panel made use of section 1.3.2.(c) to determine the simple span live load moment. The AASHTO design is based on a reinforced cast-in-place concrete slab which does not have the possible discontinuity that the transverse joints between panels in a precast system might produce. On page 150 of appendix A, an effective width for wheel load distribution was determined. The required width was 5.24 feet which is greater than

the established 4-foot width of the panel. With this difference the application of AASHTO for design of the panel was questionable.

An interesting comparison of allowable tension stress in the precompressed tensile zone from the AASHO (1969), AASHTO (1973), and Interim Specifications (1974) can be made at service load conditions after prestress losses have occurred. AASHO (1969) allows 3 $\sqrt{f'_c}$ but not to exceed 250 lb/in^2, AASHTO (1973) allows 6 $\sqrt{f'_c}$ or 3 $\sqrt{f'_c}$ for severe corrosive exposure conditions, and Interim (1974) under allowable service load stresses allows extreme fiber stress to be 0.21 times modulus of rupture from tests. Hence, the following allowable tension stresses (f_t) might be considered if f'_c equal 15,000 lb/in^2 and f_r equals 1,300 lb/in^2 as established for PIC:

1. AASHO (1969) $f_t = 250$ lb/in^2
2. AASHTO (1973) $f_t = 734$ lb/in^2 (maximum)
   or $f_t = 367$ lb/in^2 (minimum)
3. Interim (1974) $f_t = 273$ lb/in^2

The AASHTO design in appendix A was based on the 273 lb/in^2 allowable tensile stress because of the available modulus of rupture data, and it provides a more conservative design than that produced based on f_t from AASHTO (1973).

Panel Design Using Elastic Analysis

Two different and separate elastic analysis techniques were performed by the USBR and PCC to determine slab moments considering only one span of the panel as a flat plate with various boundary conditions. Additional slab moments due to differential displacement and torsional rotation of the girders were determined from a three-dimensional analysis of the assumed bridge. The USBR used an in-house indeterminate structural analysis computer program "STR5" and modeled the panels using finite bending elements, appendix A, pages 151 through 154. While PCC made use of a graphical technique of moment influence surfaces in slabs, as presented by A. Pucher in "Einflussfelder Elasticher Platten," Springer Verlag, Berlin. The PCC's analysis is shown in appendix A, pages 160 through 163.

Using the finite bending elements, an analytical model was defined which modeled three panels adjacent to each other between two girders. Each panel was 4 feet wide and 6 feet 2 inches long. The 4-foot dimension of the panels on one girder support was fixed against rotation and vertical displacement, which simulates a continuous edge of an actual panel. While the opposite 4-foot dimension was assumed free to rotate about a longitudinal bridge axis but fixed against transverse rotation and vertical displacement. The transverse joint between panels had equal vertical displacement but the panel edges adjacent to the

transverse joint had independent rotations. This simulates only a shear transfer across the transverse joint between the panels. Live load plus impact of 20,800 pounds was applied as a uniform load of 130 lb/in^2 on 8- by 20-inch elements or 144 lb/in^2 on 8- by 18-inch elements to simulate various positions of a wheel load. Plate bending moments and shears from the analysis for various loads and positions in the model are presented in appendix A starting on page 154.

Using A. Pucher's graphical technique of moment influences surfaces, one panel was modeled between two girders. The panel was 4 feet wide and 6 feet long. The 4-foot-wide edges were assumed to be fixed and the 6-foot edges were assumed to be free. A live load of 16,000 pounds was applied to the panel in two locations to determine panel bending moments. In this analysis only one panel was considered and some adjustment of moments was required because of shear transfer to adjacent panels. It was initially assumed for the live load at the free edge of the panel that the adjacent panel would carry 40 percent of the load through shear transfer in the transverse joint. A refined distribution was made by checking deformations, making a refined shear assumption, and repeating computations until panel edge compatibility existed.

From both of the elastic analyses the controlling load position for design was when the wheel load was at the panel edge. Only one wheel load was considered because more wheel loads and less tire pressure would have produced less critical design moments. Each analysis made use of adjustment factors. In the finite bending element analysis, negative moments in the panel at the girder were found to be the most critical. Since the girder flange can bend slightly and the panel is continuous over the girder, at the completely fixed support, the negative moments were reduced by 75 percent and positive moments at midspan of the panel were increased by 25 percent. Using A. Pucher's graphs the negative and positive moments in the panel were assumed equal and reduced by 20 percent by assuming panel continuity across the girder supports. A comparison of moments from the two analyses is presented in appendix A on pages 161 and 162 for live load plus impact.

Neither elastic analysis took into consideration the additional moment introduced into the slab because of differential displacement and torsional rotation of the girders due to live loadings. A three-dimensional analysis was made of the assumed bridge configuration, appendix A, pages 163 through 165. This analysis shows that an additional negative moment in the panels of 1.0 ft-kip/ft has to be added to the moments from the elastic analyses of the panels. A summary of final design moments from both analyses, which includes slab moment due to differential girder movement, is presented in appendix A, page 166.

The required prestressing was designed for both allowable stresses and load factor, both of which are controlled by tension stresses. In the design for allowable stresses, if tension stress (f_t) is based on modulus of rupture, 14 strands per panel are required. However, if f_t is based on $3\sqrt{f'_c}$ then only 12 strands per panel are required,

appendix A, page 168. For load factor design it was necessary to determine a load factor or factor of safety, appendix A, page 169. AASHTO gives a load factor of 2.3 but this is believed to be excessive and limited to girders and other main members. No consideration for precast prestressed decks is made within AASHTO. From ACI, a load factor of 2.0 was obtained, which is believed to be more applicable to this type of construction. Hence, in using the 2.0 factor of safety the USBR analysis required 10 strands per panel and PCC analysis required 12 strands per panel. If 10 strands per panel were used, much closer attention would be required in placing the strands near the edge of the panel because the panel bending moments are greater at the edge of than at the center of the panel. Since the service load design requires 12 strands per panel and PCC's analysis requires 12 strands per panel, the final prestress pattern was selected as 12 strands per panel. From appendix A, page 172, this pattern provides an ultimate moment capacity of 703.2-inch-kips for the panel.

The prestress design was based on the assumptions that the initial stress would be 0.7 of the ultimate strength of the prestressing steel or 189 kip/in^2 and the prestress loss would be 21 percent. The prestress losses due to all causes were as follows:

1. Elastic shortening = 5,000 lb/in^2
2. Shrinkage = 18,600 lb/in^2
3. Creep = 4,600 lb/in^2
4. Strand relaxation = 11,400 lb/in^2

This totals 39,600 lb/in^2 and gives a final predicted stress of 149,400 lb/in^2 or a uniform concrete stress of 530 lb/in^2.

Excessive strand relaxation would result if stress relieved strands were used in the panels because of the elevated temperatures necessary for drying the panels prior to treatment to form PIC panels. Stabilized strand which the C.F.&I. Steel Corporation estimated would have a relaxation of about 6 percent if a drying temperature of 212° F was not exceeded was selected.

A check of bending about the transverse bridge axis in the panel was made, appendix A, pages 173 and 174. It was found under service load conditions a tension stress of 514 lb/in^2 develops which exceeds $3\sqrt{f'_c}$ but this occurs in the bottom of the panel and would not affect panel durability. However, in using load factor design, the stress is 1,028 lb/in^2 which is less than the 1,300 lb/in^2 ultimate design modulus of rupture strength.

It was determined that a limited amount of longitudinal post-tensioning would be beneficial for pulling the panels together during

deck erection and to assure a permanent closure of the transverse joints in the deck. Permanent closure of the transverse joint would enhance the durability of the deck. A value of 30 lb/in^2 was believed adequate to assure permanent closure. To obtain the 30 lb/in^2 it was decided to use 3/8-inch longitudinal strands on 4-foot centers and design for a temperature differential of 160° F. The temperature differential was determined by considering a maximum temperature of 120° F and a minimum temperature of -40° F. The 30 lb/in^2 was obtained by stressing the longitudinal strands to 60 percent of the ultimate which produced a concrete stress of 48 lb/in^2 or a post-tensioning force of 55,300 pounds. This allowed for a prestress loss of approximately 37 percent due to creep in the panels and the 160° F temperature change.

A check of shear through the transverse joint was made, appendix A, pages 175 and 176. Maximum shear was found when the wheel load was on the middle panel next to the transverse joint. A shear area in the transverse joint was assumed as one-third the thickness of the panel. It was found under service load conditions the maximum shear stress was 145 lb/in^2 which is less than $1.8\sqrt{f'_c}$, and under load factor design the shear stress was 290 lb/in^2 which is less than the 750 lb/in^2 permissible shear stress established for PIC.

Bond Development in Ends of Panel

The requirements for bond development were investigated for the ends of the panel, appendix A, pages 177 through 181. Maximum positive moments in the panel due to live load plus impact were obtained from the finite bending element analysis for various loading positions. A conservative assumption was made which considered the maximum moments due to dead load plus live load plus impact to be uniform for the 4 feet of panel width. Knowing the amount of prestressing, the modulus of rupture of PIC, and assuming the 21 percent prestress losses a cracking moment was computed. Using AASHTO, required bond lengths were computed for cracking moment and ultimate moment, which were 19.2 inches and 63.9 inches, respectively.

A diagram of moment versus distance from the end of the panel was plotted, appendix A, page 181. It was found that the moments using the load factor of 2.0 were not contained under the ultimate moment capacity of the panel but were contained under the cracking moment capacity of the panel. From pullout tests it has been determined that bond strengths for steel are greater in PIC than conventional concrete. Hence, if the bond development length for ultimate moment is reduced 30 percent the load factor moments are contained under the adjusted ultimate moment capacity.

The conditions for bond development are not believed to be critical since cracking moment capacity easily contains the moments using load factors. Also, bond development is not as critical if the panel length is equal to the bridge width.

PANEL AND GIRDER FABRICATION

Panel Fabrication

The panels and related control test specimens were cast in 2 days at the Denver plant of PCC. Ten 16-foot, two 6-foot, and two 5-foot-long panels were cast. Related control test specimens consisted of six 2-foot-long shrinkage panels, fifty 4- by 4- by 30-inch bars, and one hundred forty-two 6- by 12-inch cylinders. Test bars and cylinders were made throughout the casting operation to monitor the consistency of the concrete in all panels. A drawing such as shown in figure 4 was made for each day of casting to assure placing the correct number of specimen molds at the desired locations.

Casting was performed in a flat bottom box girder bed 6 feet wide and 110 feet long, figure 5. Placing the panel forms to one side of the bed left approximately 2 feet on the other side in which to place test specimen molds. Prestressing the strands was accomplished by applying a force of 16,000 pounds to each strand which resulted in 189,000 lb/in^2 prestress in the strand. This load produced a strand elongation of about 9 inches. Figure 6 is a closeup view of a portion of the bed ready for placing concrete. In this view, the embedded plate for midpanel connection to the girder can be seen. Also in evidence are the prestressing strands and the conduit for longitudinal post-tensioning cables.

A standard PCC mix for prestressed members as shown below was used:

Cement	720 lb/cu yd
Water	35 gal/cu yd
Sand	1,110 lb/cu yd
Coarse aggregate	1,860 lb/cu yd

Admixtures:

Pozzolith 82 water reducing agent	6.0 oz/sk cement
MBVR air entraining agent	3/4 oz/sk cement

This mix was designed to yield a 28-day strength of 5,500 lb/in^2 and a 24-hour strength of 4,000 lb/in^2 for prestress release. Control cylinders tested yielded average strengths of 5,700 and 5,400 lb/in^2 for the two casts at strand release. Slump measurements were made each day of casting. The average slumps were 3.3 inches and 3.5 inches, respectively. Once concrete placement started, it was continuous until all panels were cast. Placement of the concrete took about 1-1/2 hours.

Measurements on panels were planned to obtain additional information on prestress loss due to elastic shortening, shrinkage, creep, and stress relaxation of the prestress strand. This required the installation of gage points while the panels were being cast. Five Whittemore gage points spaced 10 inches apart were installed in each of the three

2-foot-long shrinkage panels cast each day. The gage points were secured to a metal template and then inserted into the fresh concrete perpendicular to the prestress strands at the center of the panel. An invar tube extensometer was used to measure length change in the panels. Gage points for this extensometer were placed 12 feet apart, 7-3/4 inches from each side of the panels. Immediately after a trowel finish had been applied, these gage points were installed. Lifting lugs were also installed in the fresh concrete at this time. Finally a broom finish was applied to the panel surface. Since the concrete was still fresh when the broom finish was applied, great care was required not to disturb any of the gage points.

After all of the concrete had been placed and finished, a cover was placed over the bed. The bed was then heated by steam in pipes located under the bed and the concrete radiantly cured overnight at a temperature of 125° F for the first day's casting and 105° F for the second day's casting.

The day following the first casting, the cover was removed from the bed. Prior to cutting the prestressing strands, panel length and shrinkage panel measurements were made. When all measurements had been completed, the prestressing strands were cut with a torch. The same measurements were repeated to determine the effect of the prestressing. Upon completion of all measurements, the panels were removed from the bed and stacked, figure 7.

The same procedure was followed for the panels cast on the second day except that the bed remained covered for three nights before making measurements and removing the panels. Also, instead of stacking the panels at the plant, they were placed upon a truck and delivered to the impregnation facility at the Denver Federal Center.

Girder Fabrication

The girder cross section, figure 8, is similar to a proposed Colorado Division of Highways standard G54. Nine of the girders were 6 feet long and six were 12 feet 6 inches long. Since the girders were to be anchored to a test floor, the full depth and bottom configuration of the Colorado standard G54 girder were not required.

IMPREGNATION FACILITY

Impregnation of the panels posed a problem at the beginning of the program. The largest impregnation/polymerization facility in the country at that time was the USBR facility at the Denver Federal Center. This unit had been designed for treating concrete pipe and smaller test specimens and could not be used for treatment of specimens as large as the panels. Therefore, it was necessary to expand this capability to treat the panels.

Primarily the new equipment consisted of a large stainless steel impregnation/polymerization tank, a stainless steel carrier for panels, a stainless steel monomer transfer tank, and an oven. The interior diameter of the impregnation/polymerization tank is 6 feet, and it is 19 feet long. The specimen carrier is 4 feet 3 inches wide, 16 feet 9 inches long, and 2 feet 9 inches deep. The vertical monomer transfer tank is 4 feet in diameter and holds 6,000 gallons. A drawing of the impregnation/polymerization tank and specimen carrier is shown in figure 9. Figure 10 is a photograph of the complete impregnation/polymerization facility.

Four basic steps as follows were involved in the impregnation/polymerization process:

1. Drying the concrete
2. Evacuating air from the dried panels
3. Impregnating panels by immersing them in monomer under pressure
4. Polymerizing the monomer in the panels by application of heat

The most time consuming step in the process was drying the concrete. To assure full penetration of the monomer into the concrete, the concrete must be almost completely dry. The criteria establishing dry was that no further weight loss occurred on continuing exposure to elevated drying temperature. In previous PIC research, this condition was reached in 24 hours at a drying temperature of 350° F. However, discussions with industry representatives indicated that if conventional stress relieved prestressing strands were subjected to an extended drying period at 350° F, excessive stress relaxation would occur. Therefore, a strand manufacturer recommended the use of stabilized prestress strand which has lower stress losses due to strand relaxation. From tests they conducted at a temperature of 212° F the relaxation loss for stabilized strand is approximately 6 percent. Accordingly, a drying temperature of 200° F was established for this research study. Since weighing the panels was the only means for determining whether the panels were dry, it was necessary to establish a drying period which would be needed before starting treatment of the panels. Accordingly, two 6-foot-long and two 5-foot-long panels were oven dried, and weight measurements were taken after 7, 12, 14, and 15 days. No significant

weight loss was evident after 12 days. Therefore, a drying period of 2 weeks was established for the 16-foot-long panels.

A load cell, placed between the crane hook and the lifting sling, was used to weigh the panels. Before weighing the panels, the load cell was calibrated by lifting a known weight of about 5,000 pounds as shown in figure 11. The load cell can be seen between the crane hook and lifting sling in this figure. After calibrating the load cell, panels were picked up and placed in the oven as shown in figure 12. Undried panel weights were obtained at this time. Companion test cylinders were dried in the oven and impregnated with the panels.

After 2 weeks in the oven, the dried panels were transferred to the specimen carrier. Dry panel weights were obtained at this time. The carrier could hold four panels separated by 1/2-inch rods. Figure 13 shows a fully loaded carrier which was then pushed into the impregnation/polymerization tank. After the tank had been closed, a vacuum of 22 to 23 lb/in^2 was applied and held for 2 hours to evacuate air from the concrete. During this period, catalyst was mixed with the monomer in the transfer tank. Monomer was transferred to the specimen carrier to cover the panels while a partial vacuum remained in the tank. After the panels were completely submerged a pressure of 60 lb/in^2 was applied and maintained for 3 hours to force the monomer into the concrete. Following this step, the monomer was drained from the carrier. Polymerization was achieved by filling the carrier with 150° F water. This temperature was then raised to 160° F by injecting live steam into the surrounding space in the tank. Complete polymerization was obtained in about 4 hours.

TEST PROGRAM

In order to validate the design for a segmental bridge deck, comprised of individual polymer-impregnated prestressed panels, the following laboratory tests were conducted:

1. Physical properties tests to determine strength and elasticity properties of both the unimpregnated concrete and PIC used in the deck panels at ambient temperature.

2. Tests of unimpregnated concrete and PIC to determine physical properties at subzero temperatures.

3. Fatigue tests of special PIC and unimpregnated concrete beams, and of beams cut from undamaged portions of previously tested panels.

4. Tests to investigate the stress relaxation of prestress due to temperature.

5. Static test of an unimpregnated and PIC single-panel configuration.

6. Static test of a PIC three-panel configuration.

7. Fatigue test of a PIC single-panel configuration.

8. Fatigue test of a PIC three-panel configuration.

9. Shear tests to determine composite action between panels and support girders.

PHYSICAL PROPERTIES TESTS

Deck Panel Concrete

Specimens to determine the strength and elasticity properties of the deck panel concrete were obtained when the panels were cast.

Seventy-eight 6- by 12-inch unimpregnated cylinders were tested in compression to determine ultimate strength and modulus of elasticity of the concrete at ages of 1, 3, 5, 7, 14, and 28 days. Examination of these test results, table 2, shows that the first day's concrete was slightly stronger than that used in the second day of casting. The 7,800 lb/in^2 average 28-day strength for the first placement and 7,120 lb/in^2 for the second may appear to be high. However, the production operation of a prestressing plant is geared to a 24-hour turnaround time for the prestressing beds. The specified 24-hour strength is a required minimum value. Production of a concrete achieving a specified 24-hour strength usually results in a product exceeding a specified 28-day strength.

Companion 6- by 12-inch cylinders were made from the concrete in each of the 16- and 6-foot-long panels. The cylinders were stored, dried, and impregnated with their respective panels. Table 3 presents a summary of the average ultimate strength and modulus of elasticity values of these cylinders. These results show that the average strengths were reasonably consistent and that they were in excess of the 15,000 lb/in^2 used in designing the panels.

Tables 4 and 5 summarize results of flexure tests on 4- by 4- by 30-inch bars of unimpregnated concrete and PIC, respectively. The same trends that had been observed in the compression tests were found in the flexural tests. Results were quite consistent, and the average modulus of rupture was well above the 1,300 lb/in^2 assumed for the panel design.

Low Temperature Tests

Bridge decks in some areas are subjected to subzero temperatures so it was deemed desirable to determine the effect of subzero temperatures on PIC. Therefore, tests were conducted at -10° and -40° F to determine the physical properties at subzero temperatures. Since the decision to conduct these tests was subsequent to the fabrication of the panels, it was not possible to obtain test specimens from the panel concrete. However, specimens were cast later using the same materials and mix proportions used in fabricating the panels. Twenty-six 6- by 12-inch cylinders were cast for compressive strength tests. Thirty-six 3- by 6-inch cylinders were made for tensile strength tests. Twenty-six 3- by 6- by 54-inch beams were fabricated for flexure testing. One-half of the compression and flexural test specimens and 23 of the tensile test specimens were impregnated with MMA monomer and polymerized.

Both strength and elasticity properties were determined in compressive and flexural tests. Therefore, strain gages to measure longitudinal strain were cemented diametrically opposite each other at the center of the 6- by 12-inch cylinders. Strain gages were affixed at the center of the flexure beams on the top and bottom surfaces.

Since only ultimate tensile strength was determined, no strain gages were used on the 3- by 6-inch tensile test specimens.

All of the specimens were wrapped in insulation before bringing them to test temperature so there would be minimal temperature change when they were moved to the test machine. The insulation was placed so that it was easily removed in the areas required for loading during testing.

Standard tests were performed on both the compression and flexural test specimens. Tensile strengths were determined from direct tension tests. To conduct the tensile tests, 1/2-inch-thick steel plates were bonded to the ends of the cylinders with epoxy. The plates had 1/2-inch-diameter holes drilled and tapped at the center. At the time of testing, eye-bolts with three chain links connecting them to the loading heads were screwed into these holes. The chain links were used to assure a straight pull on the cylinders.

Specimens tested at -10° F were cooled by placing them in a cold room maintained at -15° F. They were cooled an additional 5° F to compensate for any warming occurring between removal from the cold room and testing. Specimen temperatures were monitored by thermocouples located under the insulation. Three days were required to cool the specimens to -15° F. They were then removed one at a time and tested. The time interval between removal and testing was short enough that the test temperature was at least as low as the desired -10° F.

To reach -40° F it was necessary to encase the specimens in dry ice. Several hundred pounds of dry ice and 5 day's time were required to lower the specimens to a temperature of -45° F. Once this temperature was achieved, the specimens were again removed one at a time and immediately tested.

Results of the compressive tests are given in table 6. Flexural test results are presented in table 7, and table 8 shows the results from the tensile tests. Values shown in these tables are the average values obtained. Definite trends are apparent from these tests. It is quite conclusively shown that plain concrete increases in both compressive and tensile strength at subzero temperatures. PIC on the other hand decreases in strength. The only exception to this trend was noted in the flexural tests at 73° F and -10° F. No definite influence of temperature was apparent on the modulus of elasticity. Even though PIC does decrease in strength at subzero temperature, it is still much stronger than unimpregnated concrete.

Simple Span Tests of Small Panels

One 6-foot and one 5-foot panel were cast each day of the panel fabrication. They were provided primarily for trial runs of the impregnation and polymerization treatment. As noted previously, these panels were used in establishing a required drying time for the deck panels. Both of the 5-foot panels and one of the 6-foot panels were impregnated. Breaking the panels permitted visual inspection to determine whether the treatment process yielded fully impregnated panels. All treated trial panels were found to be fully impregnated.

Since it was necessary to break the panels to inspect the completeness of the treatment process, test data were collected as a preliminary check on whether design assumptions had been adequate. The 6-foot panels were tested as a simple 5-foot span with a concentrated line load across the center of the span. The 5-foot panels were tested as a 4-foot span. A summary of the test results is shown in table 9. The 5-foot PIC panels had a lower first cracking strength than the 6-foot PIC panels. This was believed due to a greater prestress loss in the shorter length. However, the ultimate moment of the panels exceeded the design ultimate moment. From these tests it was concluded that the design assumptions were adequate.

Fatigue Tests of Beams

It was believed that knowledge of PIC reaction to fatigue stress compared with that of plain concrete would be valuable. Consequently, a limited program of fatigue testing was included in the scope of the study.

As with the low temperature tests, the decision to conduct fatigue tests of beams was made subsequent to casting the panels. Consequently, it was necessary to fabricate beams for use in this testing. Thirty 3- by 6- by 54-inch concrete beams were cast using the same concrete mix design which was used in panel fabrication. One-half of the beams were impregnated with MMA monomer and polymerized. Additionally, 14 beams of the same size were sawed from what appeared to be undamaged portions of PIC panels which had been previously tested. The beam size, particularly length, was dictated by the size of beam which could be tested with existing USBR facilities.

The USBR beam testing machine consists of a hydraulic power unit, servo controlled by two electronic control units, and a test frame with a capacity of six beams. If six beams are in the test frame, the force applied to three of the beams is controlled by one electronic unit while the remaining three beams are under the control of the other unit. At the outset of the program, six beams were to be tested simultaneously. However, problems developed in one of the electronic control units so in the program only three beams were tested at one time, figure 14.

Before starting fatigue testing, flexural tests were conducted to determine the static modulus of rupture for the beams. Some beams were broken while calibrating the test machine. Consequently, only two beams were available to establish the modulus of rupture for plain concrete, while three were available for PIC, and four for the sawed beams. It was recognized that these few tests were not enough to provide a good statistical evaluation of the modulii of rupture. Nevertheless, the ultimate loads to produce these modulii of rupture were computed and used as a basis for fatigue loading. Average ultimate loads were 1,880 pounds for plain concrete, 4,330 pounds for cast PIC, and 5,625 pounds for the sawed PIC beams. These loads produced modulii of rupture of 815 lb/in^2, 1,925 lb/in^2, and 2,500 lb/in^2, respectively.

It had been initially determined to conduct the fatigue tests at 70, 80, and 90 percent of ultimate load. Nine tests were to be run. A test consisted of loading three beams of the same type at one of the predetermined loads. Loading was to be applied until either a failure of one or more beams occurred or 10 million cycles were reached, whichever occurred first. A cyclic rate of 6 Hz was chosen to limit the time required for 10 million cycles to 20 days.

The first tests were conducted loading to 80 percent of ultimate load. However, both the unimpregnated concrete and PIC beams failed after very few cycles when this load was applied. Therefore, the program was revised to test at maximum loads of 50, 60, and 70 percent of the ultimate load. The minimum load was held constant at 10 percent of ultimate in all tests. Three each, plain concrete and cast PIC beams were tested at these loads. In the 50 percent test, the load was cycled between 180 and 915 pounds for plain concrete and between 430 and 2,165 pounds for cast PIC beams. No failure occurred in any beam in 10 million cycles. For the 60 percent test, the load was cycled between 180 and 1,100 pounds on the plain concrete beams and between 430 and 2,600 pounds on the cast PIC beams. One of the plain concrete beams failed after 1,736,000 cycles, while none of the PIC beams failed in 10,000,000 cycles. Loading in the 70 percent test was cycled between 180 and 1,280 pounds on the plain concrete beams and between 430 and 3,030 pounds on the cast PIC beams. Failure occurred in a plain concrete beam after 315,000 cycles and in a PIC beam after 3,045,000 cycles.

After tests on the unimpregnated concrete and cast PIC beams were completed, fatigue tests were performed on the beams sawed from previously tested PIC panels. The same test procedure used on the unimpregnated concrete and cast PIC beams were used for the sawed beams. In the 50 percent test, the load was cycled between 560 and 2,810 pounds. No failure occurred in 10 million cycles. Load was cycled between 560 and 3,380 pounds in the 60 percent test. One of the beams failed after 3,555,000 cycles. For the 70 percent of ultimate load test, loading was cycled between 560 and 3,940 pounds. One of the beams failed after only 156,000 load cycles.

The modulus of rupture computed for the beams sawed from apparently undamaged portions of previously tested PIC panels was greater than that computed for the fabricated PIC beams. It was therefore anticipated that the sawed beams would perform at least as well under fatigue loading as the fabricated panels. The failure of a sawed beam under such a low number of cycles at 70 percent of ultimate load was not understood, so three more sawed beams were tested at this load. Failure this time did not occur until 2,783,000 cycles.

The inferior performance of the sawed beams compared with the fabricated beams coupled with their inconsistent performance was puzzling. An investigation was made to find a reason for the lack of, and inconsistent performance of, these beams. In examining the beam that had failed after only 156,000 cycles when loaded to 70 percent of ultimate load, it was found that the beam was not completely impregnated at the break. Also, there appeared to be two isolated pockets that were not impregnated in the sawed beam that was tested at 60 percent of ultimate. All of the other fabricated and sawed beams indicated complete impregnation had been achieved. Another possible reason for their performance may lie in the source of these beams. As stated previously, they were sawed from PIC panels which had come from apparently undamaged portions of panels which had been failed in previous tests. No damage was visible to the naked eye in any of the beams. However, the possibility exists that there were microfractures that contributed to their inferior performance.

Test results of the beam fatigue tests are tabulated in table 10. It is recognized that the data obtained in this study are too limited to provide adequate percent ultimate load versus number of cycles diagrams. However, figure 15 is a diagram of this type for the results obtained.

PRESTRESS LOSS TESTS

As previously mentioned, the panels were designed assuming an initial stress in the prestressing strands of 70 percent of their ultimate strength or 189 kip/in^2. It was known that prestress losses would occur due to elastic shortening, creep, and shrinkage of the concrete as well as relaxation of stress in the prestressing strands. These losses were assumed as 21 percent of the 189 kip/in^2 of which 2.6 percent was attributed to elastic shortening, 6 percent to prestress strand relaxation, 2.4 percent to creep, and 10 percent to shrinkage.

Tests were performed in the laboratory to verify the accuracy of these assumptions. The corresponding percentages determined in these laboratory tests were 3.0 percent for elastic shortening, 6.5 percent for prestress strand relaxation, 4.4 percent for creep, and 7.7 percent for shrinkage. The combined effect from laboratory tests was 21.6 percent. Therefore, the assumptions used in designing the panels are believed to be valid.

Further verification of the validity of the assumed prestress losses in the panel design was achieved later in the panel tests. As will be discussed later in the report, low level static loads were applied to a single PIC panel prior to conducting a fatigue test. An accidental overload developed a longitudinal tensile crack in the panel while positioning the actuator during erection of the test configuration. A plot of the stress computed from strain gage readings is shown in figure 16. As can be seen, there is a definite change in the slope of the curve for stress versus load. This change in slope is believed to have occurred when the existing tensile crack started to open. Gages 41, 42, and 43 were located on the centerline of the loaded span. The stress at which the change in load occurred was 530 lb/in^2. The calculated prestress assuming a 21 percent prestress loss is also 530 lb/in^2. This provides further verification that the assumed 21 percent prestress loss was a valid assumption in designing the panels.

As stated in the Panel Fabrication section, gage points were installed to measure length in the 16-foot-long panels and to measure concrete shrinkage in the 2-foot-long panels. The intent was to obtain measurements from the panels which would provide information to determine prestress losses due to elastic shortening of the panels at strand release and losses due to creep and shrinkage of the concrete.

Creep and shrinkage in concrete are both influenced by the relative humidity of the surrounding air.7/8/ No relative humidity measurements were made either at the plant at the time of strand release or when measurements were made later at the Denver Federal Center. Consequently, the effect of varying relative humidity on measurements could not be determined. While temperatures were read when panel measurements were made at the Denver Federal Center, none were read at the time of strand release at the plant. Again, with no base temperature other than an estimate, temperature effects on the measurements could not be accurately determined.

It was also found while making panel length measurements at the Denver Federal Center that some of the gage points were loose. It was assumed that this had happened while the panels were being handled in removal from the precasting bed and delivery to the Denver Federal Center.

Because of the foregoing reasons, any evaluation of panel measurements for the effects of concrete creep and shrinkage on prestress losses would be invalid.

Prestress Loss Due to Elastic Shortening

While panel measurements could not be used to evaluate prestress losses due to creep and shrinkage of the concrete, they were used to determine losses due to elastic shortening at prestress release. Since panel length measurements for this purpose were made just prior to and immediately after strand release, temperature and relative humidity were of no concern. Measured values of panel shortening are shown in table 11. The average shortening of all of the panels was 0.030 inch. This change in length converts to a prestress loss of 5,626 lb/in^2 using a modulus of elasticity of 27,000,000 lb/in^2 for 7-wire prestressing strand.9/ The 5,625 lb/in^2 stress loss is 3.0 percent of the 189,000 lb/in^2 stress in the strands at release. This value is quite close to the 2.6 percent loss assumed for elastic shortening in the panel design.

Investigation of High Temperature on Stress Relaxation in Prestressing Strands

As previously stated, a prestress strand fabricator estimated that the stress relaxation in the strands would be about 6 percent if stabilized strands were used, and if the drying temperature did not exceed 212° F. To verify this estimate, an investigation of temperature effects on stress relaxation in prestress strands was included in the scope of the study.

Five devices as shown in figure 17 were fabricated to test strand relaxation at various temperatures. Two high temperature strain gages were bonded diametrically opposite each other at the center of the pipe to measure strain. Prior to testing, the devices were calibrated for both load and temperature.

Tests were conducted at temperatures of 350°, 280°, 212° and 73° F. A load of 16,000 pounds, the same as the load applied to the strands in fabricating the panels, was applied to the strand in the test device with a center pull hydrualic ram. The ram load was then removed, as it is in normal prestressing operations, using strand chucks to maintain the load in the strand. It is recognized in prestressing that a very slight slippage occurs in a strand chuck when the load is transferred from a loading system to the strand chuck. Over the long length of a prestressing bed this slippage is negligible. However, in the short 5-foot length of this test a reduction of close

to 40 percent of the strain was noted. The device was modified to include wedges between the strand chuck and the end of the pipe. With the wedges in place, it was possible to close them and bring the load back up to the desired 16,000 pounds.

One test was conducted at each of the temperatures of 280° and 350° F, while two tests were made at 212° F since the panels were dried close to this temperature. Data obtained from these tests plotted as a straight line on log-log paper, figure 18. Data from these curves are shown in table 12. At 212° F a prestress loss of 6.5 percent in 2 weeks was determined. This is very close to the 6 percent estimated by the strand manufacturer. In 2 weeks the prestress loss at 350° and 280° F was about 22.6 percent and 20.5 percent, respectively. These data were confirmed by measurements to determine the length change of the pipe during the test. Measurements were made with a 10-inch gage length Whittemore gage after the strand had been stressed but before the testing device was placed in the oven. They were repeated when the test was completed and the pipe had cooled to room temperature. At all temperatures, the stress loss was within 1 percent of those shown in table 12 after 2 weeks.

Laboratory Investigation of Prestress Loss Due to Creep in Concrete

Five 6- by 12-inch cylinders to be used for creep measurements, according to ASTM C 512-9, were obtained each day of panel casting. The cylinders had three equally spaced lines of inserts, for Whittemore gage points, embedded 8 inches apart. These test specimens were taken from the casting yard to a creep testing room at the USBR. This room is maintained at a constant relative humidity of 50 percent and 73° F temperature. Three specimens from each day's casting were placed under a constant 600 lb/in^2 compressive load about the same time prestress strands were cut to load the panels. The remaining two specimens were not loaded and served as controls. The 600 lb/in^2 stress applied on the cylinders was close to that applied on the panels by the prestressing strands.

Creep measurements were taken periodically for 120 days on the loaded and unloaded cylinders. Creep due to the sustained load was the difference in strain between the loaded and control specimens. Creep from each of the loaded cylinders was plotted, and a smooth curve was drawn through the plotted points. Figure 19 is an example for one cylinder. For each day's casting, points were picked from the curve of each cylinder. The points were averaged, and a curve representing the average creep from each day's casting was drawn, figure 20.

Data from the laboratory creep measurements were examined in light of predicting prestress loss due to creep. Over the years, numerous mathematical expressions relating creep and time have been suggested. One of the most convenient is a hyperbolic expression introduced by Ross.9/ He expresses creep, c, after time, t, under load as:

$$c = \frac{t}{a+bt}$$

where a and b are constants determined from experimental results. This expression was rewritten in the form of a straight line equation:

$$\frac{t}{c} = a+bt$$

Data from the creep curves, figure 20, were plotted with $\frac{t}{c}$ as the ordinate and t, the abscissa, and found to fit extremely well. A linear regression was run on points from the straight line curve to calculate a, the intercept of the curve and the $\frac{t}{c}$ axis, and b, the slope of the straight line. The value of a was found to be 0.044 and 0.034 for the first and second casting, respectively. The slope, b, was found to be 0.00338 and 0.00308, respectively. The limit of c as t approaches infinity is 1/b. Ultimate creep strains for each day's casting were calculated from this expression to be, respectively, 296 and 325 microinch per inch. Using an average strain value of 310 microinch per inch, the ultimate prestress loss due to creep was calculated to be 4.4 percent, which is about twice as much as estimated in the panel design.

The percent of prestress loss shown above is known to be very conservative since it was based on creep tests of unimpregnated concrete. Previous research has shown that creep is not as great in PIC as it is in unimpregnated concrete. It has been stated that for design purposes, a creep of 40 percent of that expected in unimpregnated concrete would be an adequate assumption for PIC.6/

Laboratory Investigation of Prestress Loss Due to Concrete Shrinkage

Concrete must be almost completely dry before it is impregnated and polymerized. During the drying period, the concrete, in a short period of time, is dried at least to the stage a normal concrete structure would reach in its lifetime. Virtually no further shrinkage occurs after impregnation and polymerization of the concrete. Therefore, prestress losses due to concrete shrinkage predicted for unimpregnated concrete should provide a reasonable estimate of that which will occur in PIC.

Length measurements were made on the 4- by 4- by 30-inch bars immediately when they were placed in the 50 percent relative humidity room. Periodic measurements were taken thereafter for about 120 days. The changes in length of the bars were plotted in the same manner as the creep data had been plotted. The shrinkage curves had the same general shape as the creep curves, figure 21 is an example, and could be expressed in the same manner. Constants a and b were again determined for each day of casting by a linear regression. The value of a was 0.0212 and 0.025, respectively, for the 2 days, while b was 0.0019 and 0.0018, respectively. From these values the ultimate shrinkage strain was calculated from the expression $\frac{1}{b}$ to be 526 and 554 microinch per inch, respectively, for each day.

An average ultimate shrinkage value of 540 microinch per inch was used to determine a prestress loss of 7.7 percent due to shrinkage. This is less than, but reasonably close to, the 10 percent assumed in the panel design.

PANEL TESTS

The final objective of the research program was to verify the panel design by testing both single-panel and three-panel configurations with both static and fatigue loadings. A sectional view of the test configurations is shown in figure 1. The tests did not completely simulate an actual bridge performance because the girder bending and torsional flexibilities were restrained in the tests. However, the tests did produce sufficient information to verify the adequacy of the panel design.

Throughout the following discussion, mention will be made of transverse and longitudinal directions or axes. Transverse refers to an axis which in all cases is perpendicular to the girder supports or traffic flow on a complete bridge, and longitudinal is parallel to the girder supports or traffic flow.

In order to verify the design of the panel from load tests, strains and deflections were obtained with static loadings at various loading positions shown in figure 22. Static loadings to 20 kips were used for this verification which is approximately the service load condition for design, based on a 16-kip wheel load plus 30 percent impact. Loading of the panels to 20 kips was applied in increments. Strains and deflections were obtained at each incremental load. During these static tests, strains and deflections were linear with respect to load. Strains from the tested panels were converted to stresses by assuming $E = 3{,}600{,}000\ lb/in^2$ and $E = 6{,}000{,}000\ lb/in^2$ for unimpregnated concrete and PIC, respectively.

Prior to performing any single-panel tests an elastic analysis was performed on the test configuration by analytically modeling it as a two bent planar frame considering the girder supports and panel as finite straight uniform cross section members rigidly connected. Member cross sections that simulated the girder supports were increased to take into consideration average dimensions, and the three reactions of the frame were fixed against vertical and horizontal displacement but not rotation. With this analytical model, the connection between the girder supports and panel was considered as a rigid joint which would be the case if the connection is integral.

All comparisons of test results in the three-panel tests to analytical values were based on the analytical values obtained in the finite bending element analysis used in the panel design. In this analysis the connection of the panel-to-girder support was assumed to be a fixed boundary.

From the results of the static tests on both the single-panel and three-panel configurations it was determined that the panel-to-girder connection acted more as a hinged joint rather than a rigid joint or fixed boundary. Hence, the maximum tensile bending stresses occur in the bottom surface of the panel instead of in the top surface because

the maximum bending moments about the longitudinal axis are caused by a positive moment close to the midspan rather than a negative moment at the connection. This is advantageous from the standpoint of deck durability because the first tensile crack always occurs in the bottom surface of the deck.

During static load tests of all the PIC panels, the first crack developed with a load equal to or greater than the load factor design wheel load of 42 kips. All of the first cracks were caused by positive bending moment and occurred in the bottom surface. Initially in the design of the panels, there had been a concern about the transfer of tensile strain at first crack from the PIC to the prestressing strand because of the higher modulus of rupture of the PIC. However, throughout the static testing there was no evidence of prestressing strand rupture due to the higher tensile strain energy transfer at first crack.

Ultimate static load carrying capacity of the single-panel and three-panel configurations was approximately 2.2 and 3.5 times, respectively, that of the load factor design wheel load. Ultimate load for the tests was defined as the load a test configuration could sustain without any change of deflections while the load was being maintained. Ultimate failure of the PIC panel configuration always occurred by negative moment tensile cracks developing at or over the center girder support. These failures were not destructive enough to cause collapse and the test configuration remained very much intact with reduced load carrying capability. This was not the case for the unimpregnated single-panel that was tested. The failure of an end of panel-to-girder connection in that test resulted in a destructive failure mode or collapse of the test configuration. This in turn points out the benefits of the higher compressive strength of PIC.

Fatigue-type load carrying capacity of the three-panel configuration, when subjected to the load factor design wheel load and greater, was proven to be excellent. No evidence of panel-to-girder connection failure was observed during testing to over 2 million cycles of load.

Assembly of Test Configurations

The steel floor in the USBR's vibration testing laboratory was drilled and tapped with holes to position and hold the girder supports and loading frame for the panel tests. Stems of the girder supports were secured in their proper positions of 8 feet center-to-center with pieces of steel angle bolted to the floor as shown in figure 23. The 2- by 8-inch boards bolted to the edges of the girder flange served a dual purpose. They were adjustable vertically to provide leveling control for setting the panels and also acted as a form for the grout which was placed between the girder support and the panel.

After the girder supports were in position, the test panels were placed on edge resting on a wood frame built for this purpose. The

J-hooks were welded on the bottom of the panel as shown in figures 24 and 25. Strain gages were bonded to the bottom surface. Figure 26 shows a typical installation of 2-inch-long strain gages at a point where both transverse and longitudinal strains were desired.

When all bottom surface preparations of the panel had been completed the panel was placed on the girder supports, figure 27. A temporary wood frame shown in figure 28 was attached to each of the end girder supports to provide accurate alinement and positioning of the panel. Similar procedures were followed for the erection of the three-panel configurations except that prior to pulling the panels together, 3/8-inch-thick strips of neoprene were cemented to the panel edges to contain the epoxy in the transverse panel joints. Figure 29 shows the use of a center pull ram on the longitudinal post-tensioning strand to pull the south panel to the center panel. For the three-panel tests the space left between the panels in the transverse joint was filled with epoxy while approximately a 15 lb/in^2 longitudinal post-tensioning stress was maintained in the panels. After the epoxy had cured, a final longitudinal post-tensioning stress of 30 lb/in^2 was applied to the panels.

After the panel or panels were in place, and all required transverse joint preparation was completed for the three-panel tests, the spaces between panels and girder supports were ready for grouting, figure 30. A neat cement grout of high early strength cement was used to complete the panel-to-girder connections, figure 31. High early strength cement was used to assure a 5,000 lb/in^2 compressive strength within 7 days. The grout was pumped into the space through a 3/4-inch hose which was placed lengthwise in the connection. As grout filled the space the hose was pulled back so the connection would be completely filled without large air pockets.

Strain gages were connected directly to data acquisition equipment designed to perform the measurement and control function of a complete strain data recording system. The accuracy of the system was plus or minus 0.3 percent of the reading plus or minus one count. Strain readings were recorded on printed paper tape. Linear variable differential transformers (LVDTs) were used to measure deflections of the panels and horizontal movements of the girder supports. LVDTs were individually connected to exciter demodulators which served as a power supply and balancing unit. Lead wires from the exciter demodulators were run to a separate data acquisition system. Each LVDT was bench-calibrated and measurements to the nearest 0.0001-inch were obtained. Figures 32 and 33 show, respectively, a single-panel ready for testing and the data aquisition system used to record strains and deflections. Figure 34 shows a three-panel configuration ready for testing.

Load was applied to the panel tests with a 200-kip hydraulic ram which had a 4-inch total stroke, figure 35. The load was transferred from the ram to the panel through a 150-kip capacity load cell, a spherical bearing block, and a 5- by 20-inch bearing block which simulates the HS20-44 wheel load contact area used in the panel design. Load control was possible within plus or minus 50 pounds.

Unimpregnated Single-panel Static Test

This test made use of panel No. 3 and was performed so a comparison could be made between unimpregnated concrete and PIC panels. The panel had fifty-six 2-inch strain gages bonded to it, 31 on the top surface and 25 on the bottom surface. Figure 36 shows the gage locations and identificatons. Figure 37 shows the LVDT locations and identifications. Initially the panel was loaded to 8 kips with the load in position 4, figure 22, in increments of 2 kips primarily for troubleshooting. The next loading was to 26 kips, in 2-kip increments from 0 through 10 kips and 1-kip increments from 10 through 26 kips. No cracking occurred in this loading.

Bending about the longitudinal bridge axis in the panel was fairly uniform over the width of the panel based on the transverse strains recorded at a 20-kip load, table 13. The midspan section of the panel had gage numbers 7 and 9 on the top and gage numbers 38, 39, and 40 on the bottom surface. Absolute values of strains on the top are less than those on the bottom surface at the midspan section which is probably due to the load being centered over this section. Absolute strains at adjacent sections to the midspan section have top and bottom values much closer to being equal. The panel did have some slight dishing action which is evident from the longitudinal bottom strains shown in table 14.

From the planar frame analysis of the test a moment and axial compression force at the midspan section with a load of 20 kips was determined to be 12.56 ft-kips and 10.37 kips, respectively. Taking the average of the top and bottom strains, assuming it as uniform across the 4-foot panel width, and assuming an E= 3,600,000 lb/in^2, a moment and axial compression force at the midspan section at 20-kip load was calculated to be 13.18 ft-kips and 8.93 kips, respectively. This shows fairly good correlation between analytical and test results for the midspan section. However, when this was done for other sections in the loaded span the axial force was found to be either a small compression or a small tension force. Also, two free-body diagrams were taken for the sections of panel adjacent to the midspan section. Based on moments calculated from average strains, shears at the midspan section were determined. The shears at the midspan did not equate to zero, instead there was a shear unbalance of 2.49 kips. Several other free-body diagrams were taken for other parts of the panel test configuration and the sum of forces did not balance. Hence, it was concluded that it would be quite difficult to take strain gage readings and obtain moments, axial forces, and shears to check an analytical analysis.

A plot of analytical moments and moments based on tensile strains was made, figure 38. The moments based on tensile strain were computed assuming the average strain to be uniform across the panel width, an E = 3,600,000 lb/in^2, and only the section properties of the panel. The comparison of moments in the loaded span is believed to be acceptable. However, the comparison over the middle girder support is not

as good. Moments based on strain readings over the middle girder were also computed using the section properties of the panel plus the girder flange. This yielded moments over 45 ft-kips which exceeds the analytical moments. Since the first crack in the test occurred at approximately midspan, it is believed that the panel does not act integral with the girder section as assumed in the analysis. Also, it does not act completely independent of the girder section because a negative moment tensile crack over the center girder did develop during the failure test.

A plot of analytical and measured panel displacements with 20 kips of load in position 4 is shown in figure 39. One reason the measured displacements are greater than the analytical is because the analysis assumed zero vertical displacements at the bottom of the girder supports. However, in this test the end support on the unloaded span was not tied down and lifted off the floor as shown in figure 40. This caused some cracking in the stem of the center girder support, figure 41, because of the larger amount of rotation at the center girder support. Also, some horizontal movement of the girder supports was observed.

The next loading of the panel was to failure. A preload of 20 kips was applied but a power surge caused a load surge. When the load was taken off and then applied again the strain and deflection values did not compare with those previously obtained. The panel was closely examined and found to have a transverse crack on the panel centerline and a longitudinal crack near the midspan, both of which were on the bottom of the panel.

Ultimate load for the unimpregnated single panel was 78 kips. The failure of the panel was quite abrupt and produced extensive damage as shown in figure 42. The abrupt failure of the panel was believed to have been triggered by the failure of one of the studs embedded in the panel to hold the connection plate to which the J-hooks were welded for the end panel connection. Figure 43 shows how the corner of the panel lifted up from the end girder support leaving the steel plate on the girder support.

PIC Single-panel Static Tests

Static loading tests were performed on panels No. 8 and 2. Panel No. 2 was also used for the PIC single-panel fatigue test which is described later. The strain gage locations and identifications for panels No. 8 and 2 are shown in figures 36 and 44, respectively. The LVDT locations and identifications for both panels are shown in figure 37. For these tests the end girder support in the unloaded span was restrained against uplift by welding the steel channel on the bottom of the girder support to the steel positioning angles. Load positions 4, 8, and 12 as shown in figure 22 were used with loads to 20 kips for panel No. 8. Only load position 4 was used on panel No. 2 because during erection it accidently received a static load greater

than 50 kips which produced a longitudinal bottom surface tensile crack at midspan in the loaded span. During the initial loadings on panel No. 8, to 20 kips in 4-kip increments, no cracking occurred.

Bending about the longitudinal bridge axis in panel No. 8 was fairly uniform over the width of the panel based on transverse strains recorded at the 20-kip load for load positions 4, 8, and 12, tables 15, 16, and 17. In table 15, transverse strains are given for two runs. Run 1 was obtained during the initial loading to 20 kips and run 2 was obtained during the failure load test. Since the two sets of strains compare closely, it is believed that neither the panel or girder connections were affected by the 20-kip loads in positions 8 and 12.

In the areas of high moment, which coincide with the load positions, the absolute values of strains on the top of the panel are greater than those on the bottom surface. This is opposite to what occurred on the static test of the unimpregnated single panel. This is probably due to the higher modulus of elasticity of PIC as compared to unimpregnated concrete. Also, the dishing action of the PIC panels was less than that of the unimpregnated panel which can be seen by comparing the longitudinal strains recorded at a 20-kip load in position 4, shown in table 18, to those of the unimpregnated panel, shown in table 14.

Plots of analytical moments and moments based on measured tensile strains for the load positions 4, 8, and 12 are shown in figures 45, 46, and 47, respectively. The moments based on measured tensile strains were computed assuming the average strain to be uniform across the panel width, $E = 6{,}000{,}000\ lb/in^2$, and only the section properties of the panel. The maximum positive moments, both analytical and computed, compare very closely. However, again the negative moments over the center girder support do not compare as well.

Figure 45 also shows the moments based on tensile strain readings at a 20-kip load for panel No. 2. A comparison of strains at common lines between panels No. 2 and 8 are shown in table 19. Since panel No. 2 had a tensile crack in the longitudinal direction between gage 41 and the midspan section gages 42, 43, and 44, the computed moment diagram is not very smooth at midspan. The difference between the two moment diagrams obtained using measured tensile strain is because of the tensile crack in panel No. 2. It is worthwhile to note the high tensile strains that occurred on either side of the tensile crack, indicates excellent bond between the prestress strand and the PIC.

Strain gages were placed on the bottom of panel No. 2 over the end and center girder support, refer to figure 44 for the locations of gages 36, 53, and 54. Based on the moment diagram obtained from measured tensile strains shown for panel No. 2 in figure 45, the end support does act as a hinge support for the panel. The bottom panel gages over the center girder support, which are gages 53 and 54 shown in table 19, have absolute strain values almost equal to their corresponding top panel gages. This indicates the panel acted somewhat

separate of the girder support flange instead of integrally as assumed in the analysis.

Plots of analytical and measured panel displacements with 20 kips of load at positions 4, 8, and 12 for panel No. 8 are shown in figures 48, 49, and 50, respectively, and with 20 kips of load at position 4 for panel No. 2 is shown in figure 51. In all four figures it can be seen that the measured displacements are greater than the analytical displacements in the loaded span. The analytical model assumed the panel to be integral with the girder support, but the analysis of the strain readings indicates this condition did not exist. A closer correlation between analytical and measured displacements results if the panel analysis assumes hinged supports between the panel and girder supports. A comparison of maximum measured displacement with 20 kips of load at position 4 can be made for the unimpregnated and PIC single-panel No. 8 by looking at figures 39 and 48, respectively. The unimpregnated panel's maximum measured displacement at 20 kips was 0.031 inch while the PIC panel displacement was 0.023 inch. The maximum measured displacement from panel No. 2, which was cracked, was 0.033 inch which indicates the change in the panel because of the tensile crack.

The failure test was performed on panel No. 8 with the load applied in position 4. The ultimate load on the panel was 95 kips. Figure 52 shows the crack pattern that developed in the panel during the failure test. Both cracks No. 1 and 2 were positive moment cracks and occurred at loads of 56 and 85 kips, respectively. Figure 53 shows how the cracks extended to about two-thirds of the panel thickness at ultimate failure load. Crack No. 3 occurred at 93 kips and the final crack No. 4 occurred at 95 kips. A sharp noise was heard when each crack occurred, but in no case was there evidence of prestress strand failure. The transfer of tensile strain from the PIC to the strand was without rupture of the strand. Figure 54 shows the panel over the center girder support and the intersection of cracks No. 3 and 4. The extent of the damage to panel No. 8 was the tensile cracks and a slight rotation of the end of the panel in the load span with respect to the end girder support. This was much less than that experienced in the test of the unimpregnated single panel.

PIC Three-panel Static Tests

Static loading tests were performed on two three-panel configurations. Panels No. 4, 5, and 10 were used for the first test. Panels No. 7, 1, and 11 were used for the second test and also for the PIC three-panel fatigue test which is described later. Strain gage locations and identifications for the two tests are shown in figures 55 and 56. The LVDT locations and identifications for the two tests are shown in figure 57. For these tests the end girder support in the unloaded span was restrained against uplift by welding the steel channel on the bottom of the girder support to the steel positioning angles. Load positions 1, 2, 3, and 4, as shown in figure 22, were

used with loads to 20 kips. During these initial loadings to 20 kips on the two three-panel configurations no cracking occurred.

Bending about the longitudinal bridge axis in the middle panel in the three-panel tests was not as uniform as in the single-panel tests because the three panels acted as a continuous plate. This can be seen by looking at the tranverse strains recorded along the midspan section for load positions 1, 2, 3, and 4 from the two tests; tables 20, 21, 22, and 23; respectively. In table 23, gages No. 60 and 41 are the transverse gages on the bottom of the center panel for the first and second three-panel tests, respectively. It appears that the strain value of 58 microinches per inch for gage No. 60 in table 23 is low because when the load is moved to position 3 the value of strain was higher. If the value of strain from gages No. 60 and 41 are averaged then an average strain of 90 microinches per inch is obtained. Converting this strain to a moment, assuming E = 6,000,000 lb/in^2 and uniform strain over 1 foot of panel width, a moment of 3.24 ft-kip/ft is obtained, while a comparable moment from the PIC single-panel test is 3.86 ft-kip/ft, and a moment from the finite bending element analysis is 3.26 ft-kip/ft. Based on this comparison it can be concluded that the three-panel action is working to reduce the midspan moment about the longitudinal axis. Hence, if the design of the bridge deck is based on a single-panel design, it will definitely be a conservative design. Also, by looking at tables 20 through 23 it can be seen how the maximum transverse strain along the midspan section changes as the load moves from position 1 to 4.

A maximum tensile strain observed was 121 microinches per inch from the second three-panel test with 20 kips in load position 4. Converting this strain to a moment yields a moment of 4.36 ft-kip/ft and the panels were designed for a service load condition moment of 5.36 ft-kip/ft from the elastic analysis.

Figures 58 through 61 show plots of top and bottom transverse stresses along the centerline of the center panel for load in positions 1 and 4 measured on the first and second three-panel tests and the theoretical stress as determined from the finite bending element analysis. The theoretical stresses are not plotted as a smooth curve because the points of stress were determined at the center of the finite bending elements. Close comparison between theoretical and measured transverse stresses can be made at the midspan section. However, the theoretical stresses at the center girder support are much higher than the measured stresses because the finite bending element analysis assumed a fixed support at the center girder support. The connection of the panel to the center girder support was closer to a hinge support than a fixed or integral connection.

The maximum longitudinal tensile stress was measured on the bottom surface directly under the load with a load of 20 kips in position 4. Figures 62 through 65 show plots of top and bottom longitudinal stresses measured on the first and second three-panel tests and the theoretical

stresses as determined from the finite bending element analysis for a 20-kip load in positions 1 and 4. The theoretical stresses are not plotted as a smooth curve because the points of stress were determined at the center of the finite bending elements. The longitudinal stress in the panel does decrease as the load moves toward the transverse joint between panels. The difference between the stress plots of load positions 1 and 4 shows that the transverse panel joint does not carry as much moment as would occur had the three panels been a continuous plate. However, in figure 62 the measured top longitudinal stresses on either side of the joint between the center and north panels indicates some moment carrying capacity because they are greater than the theoretical stresses.

The measured displacements along the midspan section from the first and second three-panel tests with a 20-kip load at load positions 1, 2, 3, and 4, figure 22, are shown in tables 24 and 25, respectively. It can be seen from these tables how the displacement is the largest at points either under or near the point of load. Also maximum displacements from both tests occurred when the load was not on the centerline of the center panel or in load position 4. However, for a comparison purpose the displacement due to 20 kips in position 4 in the three-panel tests was compared to 20 kips in position 4 in the PIC single-panel test. It was found that the three-panel test displacement was 62 percent of the displacement of the PIC single-panel test. It can be concluded that the adjacent panels in the three-panel test probably carried 38 percent of the 20-kip load when the load was in position 4.

The failure test for the first three-panel test which used panels No. 4, 5, and 10, was performed with the load applied in position 3. Ultimate load on the panels was 160 kips. Figure 66 shows the crack pattern that developed in the panels during the failure test. The development of the crack pattern on the bottom surface was difficult to trace because constant observations could not be performed. Crack No. 1 is believed to have occurred at a load of 70 kips and crack No. 2 in just the center panel occurred at 84 kips. This can be seen from the plot of load versus deflection of the actuator LVDT shown in figure 67. The top surface crack in the center panel first occurred at approximately 100 kips and as loading continued it developed the circular pattern around the load block as shown in figure 66. Also, crack No. 2 continued to develop across the north panel as load was applied above 100 kips. Small shear cracks developed at the transverse joints at the ends of the panels in the loaded span between the south and center panels, and center and north panels as shown in figures 68 and 69, respectively. These cracks were observed at a load of approximately 140 kips. After the 160 kips was removed, load was reapplied but only 120 kips could be sustained by the three-panel system the second time. It is worthwhile to note how well the crack pattern shown in figure 66 conforms to the yield-line theory for slabs.12/ Also, the load carry capabilities of the adjacent panels are very evident.

During the static preloading to 42 kips in position 4 of the second three-panel test prior to running the fatigue test, a bottom surface transverse crack developed in the center panel. This crack ran parallel to the 20-inch dimension of the load block and was almost on the centerline of the panel. Figure 70 shows a plot of the transverse and longitudinal stresses computed using data obtained from strain gages 41 and 44, and assuming E = 6,000,000 lb/in^2, refer to figure 56 for gage locations and identifications. Both gages were directly under the center of the load block. The crack broke the longitudinal gage 44 and affected the transverse strain. The stress at cracking in the longitudinal direction was approximately 1,000 lb/in^2. From the panel design for moment about the transverse axis with load in position 4 and a load factor design, a stress of 1,028 lb/in^2 was determined. Hence, it can be concluded that the ultimate tensile stress of 1,300 lb/in^2 that was used in design might be a little high in this instance. However, at other locations where gages remained during static testing, stress readings as high as 2,100 lb/in^2 were obtained from the two three-panel tests. Also, the crack might have originated at a point outside of the gage and the stress value would have been higher than that recorded at the gage. The maximum that the transverse gage 41 recorded was computed as 1,332 lb/in^2 before it was affected by the crack.

Another important fact about loading to the load factor design wheel load is that the size of load block should be increased. Theoretically the size of the block should be increased as the load is increased over the service load value of 20.8 kips. However, from the standpoint of testing, this would be very difficult to accomplish. Hence, when any load over the 20.8-kip service load was applied, the test configurations were under a more severe test than would occur in an actual bridge.

PIC Single-panel Fatigue Test

The fatigue test of a single-panel was performed on panel No. 2. However, prior to performing this test the panel had received an accidental overload due to equipment malfunction and a longitudinal positive moment tensile crack was present in the panel. The crack was 2 inches from the midspan section and ran nearly parallel to the section.

Even with the positive moment crack, it was believed beneficial to perform a fatigue test on the panel because this might actually occur in a panel due to overload. Therefore, the test of the panel for load cycled between 5 and 42 kips in load position 4, figure 22, at a rate of 3 Hz was more a proof load test. A 42-kip load is the load factor design wheel load using the 2.0 load factor as determined in the panel design.

During the first 140,000 cycles of load no significant changes in either strains or deflections occurred. From 140,000 to 250,000 cycles, deflections steadily increased. At 250,000 cycles the panel began emitting intermittent noises that indicated either new cracks were

developing in the panel or that the prestress strands were starting to break. The latter was true because no new cracks in the panel were evident from inspection. At about 270,000 cycles the noise stopped but the deflections continued to increase in a steady manner. After 280,000 cycles the noise of cracking started again, and at 300,000 cycles the panel would no longer hold the 42-kip maximum load. Hence, failure was determined at 300,000 cycles.

After the test was dismantled the bottom of the panel was investigated at the initial positive moment tensile crack which was the only crack in the panel. The concrete was chipped away from the bottom prestress strands and all bottom strands were failed at the point of crack as shown in figure 71. There was no evidence of any bond failure between the strand and the panel adjacent to the crack and all strands failed right at the crack. Even with all of the bottom strands failed, the panel was carrying load and the high compressive strength of the PIC precluded any compressive failure in the panel.

PIC Three-panel Fatigue Test

The fatigue test of a three-panel configuration was performed using panels No. 7, 1, and 11. Prior to performing the fatigue test, static testing was performed on the three panels with loads to 20 kips in positions 1, 2, 3, and 4, figure 22. Based on these loadings, load position 4 was selected as the point of load application for the fatigue loading.

Initially the fatigue test program was to be performed by applying 42 kips of load, the load factor design wheel load using the 2.0 load factor as determined in the panel design, for one million cycles. This was to be followed by increasing the load to 62 kips, a 3.0 load factor and cycling for 1 million cycles or until failure, and so on with a 4.0 and 5.0 load factor if necessary.

The first loading applied in position 4 to the three panels was cycled between 10 and 40 kips at a rate of 3 Hz. Prior to cycling, a static load of 42 kips was applied which produced a transverse bottom tensile crack under the load block. Since the crack was in the transverse direction, parallel to the prestressing strand, it was assumed not to significantly effect the performance of the panels. During 636,000 cycles of load no change in deflections or growth of the transverse crack from the beginning of the test was observed. Hence, the test was stopped short of the intended 1 million cycles.

The second static preload of 64 kips was applied at load position 4 before cycling between 20 and 60 kips at 4 Hz. Some growth of the transverse crack occurred during the static preload. During 1 million cycles of load only very slight change in deflections and growth of transverse crack from the beginning of the test were observed.

The third static preload of 84 kips was applied at load position 4 before cycling between 40 and 80 kips at 4 Hz. There was no indication of any other cracking during the preload. At the beginning of the cyclic test, small changes in deflections occurred and longitudinal cracks developed. After 150,000 cycles under this loading, deflections remained constant and cracks did not grow. The test was stopped after 336,000 cycles.

For the final fatigue test of the panels it was decided to cycle the load between 10 and 100 kips at 4 Hz. A static preload of 104 kips was applied at load position 4. During the preload, cracks in the longitudinal direction were extended but the panels held the 104-kip static load without any increase in deflection. From the beginning of the cyclic testing deflections increased, and at about 50,000 cycles a negative moment tensile crack occurred and the working of the transverse panel joints were observed. Cycling continued until 190,000 cycles of load had been applied.

In summary the three-panel test was subjected to over 2.1 million cycles of load, at or above the load factor design wheel load of 42 kips, without failure. Figure 72 shows the load versus deflections before and after the various cyclic tests. This deflection was measured with LVDT No. 3, refer to figure 57. At 20 kips after all the cyclic testing the deflection at LVDT No. 3 was 0.0241 inch, while before the cyclic loading it was 0.0145 inch. Even though the three-panel test was more flexible after all the cycles of load, it is believed it could have carried the load factor design wheel load of 42 kips safely for many more thousand cycles.

The ultimate load of the three-panels was obtained by statically loading the panels in position 4 and found to be 152 kips, which is just slightly less than was found for the first three-panel test. Figure 73 shows the final cracking pattern of the three panels. The north and south panels were not affected when the ultimate load of 152 kips was on the center panel. Since the north and south panels were uncracked each was loaded statically at the midspan section on the centerline of the panel.

The ultimate load held by the south panel was 100 kips and figure 73 shows the final crack pattern. First crack occurred at a load of 70 kips and was a longitudinal crack. At 85 kips the transverse crack occurred in the bottom of the panel. The negative moment tensile crack on the top of the panel occurred at 100 kips.

The ultimate load held by the north panel was 100 kips. Again, figure 73 shows the final crack pattern. First cracking consisted of two longitudinal cracks from the load block to the free edge of the panel and occurred at a load of 65 kips. At 80 kips the transverse cracks developed. The negative moment tensile crack on the top of the panel occurred at 100 kips. Again, it is worthwhile to note how well

the crack pattern shown in figure 73 does conform to the yield-line theory for slabs.

Panel-to-girder Connection Shear Tests

The midpanel panel-to-girder connection was tested by applying a load to the edge of the panel as shown in figure 74. Three shear tests were performed so as to provide a horizontal shear mechanism similar to that necessary to develop composite action. The portions of the panel connected to the center girder support from the three single-panel tests were used for these tests. Tests No. 1, 2, and 3 were from the unimpregnated single-panel, PIC single-panel fatigue, and PIC single-panel static tests, respectively.

Prior to performing the shear tests, computations were made to ascertain what amount of horizontal shear stress would be required in the connection. Based on the load factor design wheel load of 41,600 pounds as the maximum shear that the girder-panel section would have to carry and an 8-foot effective width of panel or deck acting with the girder, a horizontal shear stress of 24 lb/in^2 was determined at the bottom of the panel. The effective shear area between the panel and girder was 28 by 48 inches which yields a required shear force on the edge of the panel of 32 kips.

Figure 75 shows the shear load versus panel movement for the three tests. The tests indicate that there was essentially zero bond strength available between the panel and the grout. However, shear transfer by dowel action of the J-hooks was available and provided load carrying capacity, similar to that of concrete slabs working compositely with studded steel girders. Bond was available from the grout to the top of the girder support indicating that the projected web steel from the girder to the grout can be designed as normal cast-in-place decks on concrete girders. Consequently, the full loading system is predictable and composite action can be assured by standard design procedures.

NONDESTRUCTIVE TEST EVALUATIONS

A variety of nondestructive test methods were studied for use on PIC to evaluate their potential for monitoring quality control. These included ultrasonic pulse velocity, ultrasonic radiography, gamma ray and neutron transmission, infrared radiography, microwave transmission, dielectric and electrical resistivity, and impact hammer. Absorption, permeability, specific gravity, and length change measurements might also be included. Although there is sufficient theoretical basis for each of the various methods, the heterogeneous nature of concrete makes the practical applications of any one or a combination of methods extremely difficult. These methods work best with a homogeneous material in which a flaw, defect, or change in composition or uniformity can be readily detected. The use of a nondestructive test method requires extensive calibration and standardization for a particular concrete unit. Even with careful concrete control practices, the variations between batches of the same mix present difficulties. The more practical approach appears to be in good process control to insure uniformity of treatment and testing of selected specimens to verify product quality.

Ultrasonic Pulse Velocity

Ultrasonic pulse velocity has been extensively investigated for use with conventional concrete. Commercial instruments are readily available. The velocity measurements are very sensitive to changes in density, fractures, moisture content, and to the amount of polymer in PIC. Since the velocity is sensitive to each of these parameters the interpretation is difficult.

A series of tests were made on 3- by 6-inch cylinders to observe the effects of moisture content and polymer loading on pulse velocity.

The results are shown in figure 76. The data show that pulse velocity increases with increased moisture and with increased polymer loading. The changes in pulse velocity look fairly uniform with the exception of the value of 14,600 ft/sec for concrete containing 0.7 percent moisture.

Ultrasonic pulse velocity measurements were made on panels No. 9 and 10 before and after drying and after polymerization. Panel No. 10 had lower pulse velocities at the undried, dried, and polymerized conditions than panel No. 9 or the 3- by 6-inch control cylinders, figure 77. According to the weight recorded for the panels, there does not appear to be a significant difference in density. While it is possible that the lower velocities for panel No. 10 in the undried and dried condition are perhaps due to a lower moisture content, panel No. 10 in the polymerized condition had a higher polymer loading than panel No. 9. No satisfactory explanation can be made for the lower pulse velocities in panel No. 10. The pulse velocities for panel No. 9 correspond closer with the 3- by 6-inch control cylinders,

especially in the dried and polymerized conditions. However, the close correlation may be somewhat fortuitous as panel No. 9 is prestressed and was made from a richer and denser concrete mix than the 3- by 6-inch control cylinders.

The suitability of the ultrasonic pulse velocity method remains an open question. A more comprehensive effort would be required to determine if the variations between different specimens can be accounted for and if reliable measurements can be consistently achieved.

Microwave Transmission

The National Bureau of Standards (NBS), Boulder, Colorado, has an electromagnetic nondestructive test method under development. The apparatus is a microwave transmitter and receiver with a data display. In the normal procedure, microwaves are transmitted through a medium and reflected back by interfaces or changes within the medium in a manner somewhat similar to the seismic reflection method used in geophysical exploration. The test can also be conducted by transmission through the specimen. The system is sensitive to abrupt changes in dielectric characteristics, and under appropriate conditions, can be used to detect layering, voids and cracks, areas of high moisture content, thickness of surface and subsurface layers, texture of surface layer, moisture content, packing density of subsurface layers, thickness of surface and subsurface layers, and buried objects.

The instrument operates over a range of frequencies from 0.1 to 10 GHz and sweeps continuous wave band widths of from 4,000 to 8,000 MHz. The penetration of the material is dependent upon dielectric properties and decreases as the frequency increases. In the normal mode of operation, the analysis of data are based upon wave attenuation.

Samples of PIC and water-saturated, air-dry (50 percent relative humidity), and oven-dried concrete were tested. Results are shown in figure 78. The test is very sensitive to moisture and shows a small but detectable difference between oven-dried and PIC. It should be noted that both the ultrasonic pulse velocity and the microwaves show good sensitivity to the presence of moisture; but the ultrasonic method shows roughly the same effect for the presence of polymer as for the presence of moisture and the microwave method shows only a minor effect from the presence of polymer.

The microwave technique is theoretically sound, the electronic components of the apparatus are commercially available, and the basic developmental work has already been done by NBS. However, there would be significant costs in developing the technique for concrete applications. These expenses would be for assembling portable and compact equipment, and for performing the necessary standardization and calibration work.

Neutron and Gamma Ray

Neutron and gamma ray measurements were made with a commercial nuclear moisture and density determination apparatus. Moisture determination is made from gamma ray measurements. The instrument was operated in a back reflection mode on a 3-foot by 3-foot by 4-inch-thick concrete slab at two locations on the slab. Measurements were made with the concrete in air-dried and oven-dried conditions, and after surface impregnation and polymerization. The polymer was located at the top surface of the slab, extending into the slab to a depth of approximately 1 inch. These measurements are considered very rough and should be considered as only indicative of what the test method is capable of doing rather than as a precise experiment. The main problems encountered in performing the experiment were:

1. The transmitter and receiver were placed directly on the concrete surface. The concrete surface is relatively rough which quite likely produced some loss of radiation from scattering and a small but undetermined error in readings. This loss could possibly be minimized by supporting the transmitter and receiver a fixed distance from the concrete surface or by changing the mode of operation to direct transmission through the specimen.

2. Sometime after the experiment, a defect in an electronic component of the instrument was detected. This likely introduced error in the measurements.

Results are shown in table 26. The neutron moisture determinations and the gamma ray density determinations show some relationship to the actual condition of the concrete. The calculated values for density and moisture or polymer content are lower than the actual values and probably represent errors in measurement and calibration. The indicated moisture content from neutron measurements for oven-dried concrete is attributed to water of hydration in the portland cement which is not free water.

Other Nondestructive Tests

Ultrasonic resonant frequency. - This is a standard procedure (ASTM Designation C 215-60) for evaluation of the freeze-thaw test and is used to determine dynamic modulus of elasticity. Results are customarily expressed as the square of the resonant frequency or converted to dynamic modulus of elasticity. Polymer impregnation produces a 30 to 60 percent increase in resonant frequency squared. This method is considered more applicable for durability tests than for determination of product quality or correlation with structural properties.

Acoustic impact. - This is a relatively new test. So far as is known, only one company manufacturers a specific device for this type of test. The test was originally developed for detecting fractures in rivets and fasteners. The test consists of mechanically striking the test specimen and measuring the time for the shock wave to dampen to a

predetermined value. This test procedure showed excellent correlation with measurements conducted according to ASTM Designation C 215-60. It was observed that the presence of moisture had no effect on resonant frequency, and that polymer impregnation increased the square of resonant frequency by about 40 percent.

Neutron radiography. - Neutron radiography is similar to neutron moisture methods, based upon the selective attenuation of thermal neutrons by hydrogen, except a picture is the end product instead of a dial reading. Neutron radiographs of PIC are difficult to interpret due to overlapping and extensive shadows of the aggregate particles. The method is potentially useful for observing very large variations in polymer loading within a sample; however, the equipment is expensive and further application of this method is not anticipated.

Infrared radiography. - A device is on the market which produces an image derived from the infrared radiation emitted by an object. The apparatus is fairly sensitive and can detect variations of about 1° C in surface temperature. A brief test with this apparatus indicated that under ideal conditions polymer-impregnated zones in a concrete specimen could be distinguished from unimpregnated zones; however, unequal heating or cooling of the specimen can easily mask the effects of the polymer.

Acoustic emission. - A method in which a transducer "hears" subaudible noise emitted when a material is stressed. The rate and amplitude of the stress waves may be analyzed to determine if a structure is nearing failure. Grids of transducers are used to locate flaws. This method requires extensive experience and calibration with a particular material before it can be used as an analytical tool.

Electrical resistivity and dielectric constant. - Laboratory equipment was assembled to investigate electrical resistivity and dielectric constant measurements as nondestructive test methods for PIC. Although PIC generally has a much lower dielectric constant and greater electrical resistivity than unimpregnated concrete, the dielectric constant and electrical resistivity could not be related with polymer loading in test specimens. A test of nine fully impregnated concrete specimens with polymer loadings of 6.7 to 8.0 weight percent had dielectric constants ranging from 6.56 to 7.23 and resistivities ranging from 46.9 to 69.0 million ohm meters. A set of partially impregnated concrete specimens with polymer loadings of 3.9 to 5.2 weight percent had dielectric constants from 6.87 to 7.18 and resistivities of 50.1 to 56.9 million ohm meters which are within the range of values observed for the fully impregnated concrete specimens.

Impact hammer. - The impact hammer is a commercially available device designed primarily for field testing of concrete. The instrument measures hardness by impacting a steel rod against the test surface and observing the rebound. The rebound number is considered indicative of quality; the higher the rebound number, the higher the quality. The

instrument has been used to obtain information on the extent of curing in concrete and to delineate unsound from sound zones in concrete structures. Attempts have been made to correlate rebound number with strength but have not been successful except possibly under carefully controlled experiments with a known concrete mix. The impact hammer tests the surface of the concrete to a depth of about 1 to 2 inches and is not sensitive to the condition of the concrete in the interior of the specimen. Rebound readings are influenced by surface conditions, orientation of the hammer, effects of coarse aggregate particles immediately below the hammer, size of the specimen, and the restraint placed on the specimen to hold it in place, all of which are not related to quality or strength of the concrete. Impact hammer tests generally show PIC to give a rebound number about 20 to 65 percent greater than unimpregnated concrete.

Summation. - Although a number of nondestructive tests appear to have potential for quality control in the manufacture of PIC, considerable development work would be required. This was beyond the financial capabilities of this program, and none have been pursued further. Good process control and treatment of companion specimens for destructive tests appear to be the most practical techniques at this time.

CONCLUSIONS

The inherent structural and durability properties of PIC make it an excellent bridge deck material. Many innovations for fabricating processing, and erecting PIC bridge decks systems are anticipated when an actual application is undertaken. It is believed that adequate information is documented within this report to benefit the implementation of this system. Based on this research program the use of PIC can be considered a viable bridge deck material. Conclusions drawn from this study are as follows:

1. Assumed design strength and elastic properties of PIC, using methyl methacrylate as the monomer system, were proven adequate and can be used with confidence.

2. The prestressed PIC panel system can be accurately analyzed by presently developed elastic analysis procedures for flat plates.

3. Initial design concern that the prestressing strand might rupture at development of tension cracks because of the high tensile strain energy transfer from the PIC to the prestressing strand was dispelled. Results of this study show that ultimate failure of PIC panels is not abrupt or destructive in nature and warning of impending failure can be recognized prior to collapse.

4. Stabilized prestressing strand rather than stress relieved prestressing strand, should be used for PIC panels to reduce prestress losses due to strand relaxation caused by the elevated drying temperature.

5. Even though the panels are subjected to elevated temperatures, prestress losses can be accurately predicted when all factors are considered.

6. Transverse joints between panels provided effective shear transfer and some moment capacity.

7. Adequate horizontal shear transfer for composite action of panel-to-girders was available through dowel action of the J-hooks.

8. The connection between the panel and the center girder support is actually somewhere between a pinned joint and integral joint condition. Longitudinal panel bending moment was transferred from the panel to the center girder support but the transfer was not as great as determined by the elastic analyses which assumed an integral joint.

9. The PIC panel system has excellent capability to sustain the load factor design wheel load of 42 kips during cyclic loading conditions for more than a million cycles of loading.

10. The fatigue testing of nonprestressed unimpregnated concrete and PIC beams was too limited to be classified as a complete fatigue study. However, available test results indicate that fatigue failure will occur at less than 10 million cycles if the flexure stress is greater than 50 percent of ultimate in unimpregnated concrete and greater than 60 percent in PIC.

11. Quality control of impregnation by weight is for the most part reliable. However, complete assurance of impregnation and polymerization cannot be obtained with this method.

12. Some nondestructive test methods are theoretically sound and with further development may provide means for quality control of impregnation and polymerization. However, investigations of various methods did not indicate any to be as reliable as weight measurements.

RECOMMENDATIONS

It is strongly recommended that FHWA implement the results of this research by sponsoring with state highway departments the design and construction of one or more experimental bridges using prestressed PIC panels for the decks. The designs should use panels of sufficient length to span the full width of the bridges, and panel widths greater than 4 feet should be considered to reduce the number of transverse joints in the finished decks.

The bridges for implementation of prestressed PIC panels do not have to be restricted to only straight, flat bridges as considered in this study. The panel shape can be varied from rectangular to skewed parallelogram or trapezoidal to form skew bridges or bridges on horizontal curves, respectively. A panel system need not be limited to concrete girders. However, since this study was based on usage of prestressed concrete girders, such girders should be used for the initial field evaluation of this concept of bridge decking.

It is also recommended that future research and development studies be directed at making more use of the high compressive strength of PIC, which was not done in this study. This would include the use of post-tensioning as well as pretensioning for both the deck panels and girders. Segmental girders of PIC also should be considered. Segmental girders, as long as the panels, could be treated in the same impregnation chamber. Pretensioning might still be necessary in panels with the post-tensioning system because of handling stresses prior to treatment and erection stresses. These design studies should be directed at actual applications rather than general studies so the benefits of PIC can be evaluated as compared to steel girders or concrete girders with a conventional concrete deck.

Bridges located where conventional concrete deterioration is severe, either because of constant exposure to salt water conditions or because of severe freeze-thaw conditions, could warrant the extra initial costs that are associated with this type of construction. In the long term, the unit cost per year of service should be considerably reduced because of the improved durability of PIC.

Some other problems associated with bridges such as pilings, piers, pier caps, expansion joints, curbs, railings, etc., might be solved with PIC. Each problem should be isolated as much as possible and serious study performed to solve it. These studies are strongly recommended to make full use of PIC in the total structure.

REFERENCES

1. Steinberg, M., Dikeou, J. T., Kukacka, L. E., Backstrom, J. E., Colombo, P., Rubenstein, S., Kelsch, J. J., and Manowitz, B., "Concrete-Polymer Materials, First Topical Report," BNL 50134 (T-590) and USBR General Report No. 41, Dec. 1968

2. Steinberg, M., Dikeou, J. T., Kukacka, L. E., Backstrom, J. E., Colombo, P., Hickey, K. B., Auskern, A., Rubenstein, S., Manowitz, B., and Jones, C. W., "Concrete-Polymer Materials, Third Topical Report," BNL 50218 (T-560) and USBR REC-OCE-70-1, Dec. 1969

3. Dikeou, J. T., Steinberg, M., Cowan, W. C., Kukacka, L. E., DePuy, G. W., Auskern, A., Smoak, W. G., Colombo, P., Wallace, G. B., Hendrie, J. M., and Manowitz, B., "Concrete-Polymer Materials, Third Topical Report," USBR REC-ERC-71-6 and BNL 50275 (T-602), Jan. 1971

4. Dikeou, J. T., Steinberg, M., Cowan, W. C., Kukacka, Colombo, P., Wallace, G. B., Hendrie, J. M., and Manowitz, B., "Concrete-Polymer Materials, Fourth Topical Report," USBR REC-ERC-72-10 and BNL 50328, Jan. 1972

5. Steinberg, M., Cowan, W. C., Kukacka, L. E., DePuy, G. W., Auskern, A., Columbo, P., Romano, A., Causey, F. E., Lockman, W. T., and Smoak, W. G., "Concrete-Polymer Materials, Fifth Topical Report," USBR REC-ERC-73-12 and BNL 50390, Dec. 1972

6. Cowan, W. C., "Structural Properties of Concrete Polymer Materials Summary Report," USBR GR-2-75, June 1975

7. Neville, A. M., "Properties of Concrete," Textbook, 1963, pp 286-325

8. L'Hermite, R., "Volume Changes of Concrete," Proceedings, Fourth International Symposium on the Chemistry of Cement," Washington, D.C., 1960, pp 659-694

9. Prestressed Concrete Institute, "PCI Post-tensioning Manual," 1972, p 160

10. Ross, A. D., "Concrete Creep Data," The Structural Engineer, London, England, 1937, pp 314-316

11. McCafferty, R. M., "USBR Vibration Test System," 41st Shock and Vibration Symposium, Air Force Academy, Colorado Springs, Colorado, Oct. 1970

12. Ferguson, P. M., "Reinforced Concrete Fundamentals," Textbook, 1958, pp 251-276

Table 1. Summary of structural and durability properties of MMA impregnated concrete.

Property	Unimpregnated concrete controls	MMA 1/ impregnated concrete	
		R 2/	T 2/
Compressive strength, 3/ lb/in^2	5,270	20,260	18,160
Modulus of elasticity, 10^6 lb/in^2	3.5	6.3	6.2
Tensile strength, 3/ 4/ lb/in^2	420	1,630	1,510
Modulus of rupture, 5/ lb/in^2	740	2,640	2,290
Water absorption, percent	6.4	1.08	0.34
Water permeability, 10^{-4} ft/yr	5.3	0.8	1.4
Freeze-thaw durability			
Number of cycles	740	10,340	3,650
Percent weight loss	25	12	2
Sulfate attack			
Test cycle, days	480	1,436	1,436
Percent expansion	0.467	0.032	0.017
Resistance to acid (15 percent HCl)			
Exposure, days	105	1,395	1,395
Percent weight loss	27	13	10
Resistance to acid (15 percent H_2SO_4)			
Exposure, days	49	126	119
Percent weight loss	35	29	26

1/ Methyl methacrylate.
2/ R = radiation treatment; T = thermal-catalytic treatment.
3/ Compression and tension cylinders 3- by 6-inch cylinders.
4/ Tensile strengths determined by direct tension method.
5/ Flexural strength obtained from 3- by 3- by 16-inch bars.

Table 2. Summary of strength and elastic modulus of unimpregnated 6- by 12-inch cylinders.

Age at testing (days)	Day of casting	No. of specimens	Type of cure	Average ultimate strength (lb/in^2)	Average elastic modulus (10^6 lb/in^2)
1	1	5	Air	5,730	3.23
3	1	5	Air	6,210	3.32
3	2	5	Air	5,430	3.16
5	2	5	Air	5,490	3.28
7	1	5	Air	6,460	3.35
7	1	5	Fog	6,500	3.70
7	2	5	Air	5,940	3.35
7	2	5	Fog	6,020	3.40
7	1	6*	Air	6,280	3.30
7	2	6*	Air	5,900	3.33
14	1	5	Air	7,240	3.76
14	1	4	Fog	6,760	3.79
14	2	5	Air	6,570	3.58
14	2	4	Fog	6,100	3.58
28	1	5	Air	7,800	3.98
28	1	4	Fog	7,040	3.86
28	2	5	Air	7,120	3.58
28	2	4	Fog	6,490	3.50
31	1	5	Oven dried	8,490	+
84	2	5	Oven dried	7,440	+

* Three specimens taken at beginning of casting and three at the end of casting.
+ Elastic modulus not determined.

Table 3. Summary of the polymer loadings of panels and companion 6- by 12-inch cylinders impregnated with the panels and average strength and elastic modulus of the cylinders.

Panel number	Panel length (feet)	Panel polymer loading, weight %	Cylinder, average polymer loading, weight %	Average ultimate strength (lb/in^2)	Average elastic modulus (10^6 lb/in^2)
1	16	6.50	5.80	18,730	6.1
2	16	6.96	5.73	18,170	6.1
4	16	5.10	5.34	17,430	6.5
5	16	5.42	5.34	19,430	6.3
7	16	5.87	5.47	18,970	6.1
8	16	5.50	5.15	17,210	6.0
9	16	4.65	5.80	18,720	6.1
10	16	4.84	5.42	18,580	6.1
11	16	4.46	5.96	17,980	6.0
12	6	4.60	5.87	18,030	6.0

Panels No. 3 (16 feet) and 6 (6 feet) were not impregnated.

Table 4. Summary of flexural tests on unimpregnated 4- by 4- by 30-inch bars

Age at testing (days)	Day of casting	No. of specimens	Type of cure	Average flexural modulus (10^6 lb/in^2)	Average modulus of rupture (lb/in^2)
7	1	5	Air	3.6	578
7	2	5	Air	3.7	599
28	1	5	Air	4.0	628
28	2	5	Air	3.8	609

Table 5. Summary of flexural tests on impregnated 4- by 4- by 30-inch bars.

Polymer loading (wt. %)	Day of casting	No. of specimens	Average flexural modulus (10^6 lb/in^2)	Average modulus of rupture (lb/in^2)
4.92	1	5	6.63	2,235
5.15	1	5	6.52	2,144
5.19	2	5	6.20	2,017
5.18	2	5	6.36	1,982

Table 6. Low temperature compressive tests of plain concrete and PIC 6- by 12-inch cylinders.

Temperature °F	Average modulus of elasticity (10^6 lb/in^2)		Average ultimate strength (lb/in^2)	
	Plain	PIC	Plain	PIC
73	3.49	5.74	5,165	18,355
-10	4.03	6.29	6,670	16,890
-40	4.23	6.49	7,710	15,485

Table 7. Low temperature flexural tests of plain concrete and PIC 4- by 4- by 30-inch bars.

Temperature °F	Modulus of elasticity (10^6 lb/in^2)		Modulus of rupture (lb/in^2)	
	Plain	PIC	Plain	PIC
73	4.26	6.06	850	2,020
-10	3.98	6.44	820	2,180
-40	4.08	6.18	1,075	1,965

Table 8. Low temperature tensile tests of plain concrete and PIC 3- by 6-inch cylinders.

Temperature °F	Ultimate tensile strength (lb/in^2)	
	Plain	PIC
73	405	1,405
-10	475	1,370
-40	485	1,330

Table 9. Simple span flexural tests of small panels.

Panel length (ft)	Polymer loading (% wt.)	Design ultimate moment (in.-kip)	First crack			Ultimate moment (in.-kip)
			Moment (in.-kip)	Comp. stress (lb/in^2)	Tension stress (lb/in^2)	
6.0	4.6	703	690.0	2,930	1,860	817.5
5.0	4.8	703	504.0	2,280	1,220	810.0
5.0	5.2	703	540.0	2,410	1,340	780.0
1/ 6.0	0.0	635	270.0	1,470	400	678.0

1/ This panel was dried in case it would have been necessary to run another trial impregnation.

Table 10. Summary of data from fatigue tests of 3- by 6- by 54-inch unimpregnated concrete and PIC beams.

Type of beam 1/	Ultimate load (lbs.)	Percent of ultimate load					
		50%		60%		70%	
		Load range	Cycles 2/	Load range	Cycles 2/	Load range	Cycles 2/
Plain concrete	1,880	180-915	10 million	180-1,100	1,736,000	180-1,280	315,000
Fabricated PIC	4,330	430-2,165	10 million	430-2,600	10 million	430-3,030	3,045,000
Sawed PIC	5,625	560-2,810	10 million	560-3,380	3,555,000	560-3,940	2,783,000

1/ Three beams of each type were tested at each load level.
2/ Testing was terminated when at least one of the three beams failed or when 10 million cycles was reached.

Table 11. Measured values of panel shortening at prestress strand release.

Panel No.	Day of casting	Side of panel	Shortening (inches)	Prestress loss (%)
1	1	East	0.027	2.7
		West	0.029	2.9
2	1	East	0.033	3.3
		West	0.032	3.2
3	1	East	0.033	3.3
		West	0.034	3.4
4	1	East	0.029	2.9
		West	0.031	3.1
5	1	East	0.031	3.1
		West	0.031	3.1
Mean			0.031	3.1
7	2	East	0.030	3.0
		West	0.024	2.4
8	2	East	0.034	3.4
		West	0.032	3.2
9	2	East	0.028	2.8
		West	0.026	2.6
10	2	East	0.027	2.7
		West	0.029	2.9
11	2	East	0.027	2.7
		West	0.028	2.8
Mean			0.029	2.9

Table 12. Prestress loss due to temperature in unbounded prestress strand.

Prestress Loss - Percent

Temperature ° F	Time (days) 2	4	6	10	14
350	13.1	15.8	17.7	20.8	22.6
280	11.4	14.0	15.7	18.4	20.5
212	4.3	4.9	5.4	6.0	6.5
73	1.3	1.5	1.6	1.8	1.9

Table 13. Measured transverse strains in unimpregnated single-panel with 20-kip load in position 4.

Top of panel			Bottom of panel		
Gage No.	Strain* (10^{-6} in/in)		Gage No.	Strain (10^{-6} in/in)	
1	- 7		32	8	
2	- 1		33	- 7	
3	- 19		34	17	
4	-107		35	108	
5	-110		36	105	
6	-109		37	112	
7	-145		38	166	
8	-	Midspan	39	160	Midspan
9	-144		40	158	
13	- 92		44	90	
14	- 88		45	94	
15	- 82		46	82	
16	28		47	-25	
17	34		48	-31	
18	28		49	-21	
19	81				
20	82				
21	75				
22	51				
23	60				
24	60				
25	52		50	-34	
26	58		51	-40	
27	60		52	-43	
28	45		53	-32	
29	33		54	-24	
30	27		55	-17	
31	15		56	-10	

* Minus strain is compression.
Load position is shown in figure 22.

Table 14. Measured longitudinal strains in unimpregnated single-panel with 20-kip load in position 4.

Top of panel		Bottom of panel	
Gage No.	Strain* (10^{-6} in/in)	Gage No.	Strain (10^{-6} in/in)
10	27	41	-23
11	-	42	67
12	31	43	-23

* Minus strain is compression.
Load position is shown in figure 22.

Table 15. Measured transverse strains in panel No. 8 with 20-kip load in position 4.

Top of panel			Bottom of panel		
Gage No.	Run 1 strain* (10^{-6} in/in)	Run 2 strain (10^{-6} in/in)	Gage No.	Run 1 strain (10^{-6} in/in)	Run 2 strain (10^{-6} in/in)
1	- 9	- 11	32	0	4
2	- 4	1	33	- 3	- 2
3	- 13	- 15	34	4	9
4	- 85	- 83	35	73	74
5	- 78	-	36	63	70
6	- 86	- 85	37	78	78
7	-118	-114	38	107	103
8 Mid-	-	-	39 Mid-	124	105
9 span	-115	-109	40 span	105	99
13	- 70	- 74	44	66	72
14	- 66	- 70	45	58	62
15	- 67	- 72	46	60	63
16	11	7	47	- 21	- 18
17	17	11	48	- 20	- 19
18	15	8	49	- 24	- 21
19	56	59			
20	46	47			
21	57	51			
22	41	43			
23	41	43			
24	37	34			
25	28	24	50	- 28	- 33
26	24	24	51	- 29	- 32
27	26	24	52	- 27	- 30
28	18	17	53	- 21	- 25
29	13	12	54	- 15	- 18
30	6	7	55	- 6	- 13
31	1	2	56	- 3	- 6

* Minus strain is compression.
Load position is shown in figure 22.
Run 1 was initial test to 20 kips and Run 2 was 20-kip load during failure test.

Table 16. Measured transverse strains in panel No. 8 with 20-kip load in position 8.

Top of panel		Bottom of panel	
Gage No.	Strain* (10^{-6} in/in)	Gage No.	Strain (10^{-6} in/in)
1	-50	32	42
2	-	33	49
3	-52	34	45
4	-98	35	87
5	-	36	86
6	-96	37	91
7	-75	38	68
8 Midspan	-	39 Midspan	61
9	-73	40	75
13	-27	44	30
14	-22	45	25
15	-25	46	29
16	20	47	21
17	23	48	17
18	25	49	24
19	46		
20	40		
21	48		
22	28		
23	27		
24	24		
25	13	50	17
26	12	51	17
27	11	52	15
28	9	53	13
29	6	54	11
30	3	55	7
31	- 1	56	3

* Minus strain is compression.
Load position is shown in figure 22.

Table 17. Measured transverse strains in panel No. 8 with 20-kip load in position 12.

Top of panel		Bottom of panel	
Gage No.	Strain* (10^{-6} in/in)	Gage No.	Strain (10^{-6} in/in)
1	-60	32	52
2	-	33	87
3	-64	34	56
4	-74	35	65
5	-	36	58
6	-74	37	67
7	-44	38	40
8 Midspan	-	39 Midspan	30
9	-45	40	35
13	- 8	44	7
14	- 5	45	2
15	- 9	46	4
16	23	47	-28
17	19	48	-23
18	26	49	-33
19	39		
20	32		
21	39		
22	21		
23	21		
24	15		
25	9	50	- 8
26	8	51	- 7
27	6	52	- 6
28	6	53	- 6
29	4	54	- 6
30	4	55	- 4
31	3	56	- 1

* Minus strain is compression.
Load position is shown in figure 22.

Table 18. Measured longitudinal strains in panel No. 8 with 20-kip load in position 4.

Top of panel			Bottom of panel		
Gage No.	Run 1 strain* (10^{-6} in/in)	Run 2 strain (10^{-6} in/in)	Gage No.	Run 1 strain (10^{-6} in/in)	Run 2 strain (10^{-6} in/in)
10	21	22	41	-22	-25
11	-	-	42	48	38
12	23	20	43	-19	-21

* Minus strain is compression.
Load position is shown in figure 22.
Run 1 was initial test to 20 kips and run 2 was 20-kip load during failure test.

Table 19. Comparison of average measured transverse strains in panels No. 2 and 8 with 20-kip load in position 4.

Top of panel			Bottom of panel		
Gage Nos. in panel 2	Average strain* from panel 2 (10^{-6} in/in)	Average strain from panel 8 (10^{-6} in/in)	Gage Nos. in panel 2	Average strain from panel 2 (10^{-6} in/in)	Average strain from panel 8 (10^{-6} in/in)
1	6				
2,3,4	2		36	1	
5	- 12				
6,7,8	- 31	- 8	37,38,39	34	2
9	-103	- 83	40	89	73
10	-122		41	141	
11,12,13 (Midspan)	-160	-114	42,43,44 (Midspan)	121	107
17	-136		48	125	
18	- 83	- 70	49	70	64
19,20,21	6	12	50,51,52	- 11	- 20
22	30				
23,24,25	45	53	53	- 48	
26	55				
27,28,29	54	40			
30	55		54	- 59	
31,32,33	49	25	55,56,57	- 52	- 30
34	24	12	58	- 26	- 16
35	1	2	59	- 3	- 4

* Minus strain is compression.
Load position is shown in figure 22.

Table 20. Measured transverse strains along midspan section from three-panel tests with 20-kip load in position 1.

Top of panel				Bottom of panel			
First test		Second test		First test		Second test	
Gage No.	Strain* (10^{-6} in/in)	Gage No.	Strain (10^{-6} in/in)	Gage No.	Strain (10^{-6} in/in)	Gage No.	Strain (10^{-6} in/in)
9	- 5			56	10		
10	-13			57	12		
11	-21	54	-18	58	15	55	17
12	-26	11	-31	59	23	40	27
13	-55	12	-43	60	46	41	55
14	-83	13	-94	61	72	42	94
15	-77	56	-96	62	71	57	96
16	-54	58	-57	63	50	59	57
17	-37			64	36		

* Minus strain is compression.
Load position is shown in figure 22.

Table 21. Measured transverse strains along midspan section from three-panel tests with 20-kip load in position 2.

Top of panel				Bottom of panel			
First test		Second test		First test		Second test	
Gage No.	Strain* (10^{-6} in/in)	Gage No.	Strain (10^{-6} in/in)	Gage No.	Strain (10^{-6} in/in)	Gage No.	Strain (10^{-6} in/in)
9	-12			56	8		
10	-11			57	12		
11	-22	54	-18	58	20	55	18
12	-28	11	-30	59	32	40	26
13	-61	12	-44	60	51	41	53
14	-69	13	-80	61	63	42	78
15	-73	56	-77	62	69	57	79
16	-49	58	-48	63	44	59	49
17	-36			64	34		

* Minus strain is compression.
Load position is shown in figure 22.

Table 22. Measured transverse strains along midspan section from impregnated three-panel tests with 20-kip load in position 3.

Top of panel				Bottom of panel			
First test		Second test		First test		Second test	
Gage No.	Strain* (10^{-6} in/in)	Gage No.	Strain (10^{-6} in/in)	Gage No.	Strain (10^{-6} in/in)	Gage No.	Strain (10^{-6} in/in)
9	-12			56	9		
10	-14			57	13		
11	-32	54	-26	58	26	55	28
12	-36	11	-43	59	37	40	41
13	-74	12	-58	60	63	41	62
14	-81	13	-81	61	75	42	78
15	-60	56	-56	62	55	57	58
16	-32	58	-35	63	31	59	37
17	-25			64	18		

* Minus strain is compression.
Load position is shown in figure 22.

Table 23. Measured transverse strains along midspan section from impregnated three-panel tests with 20-kip load in position 4.

Top of panel				Bottom of panel			
First test		Second test		First test		Second test	
Gage No.	Strain* (10^{-6} in/in)	Gage No.	Strain (10^{-6} in/in)	Gage No.	Strain (10^{-6} in/in)	Gage No.	Strain (10^{-6} in/in)
9	-16			56	17		
10	-24			57	23		
11	-41	54	-39	58	37	55	36
12	-54	11	-63	59	53	40	56
13	-66	12	-99	60	58**	41	121
14	-58	13	-65	61	51	42	60
15	-40	56	-43	62	35	57	40
16	-24	58	-26	63	19	59	28
17	-14			64	13		

* Minus strain is compression.
** Strain value believed to be incorrect.
Load position is shown in figure 22.

Table 24. Displacements along midspan section with 20-kip load for first three-panel test.

Load position*	Displacement measured with LVDTs** (inches)				
	1	2	3	4	5
1	0.0047	0.0059	0.0093	0.0153	0.0157
2	0.0051	0.0063	0.0098	0.0152	0.0147
3	0.0071	0.0087	0.0122	0.0159	0.0120
4	0.0098	0.0115	0.0142	0.0121	0.0086

* See figure 22 for load positions.
** See figure 57 for LVDT locations and identifications.

Table 25. Displacements along midspan section with 20-kip load for second three-panel test.

Load position*	Displacement measured with LVDTs** (inches)				
	1	2	3	4	5
1	0.0038	0.0061	0.0113	0.0157	0.0191
2	0.0042	0.0066	0.0115	0.0155	0.0175
3	0.0064	0.0088	0.0135	0.0138	0.0137
4	0.0086	0.0122	0.0145	0.0135	0.0109

* See figure 22 for load positions.
** See figure 57 for LVDT locations and identifications.

Table 26. Neutron and gamma ray moisture and density determination.

Condition of concrete	Gravimetric measurements		Neutron and gamma ray measurements			
			Position No. 1		Position No. 2	
	Density lb/ft^3	Weight of moisture or polymer lb/ft^3	Density lb/ft^3	Weight of moisture or polymer lb/ft^3	Density lb/ft^3	Weight of moisture or polymer lb/ft^3
Air dry	146.5	8.5	131.5	6.0	130.0	6.2
Oven dry	138.0	0	122.5	1.4	117.5	1.4
Surface polymerized	139.6	1.6	122.5	4.3	121.0	4.2

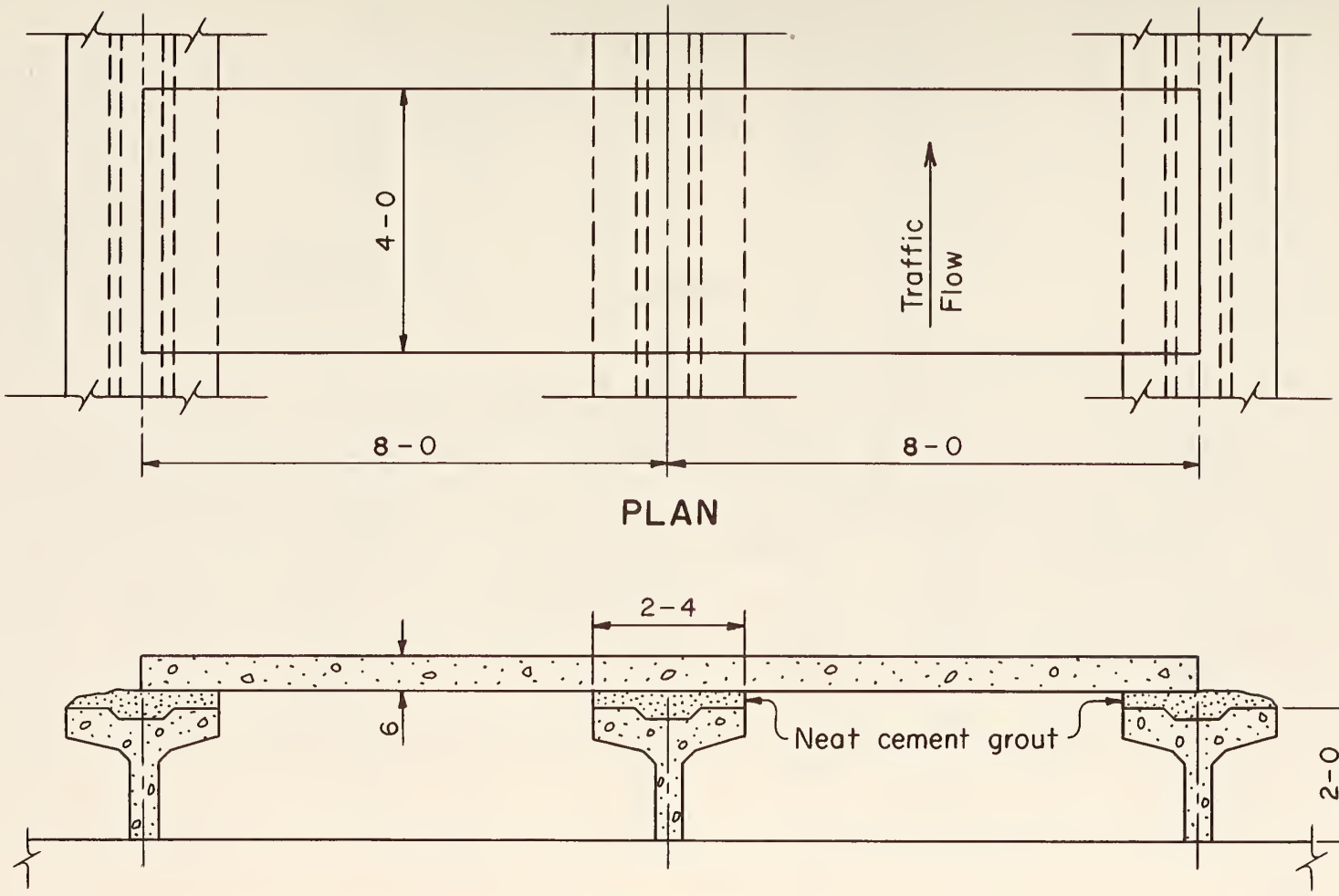

Figure 1. Plan and section of a single panel and girder support.

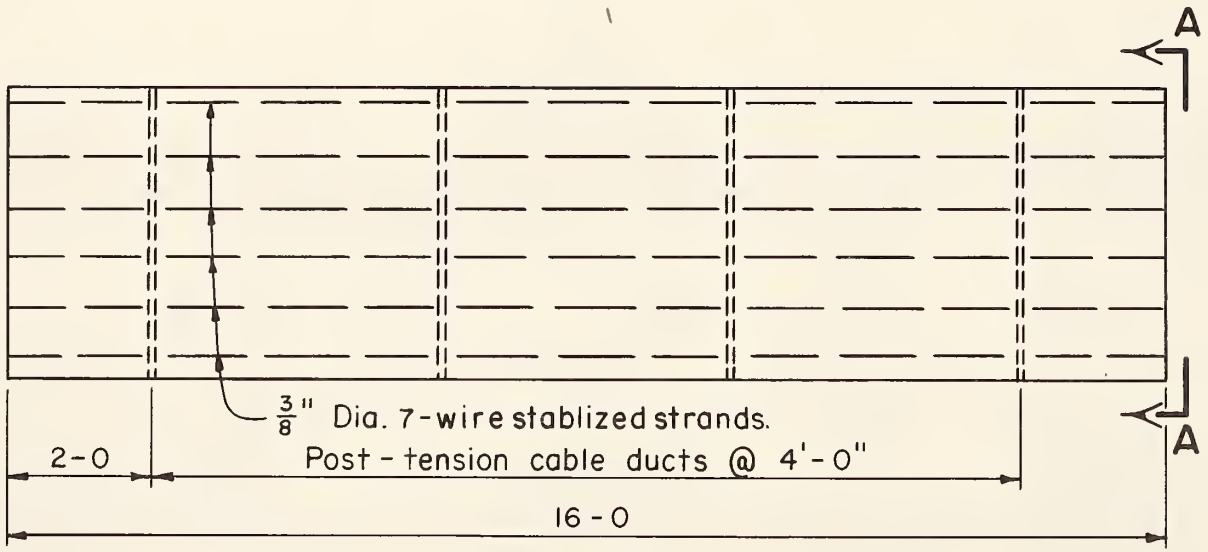

PLAN

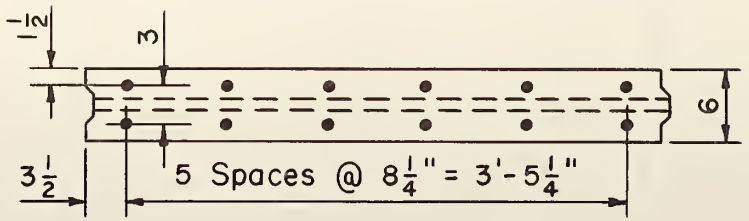

ELEVATION A-A

Figure 2. Design layout for panels.

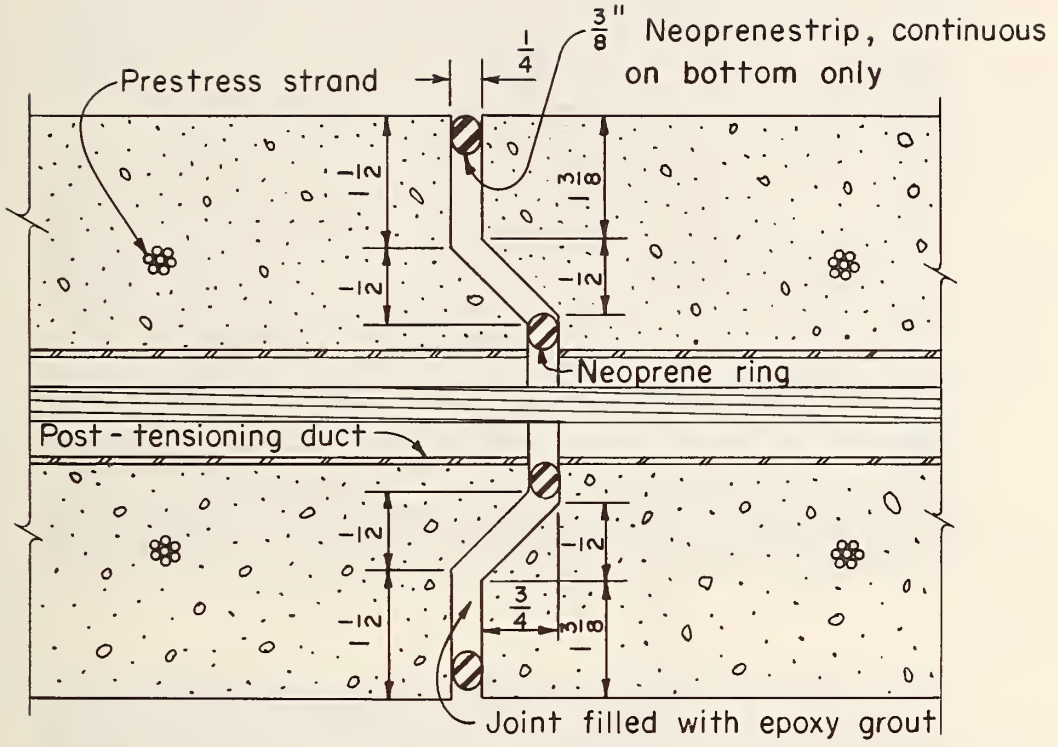

PANEL TO PANEL CONNECTION

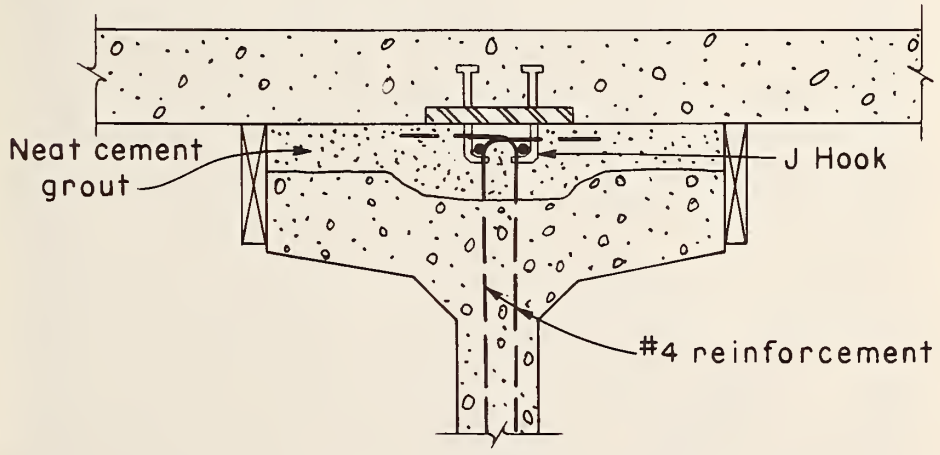

PANEL TO GIRDER CONNECTION

Figure 3. Details of panel to panel and panel to center girder connections.

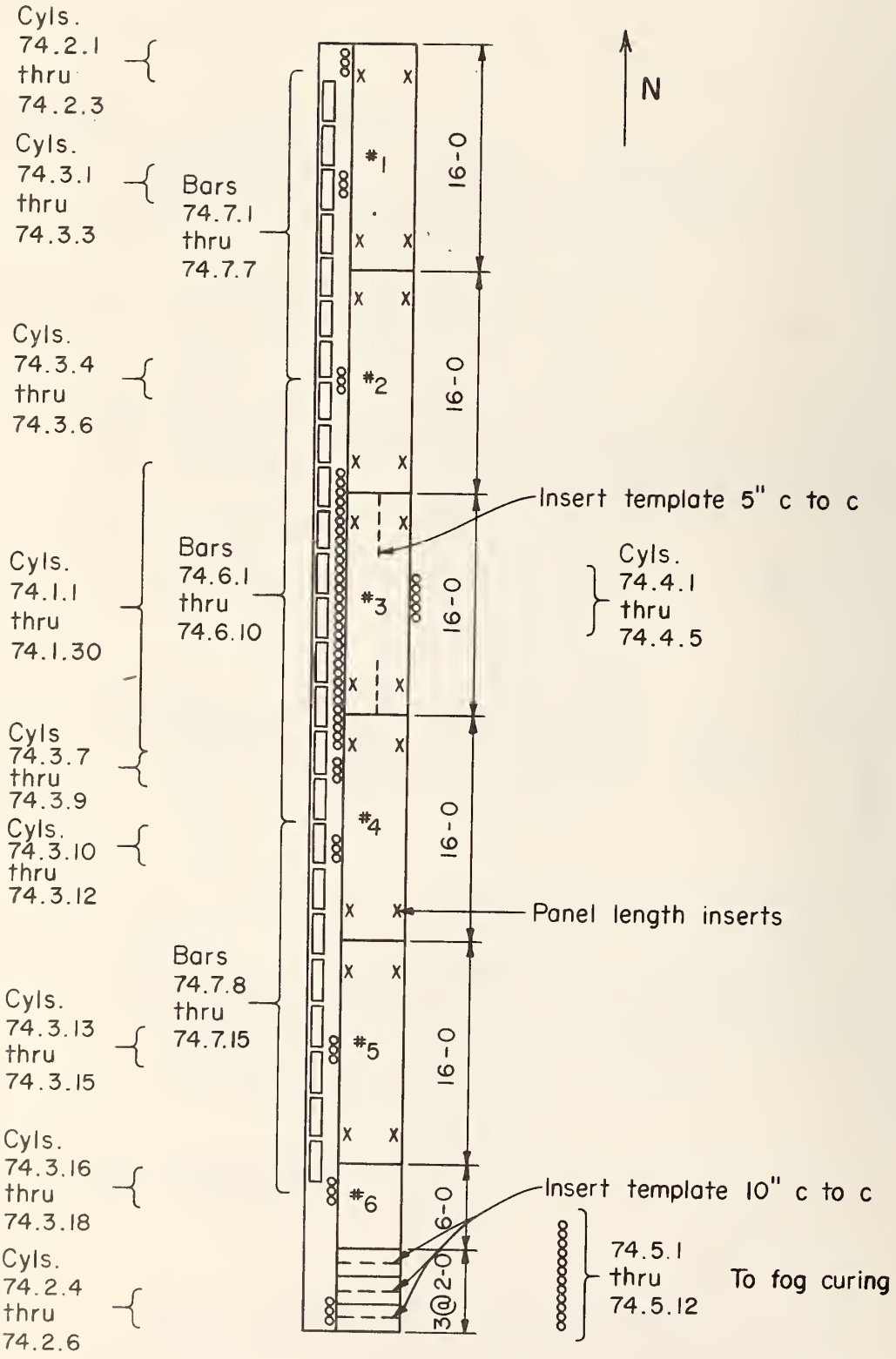

Figure 4. Schematic layout for casting panels and test specimens.

Figure 5. Panel casting bed just prior to placing concrete.

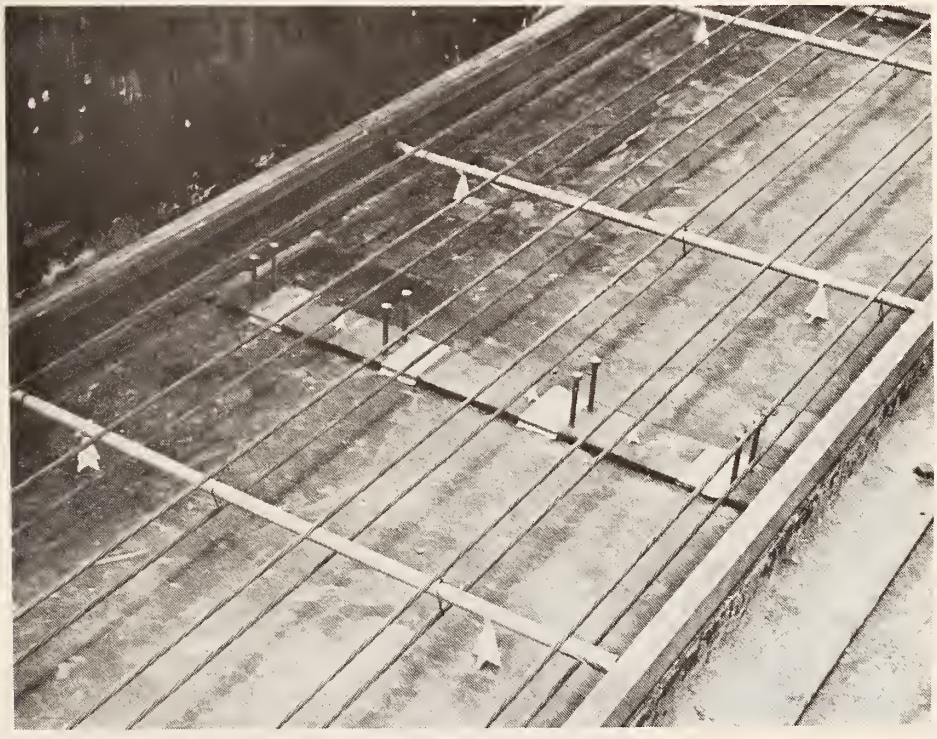

Figure 6. Prestressing strand, conduits for post-tensioning cables, and plate for center girder to panel connection.

Figure 7. Panels stacked after removal from casting bed.

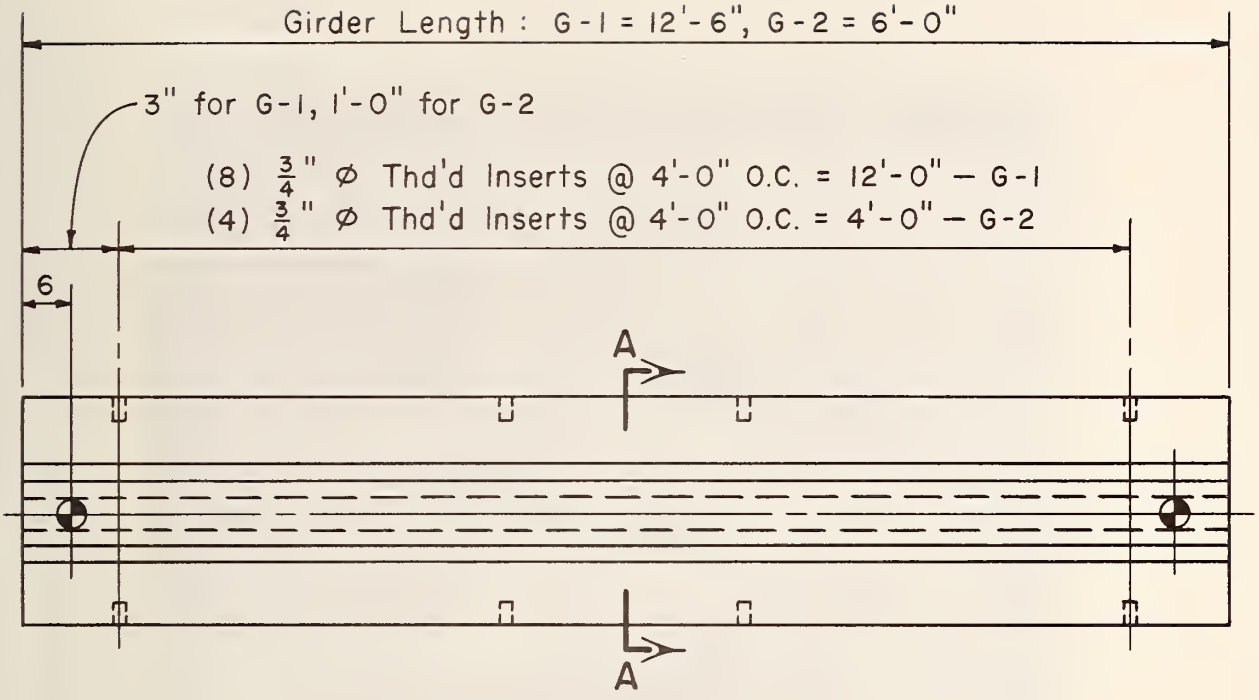

PLAN VIEW

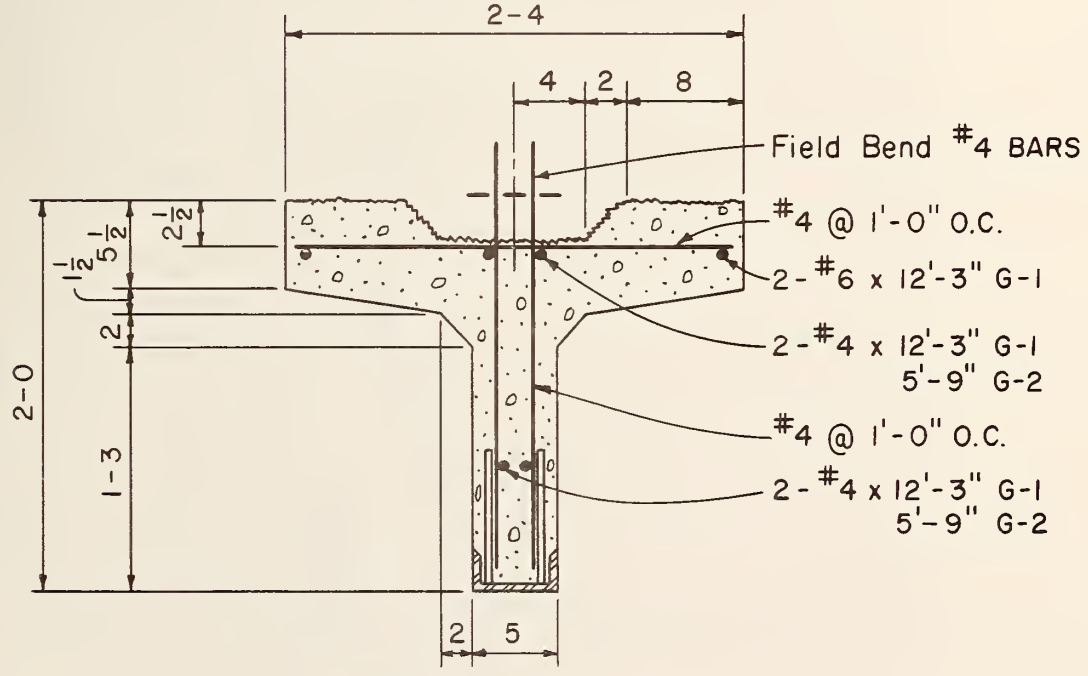

SECTION A-A

Figure 8. Details for fabrication of support girders.

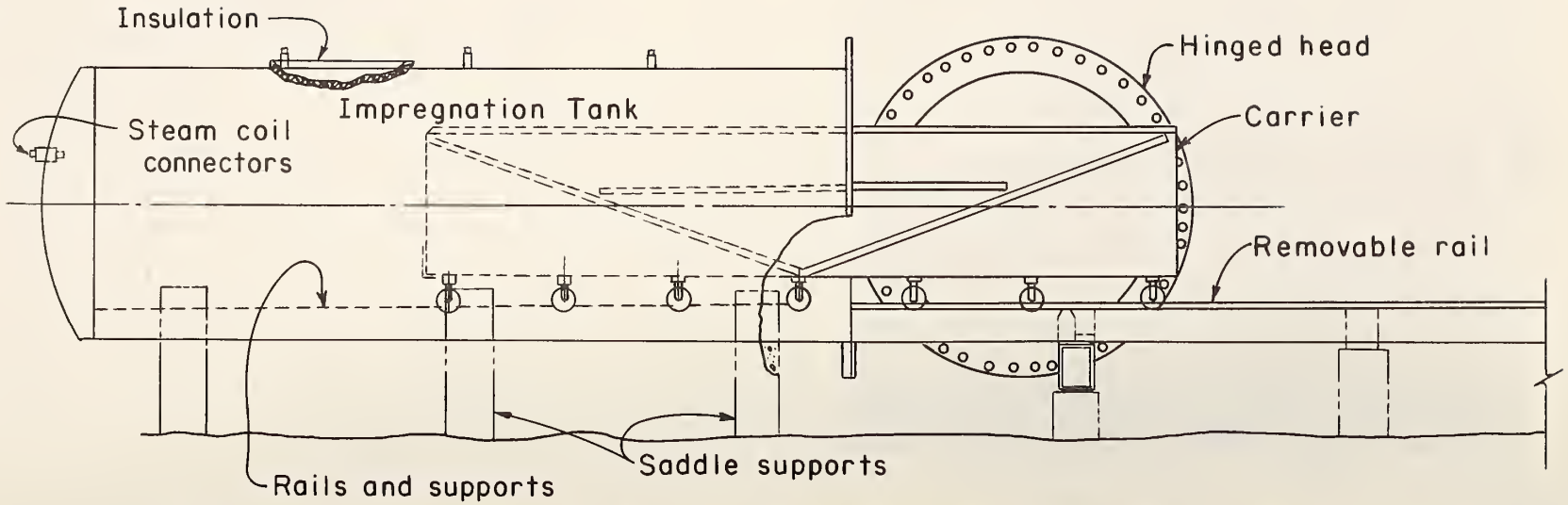

Figure 9. Schematic drawing of the impregnation/polymerization tank and panel carrier.

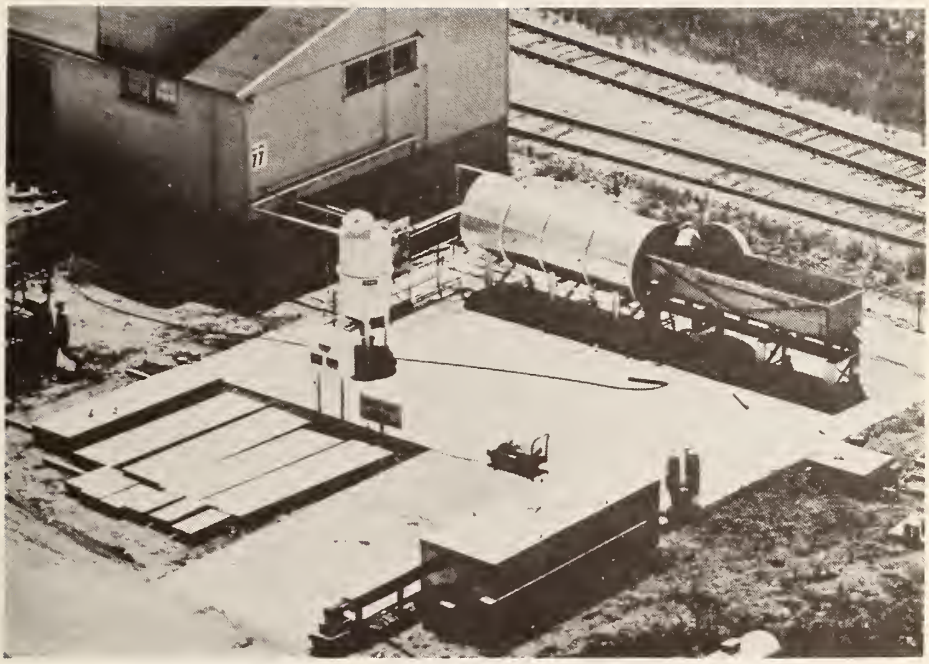

Figure 10. Overall view of the impregnation/polymerization facility.

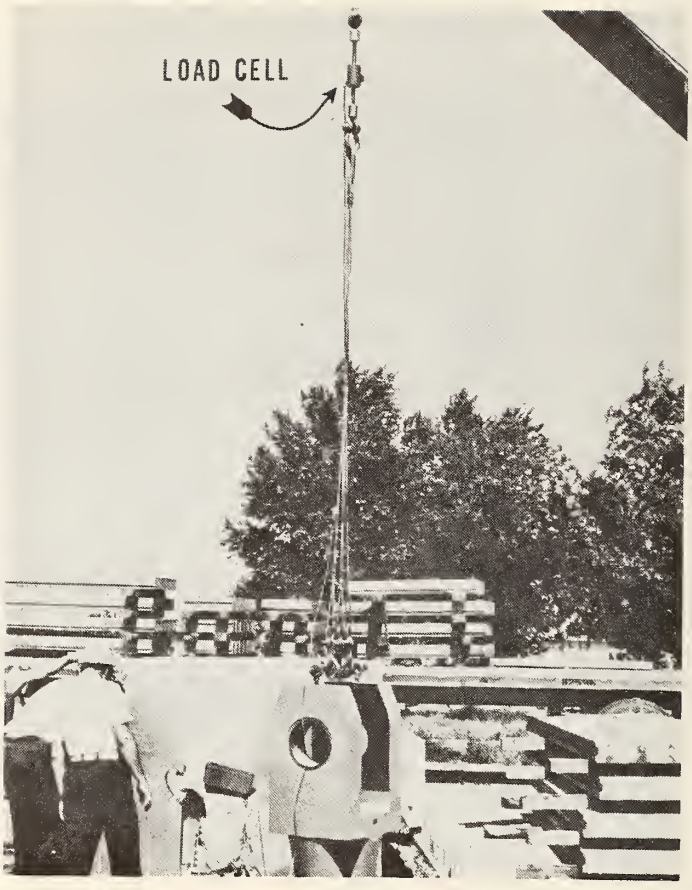

Figure 11. Calibrating the load cell prior to weighing the panels.

Figure 12. Placing a panel in the drying oven.

Figure 13. Carrier containing four panels ready for impregnation.

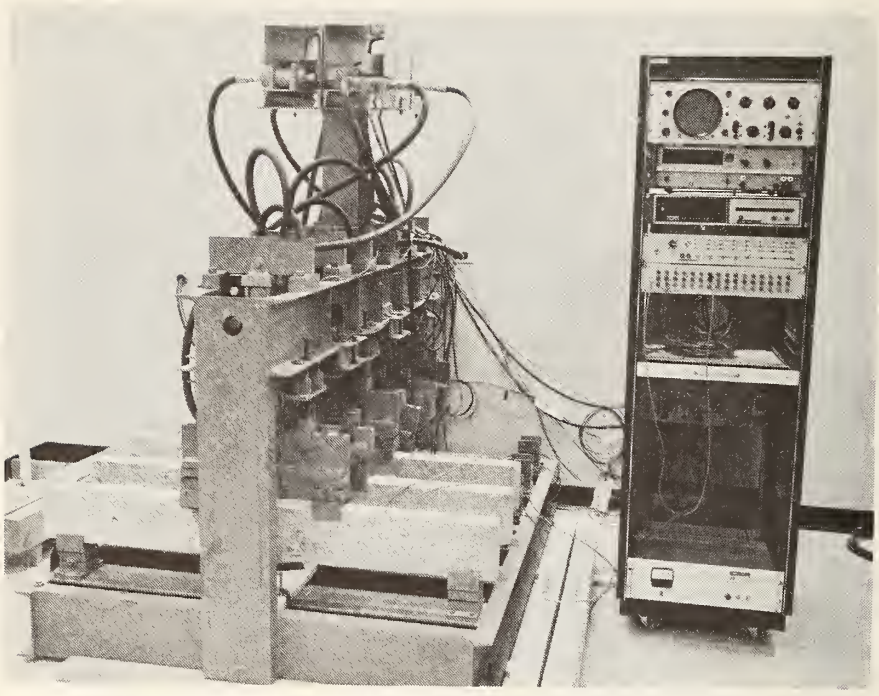

Figure 14. Beam fatigue testing machine.

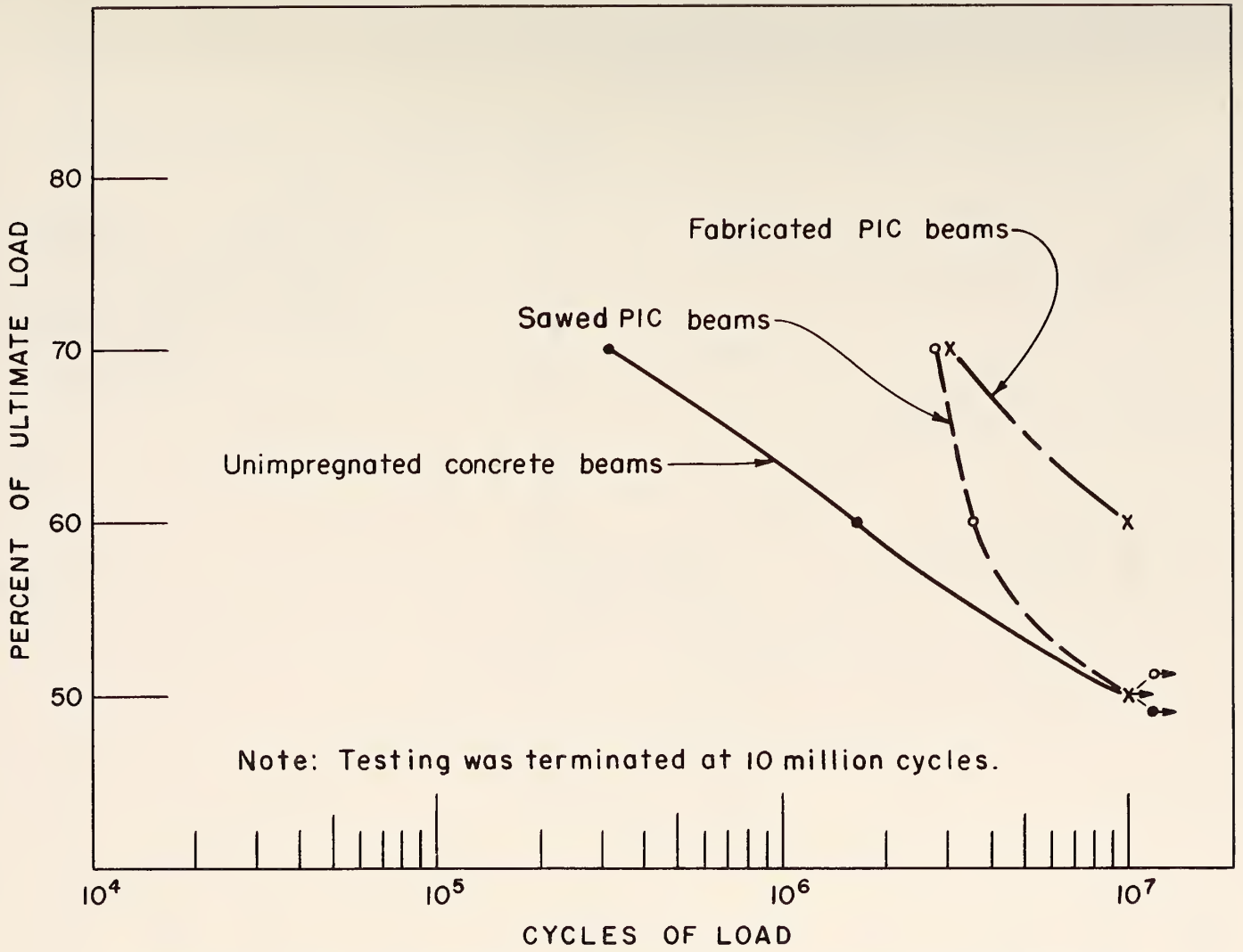

Figure 15. Curves from fatigue tests of PIC and unimpregnated concrete 3-by 6-by 54-inch beams.

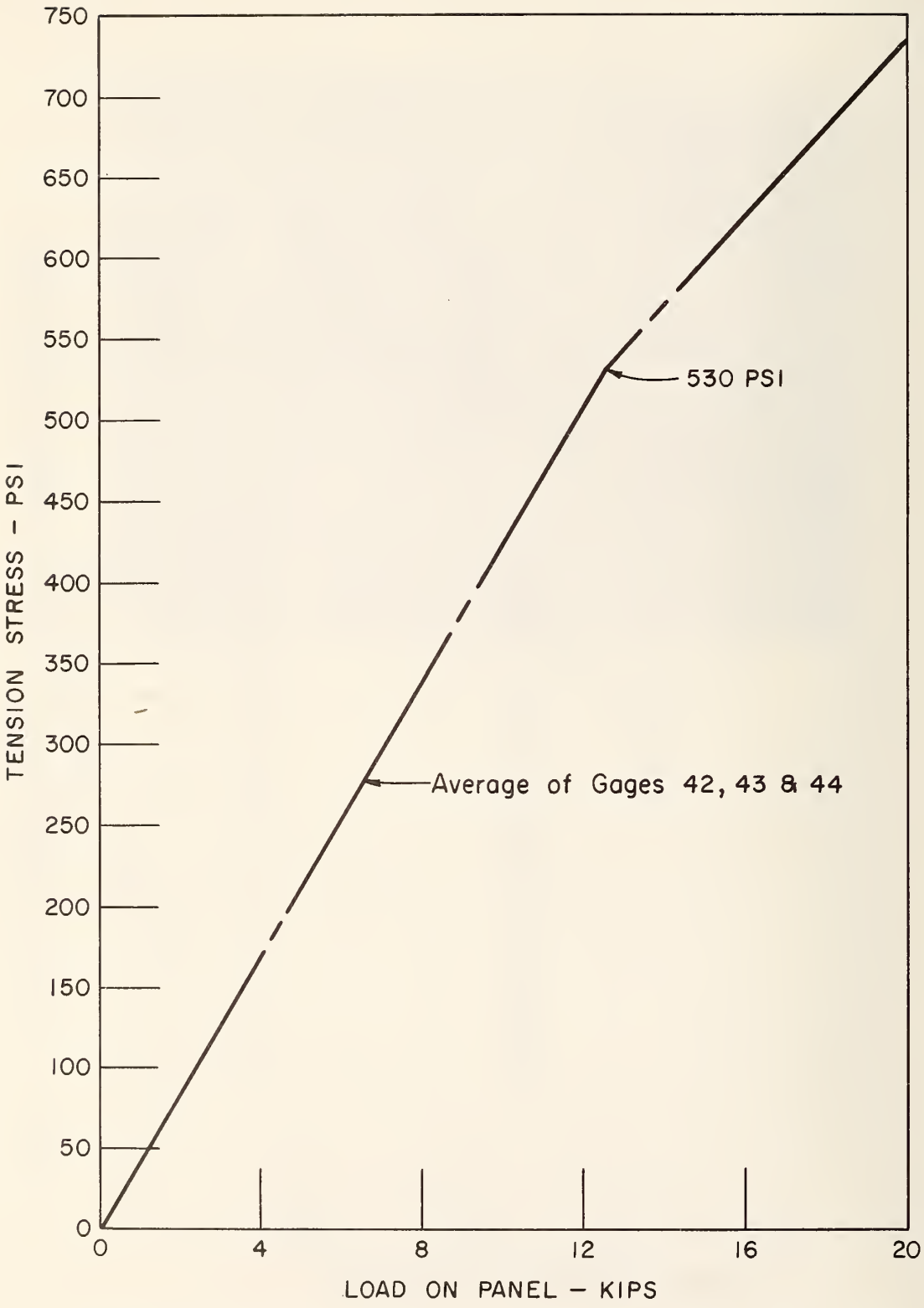

Figure 16. Change in slope of a curve of stress versus load occurring when the tension stress equals the compressive prestress in a cracked PIC panel.

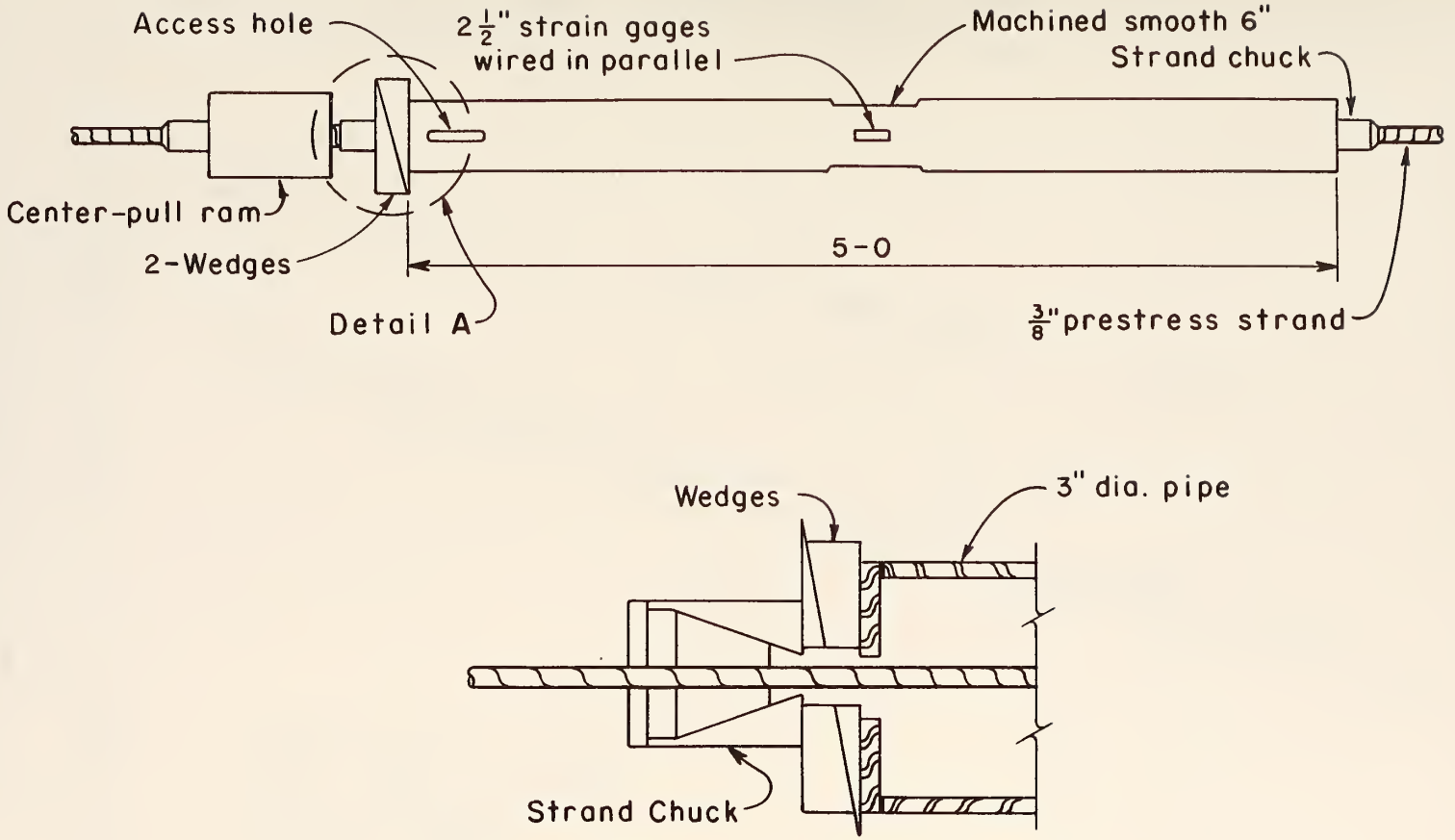

Figure 17. Loading frame used in tests to determine effects of high temperatures on prestress relaxation.

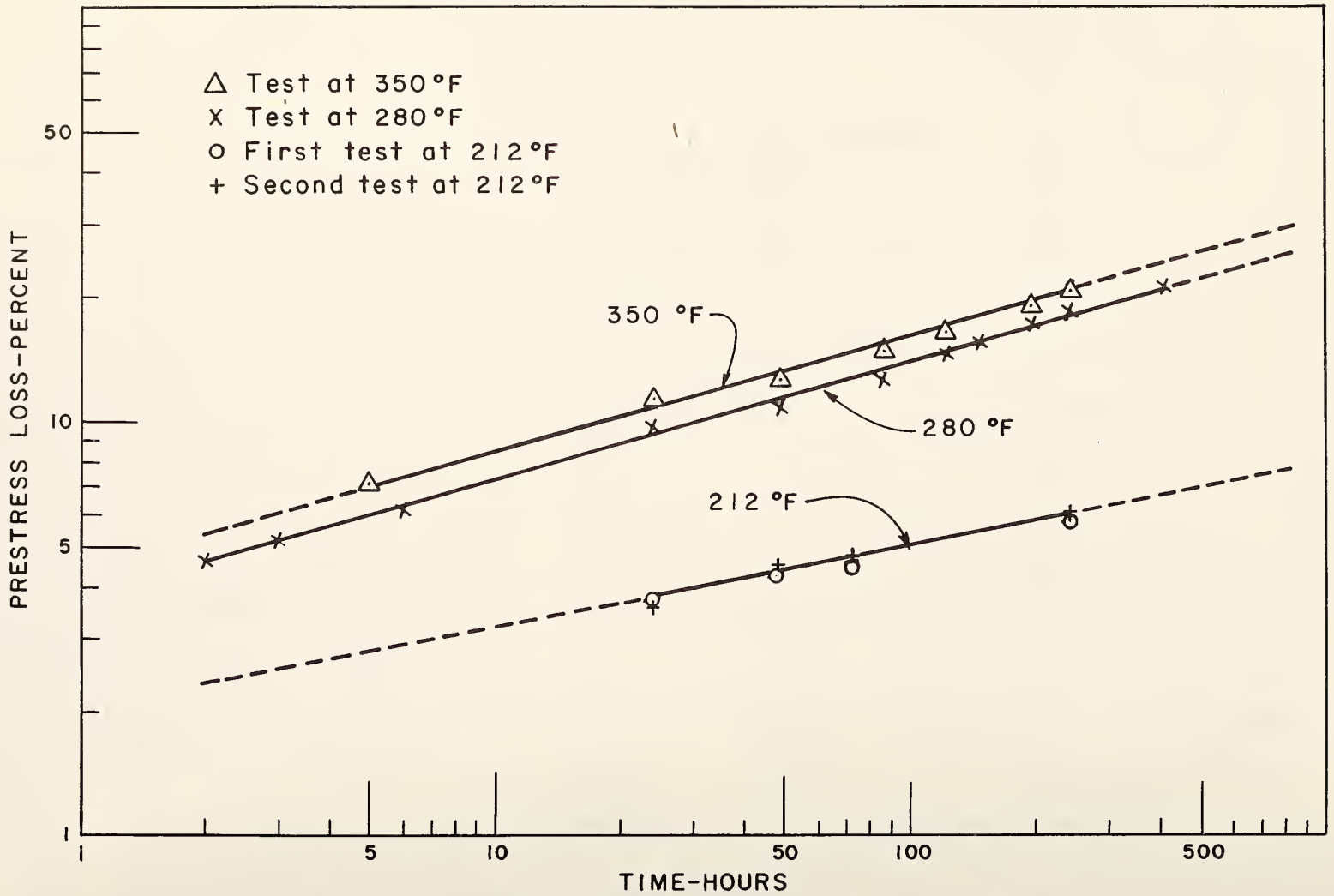

Figure 18. Percent of prestress loss due to temperature in unbonded prestress strand.

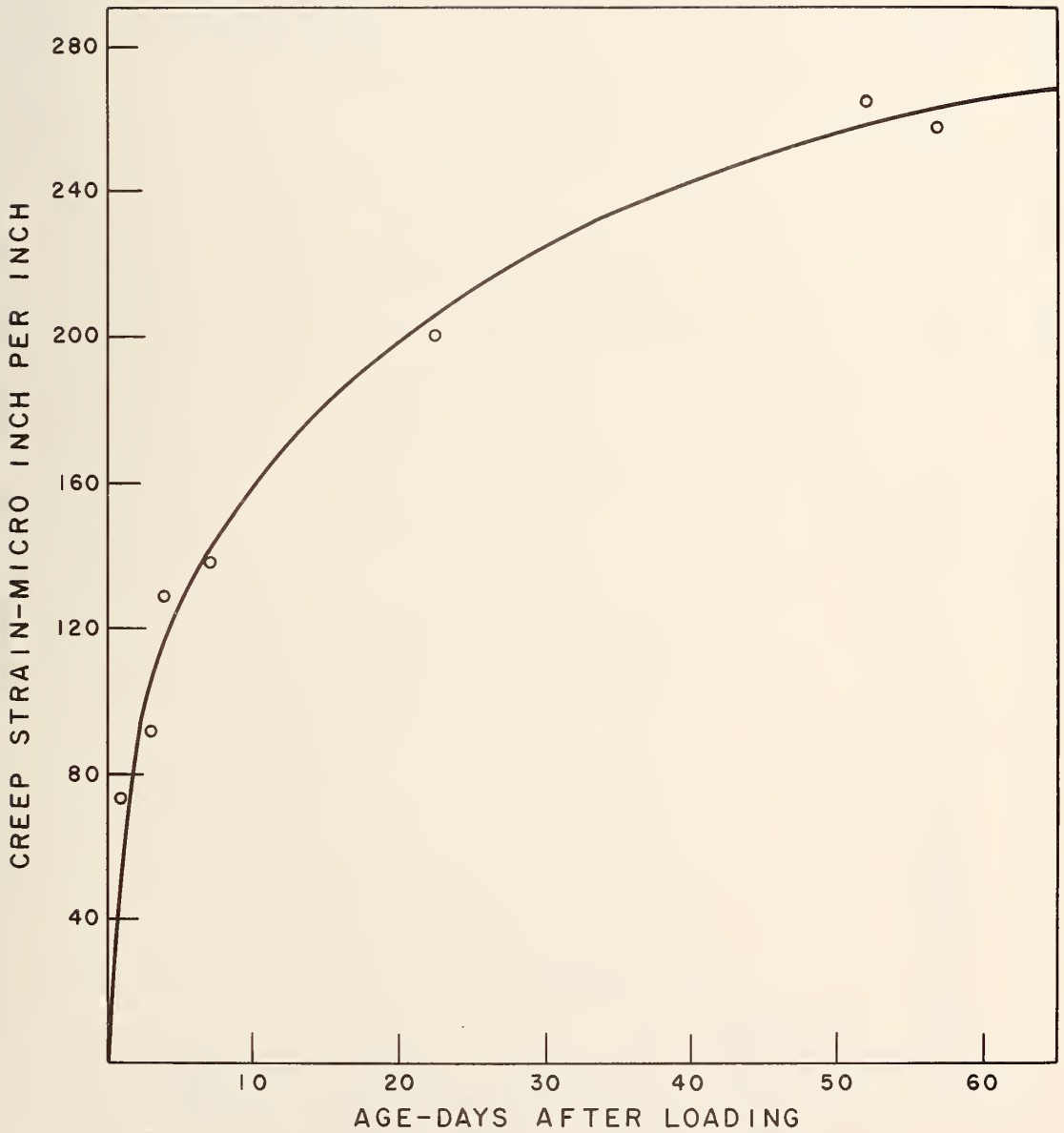

Figure 19. Creep for a typical unimpregnated concrete 6-by 12-inch cylinder.

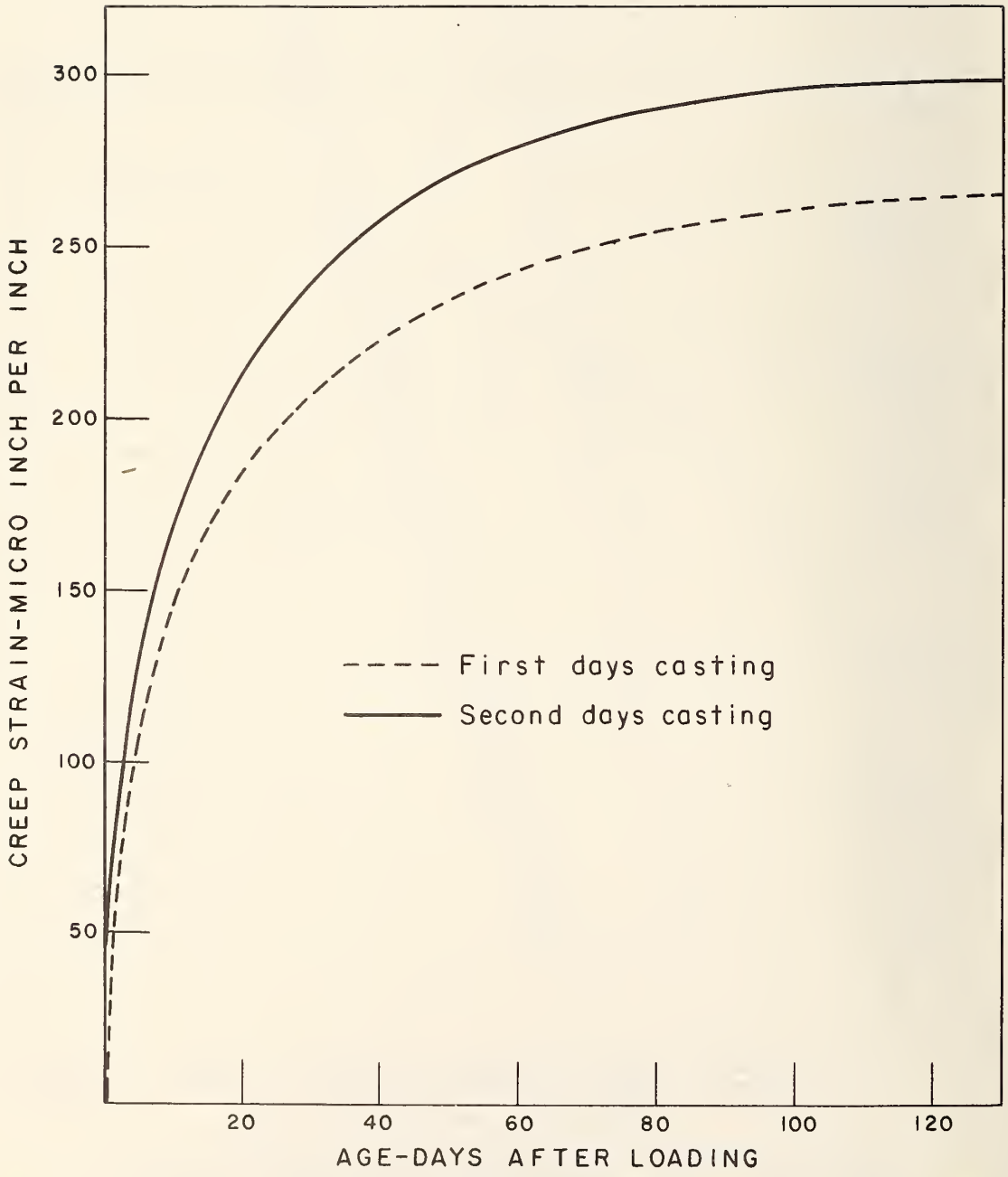

Figure 20. Curves of the average concrete creep from each day of casting.

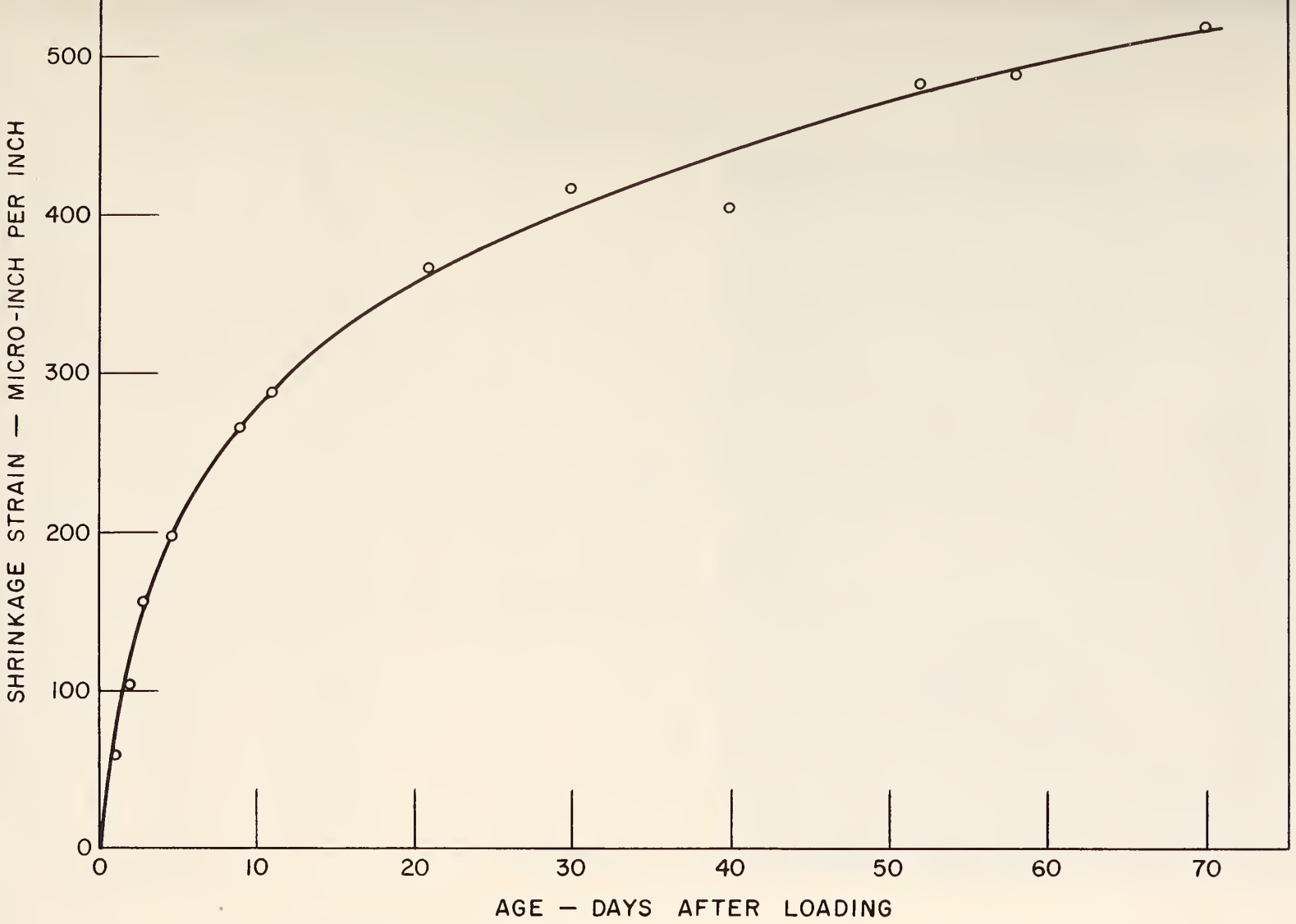

Figure 21. Shrinkage curve for a typical unimpregnated concrete 4-by 4-by 30-inch bar.

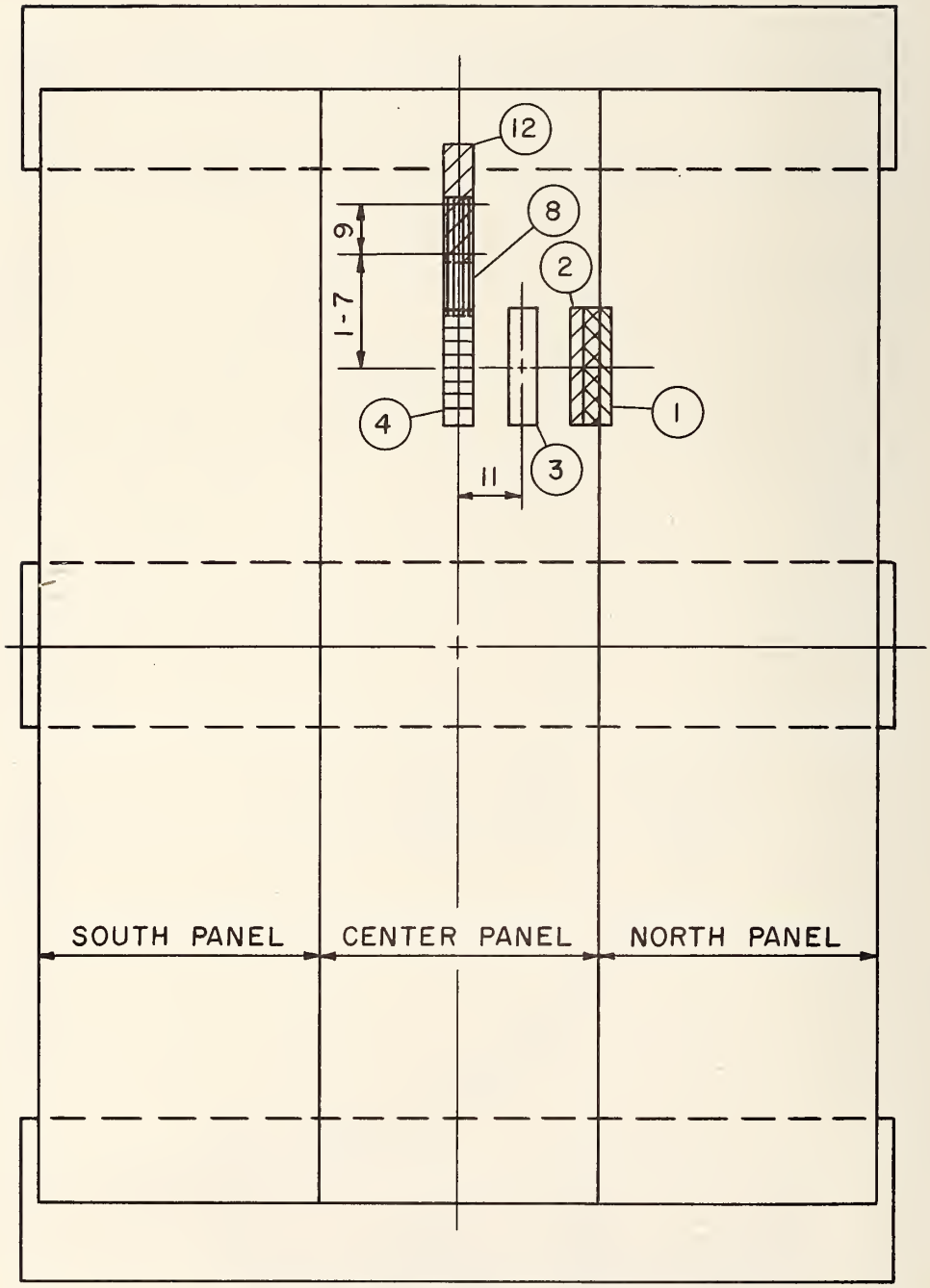

Figure 22. Load positions and identifications for both single-panel and three-panel tests.

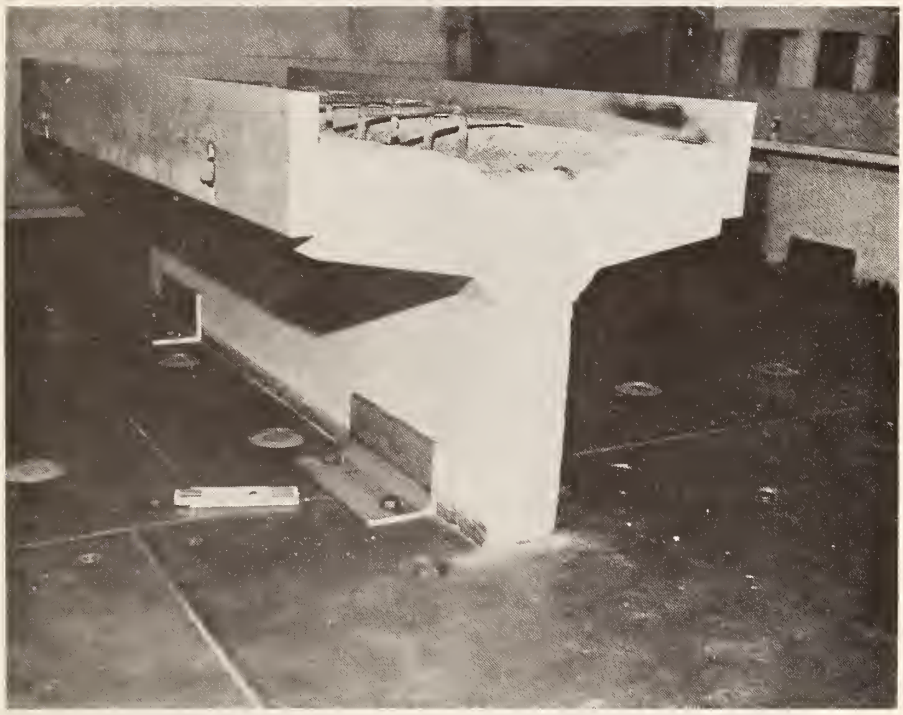

Figure 23. Girder support for the end of a panel attached to the test floor.

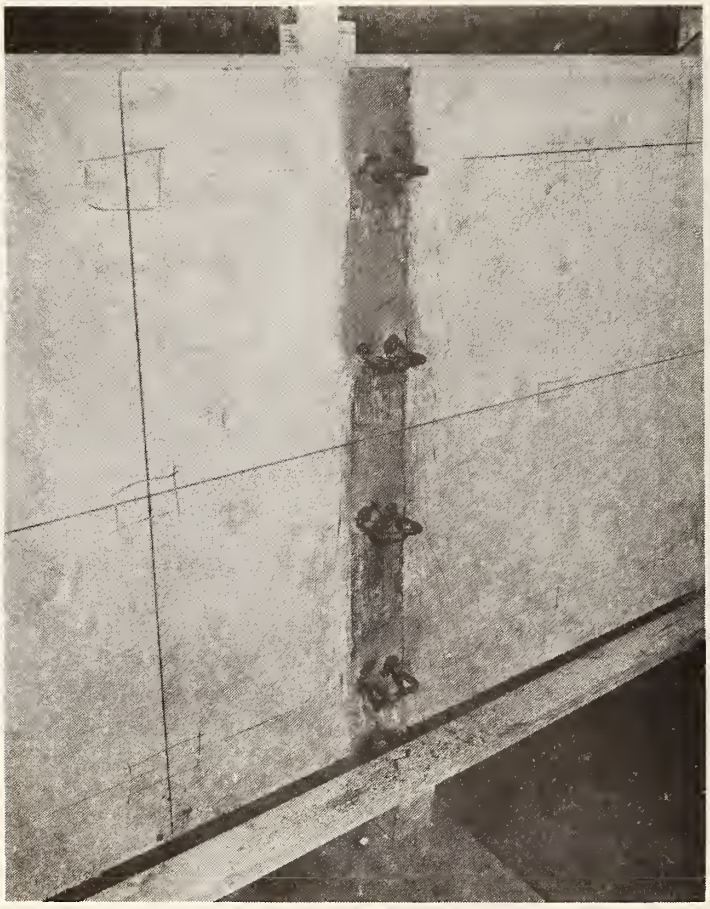

Figure 24. J-hooks welded to the bottom of a panel for the center girder support to panel connection.

Figure 25. J-hooks welded to the bottom of a panel for an end girder support to panel connection.

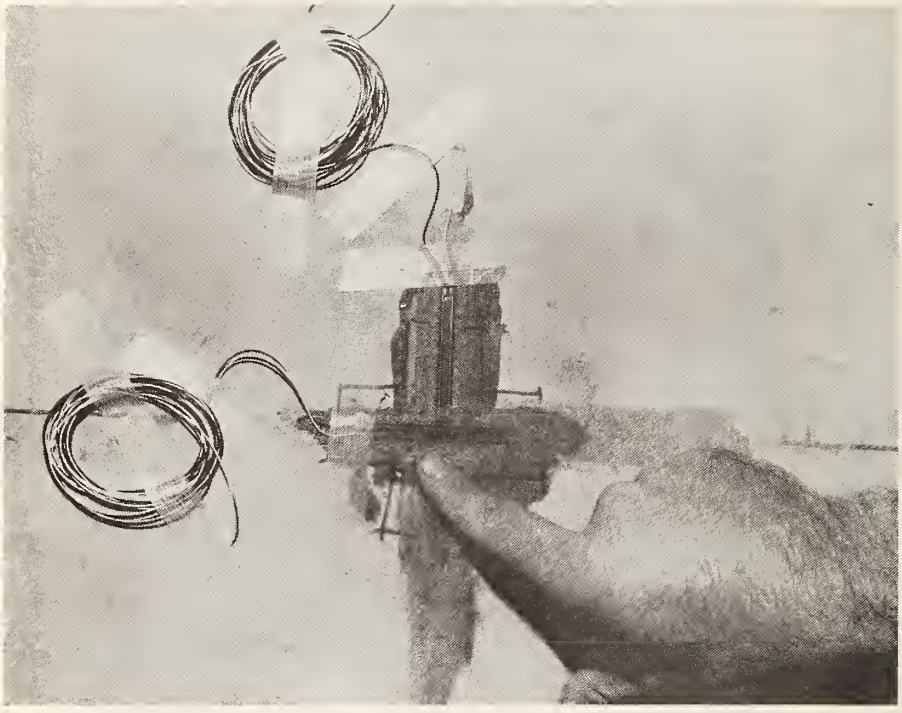

Figure 26. Typical strain gage installation where both transverse and longitudinal strain was desired.

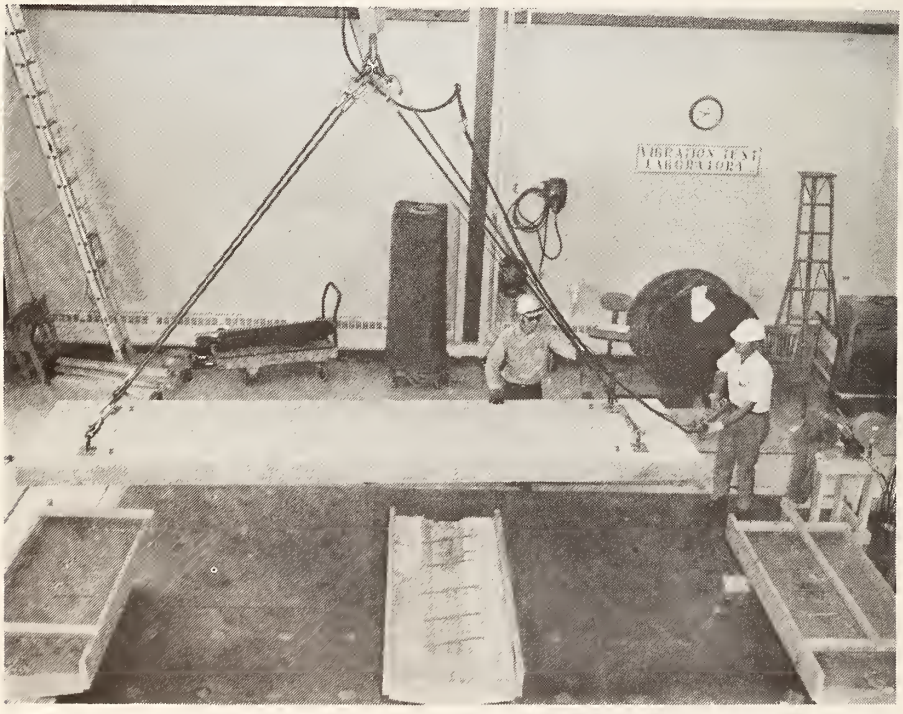

Figure 27. Placement of a panel onto the girder supports.

Figure 28. Frame on end girder support used for panel alignment.

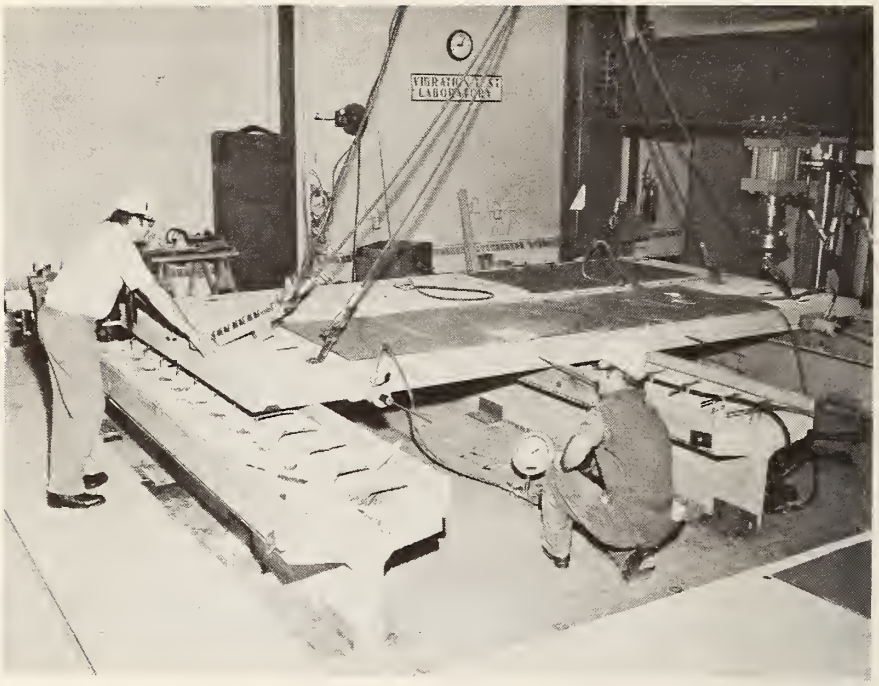

Figure 29. Pulling the south panel to the center panel by using the longitudinal post-tensioning strands.

Figure 30. Joint between panel and girder support at center of the panel prior to grouting.

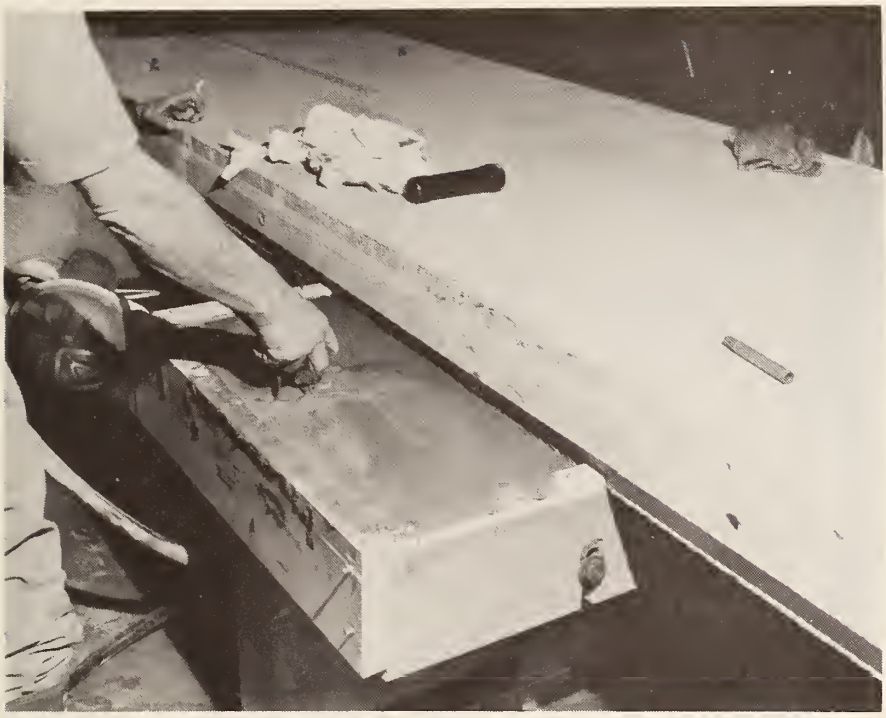

Figure 31. Grouting of the panel to the center girder support.

Figure 32. Single-panel test setup.

Figure 33. Data acquisition system used in single-panel testing.

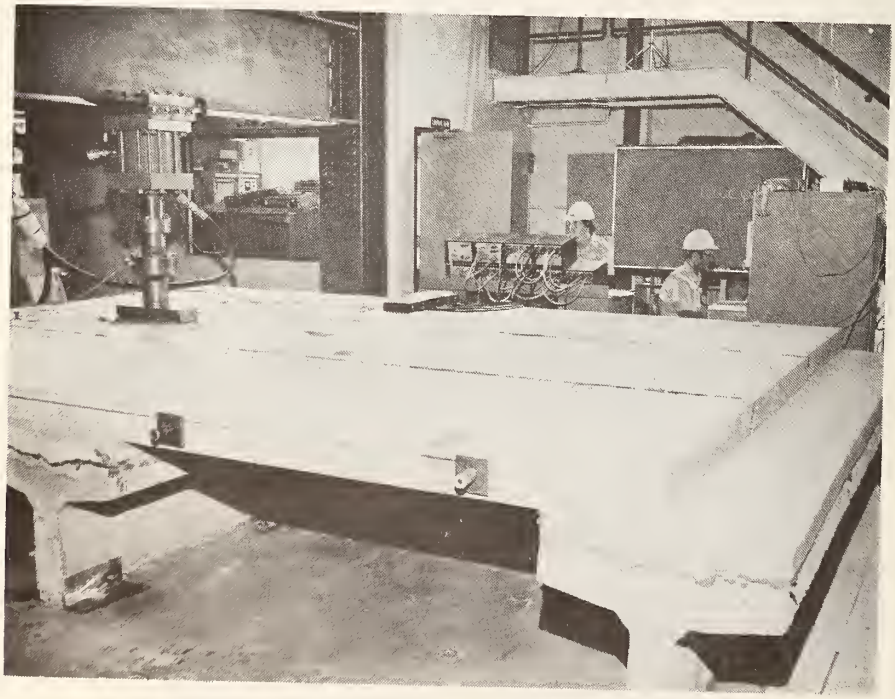

Figure 34. Three-panel test setup.

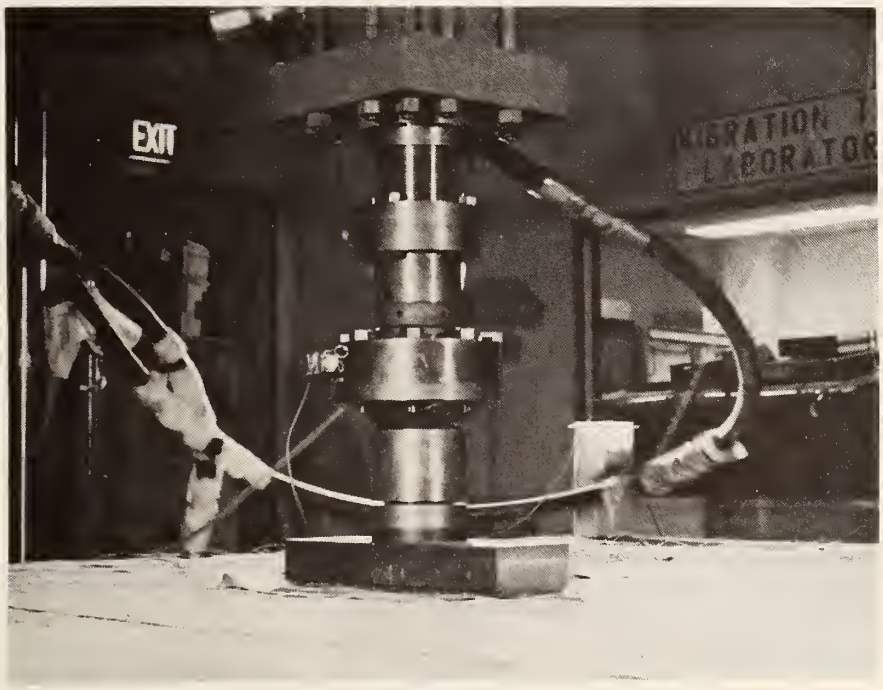

Figure 35. Hydraulic ram, load cell, and 5-by 20-inch bearing block used to load the panels.

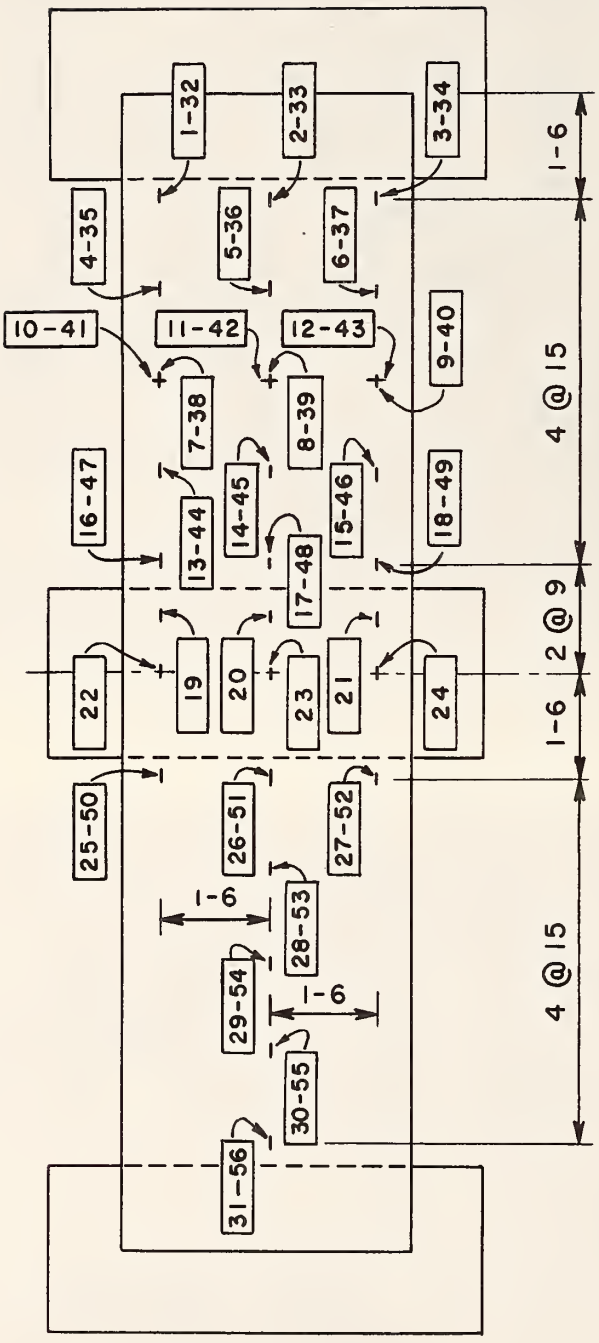

Note: Single numbers-gage on top surface only.
[X-Y] X is on top surface, Y is on bottom surface.

Figure 36. Strain gage locations and identifications for unimpregnated panel No. 3 and PIC panel No. 8 single-panel static tests.

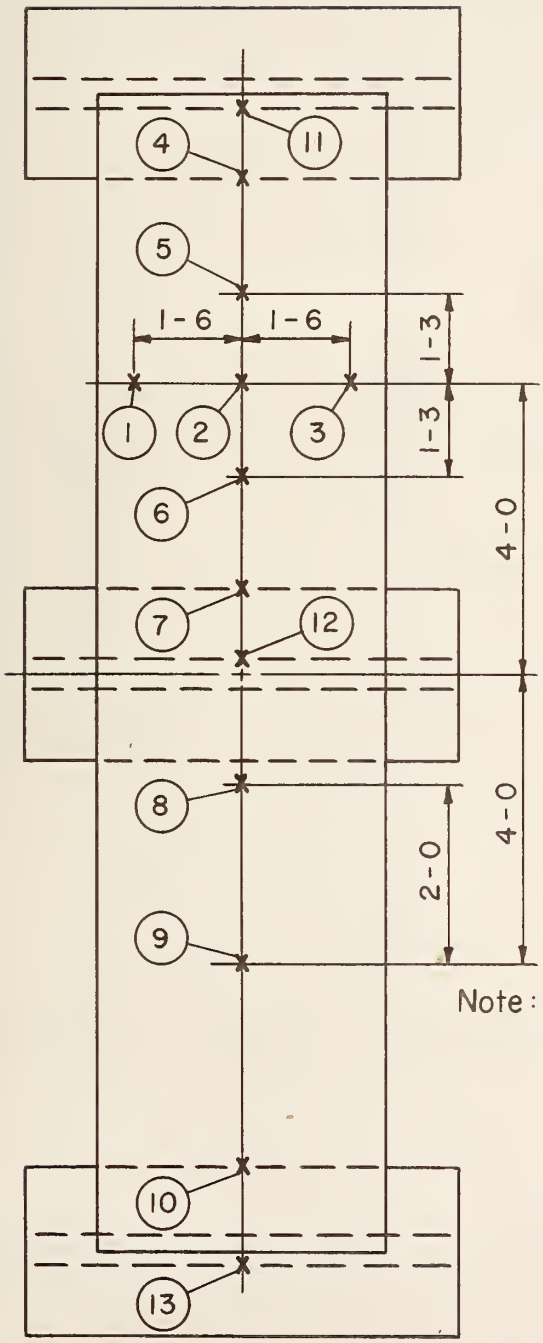

Note: LVDT's 4, 7, and 10 measure movement on girder flange. Nos. 11, 12, and 13 measure movement at bottom of girder stem. All others measure vertical movement of the bottom panel surface.

Figure 37. LVDT locations and identifications for unimpregnated and PIC single-panel tests.

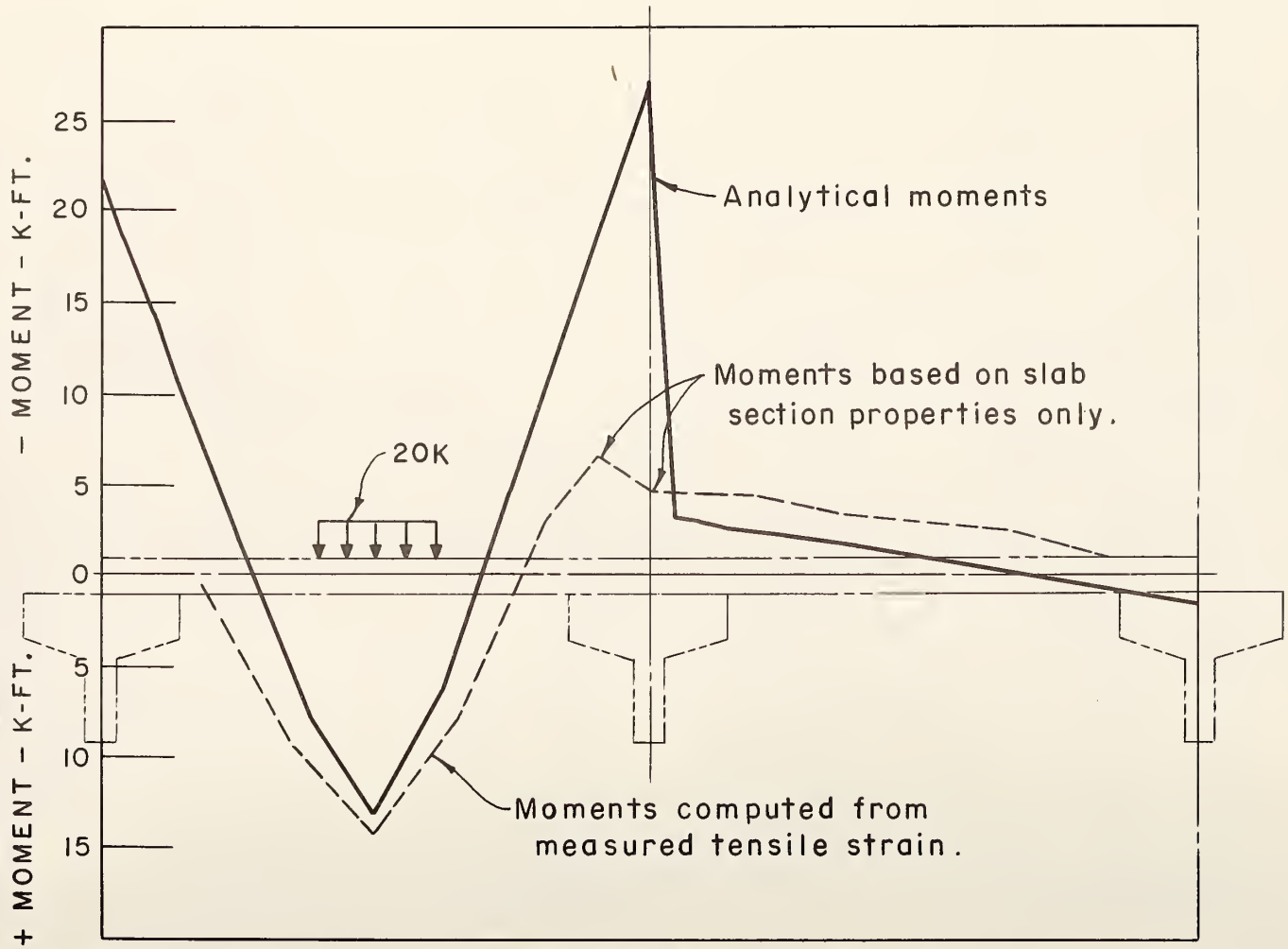

Figure 38. Plot of analytical moments and moments computed from tensile strains on the unimpregnated single-panel, 20 kip load at position 4.

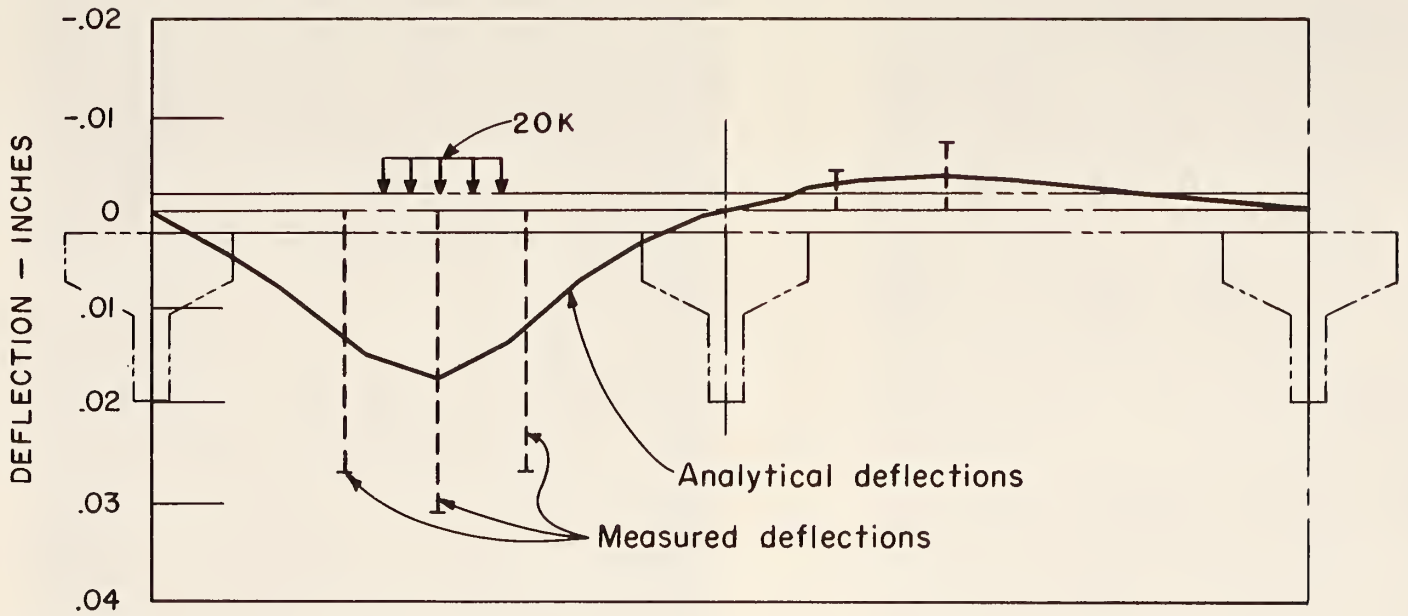

Figure 39. Plot of analytical and measured displacements on unimpregnated single-panel, 20 kip load at position 4.

Figure 40. Bottom of end girder support in unloaded span lifting off the test floor during unimpregnated single-panel test.

Figure 41. Cracks in the stem of the center girder support during failure test of the unimpregnated single-panel.

Figure 42. Failure of unimpregnated single-panel.

Figure 43. Failure of stud between embedded plate and panel at the end of the panel of the unimpregnated single-panel.

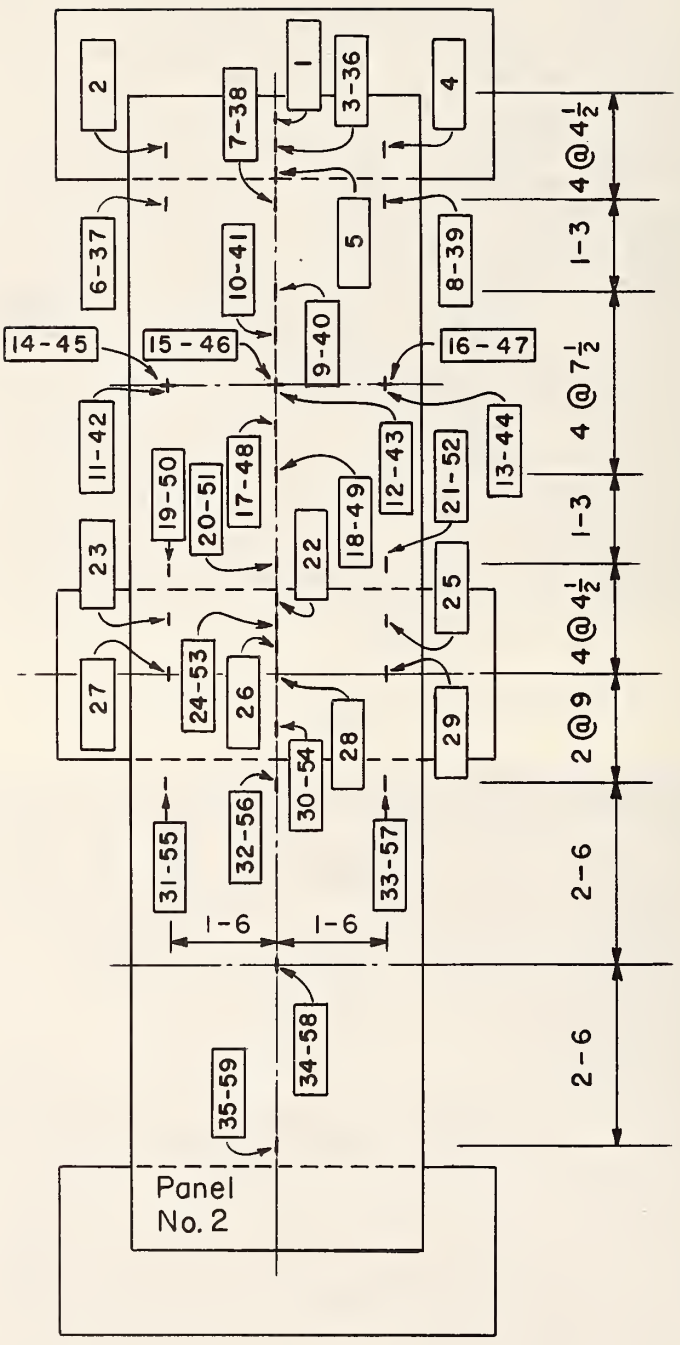

Note: Single numbers-gage on top surface only.
[X-Y] X is on top surface, Y is on bottom surface.

Figure 44. Strain gage locations and identifications for PIC single-panel No. 2, which was also used for the PIC single-panel fatigue test.

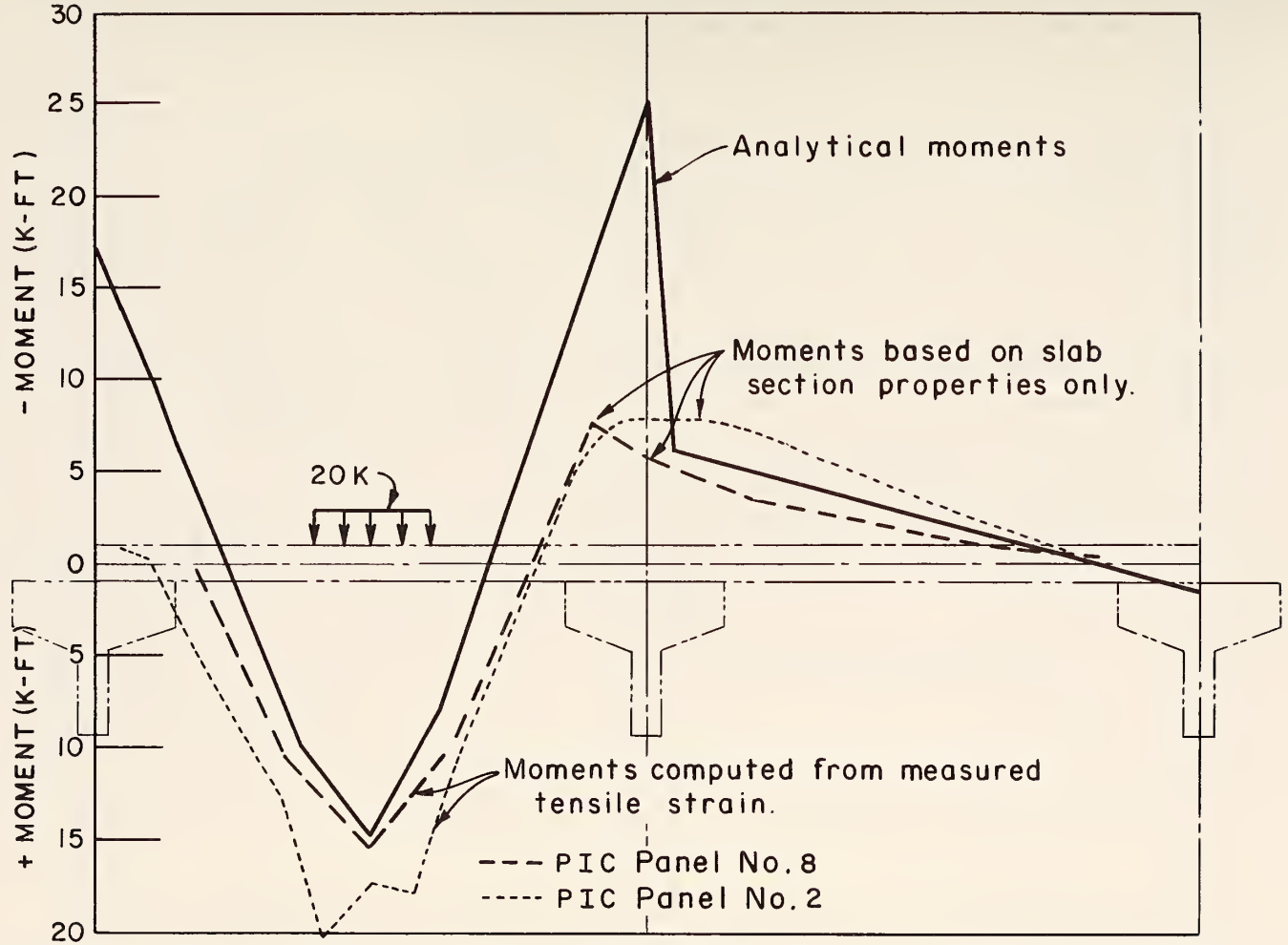

Figure 45. Plot of analytical moments and moments computed from measured tensile strains on PIC single-panels, 20 kip load at position 4.

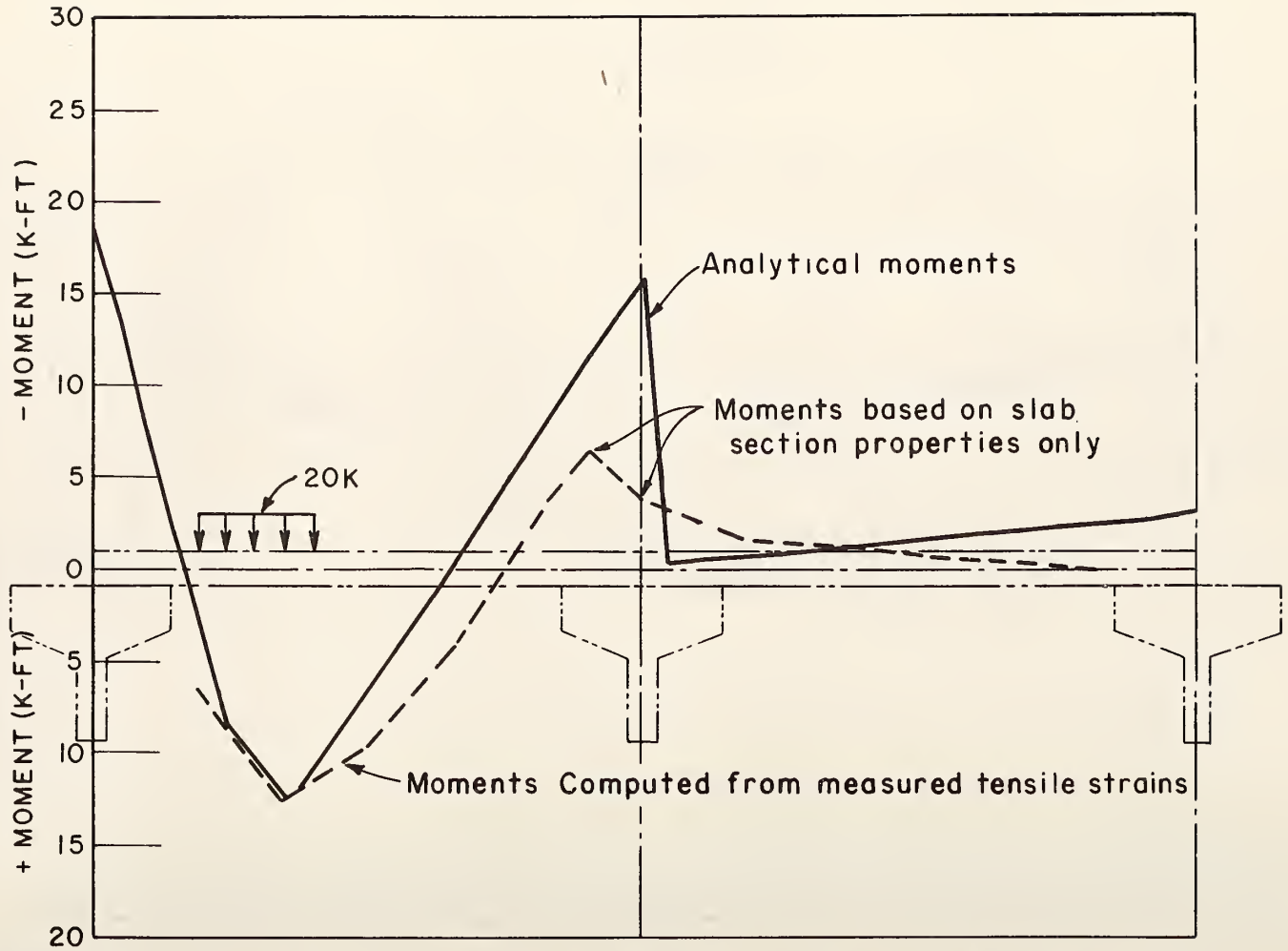

Figure 46. Plot of analytical moments and moments computed from measured tensile strains on PIC single-panels, 20 kip load at position 8.

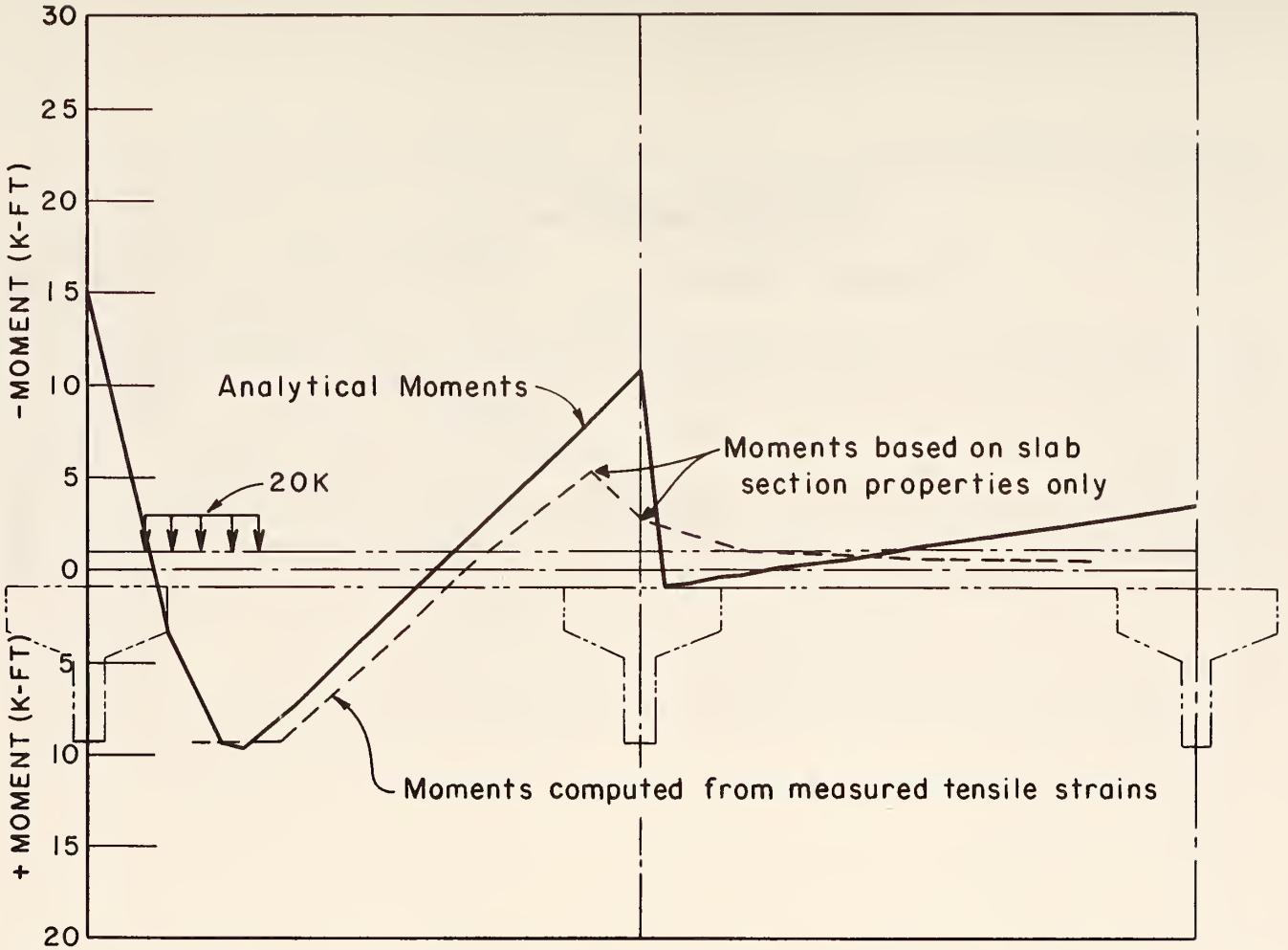

Figure 47. Plot of analytical moments and moments computed from measured tensile strains on PIC single-panels, 20 kip load at position 12.

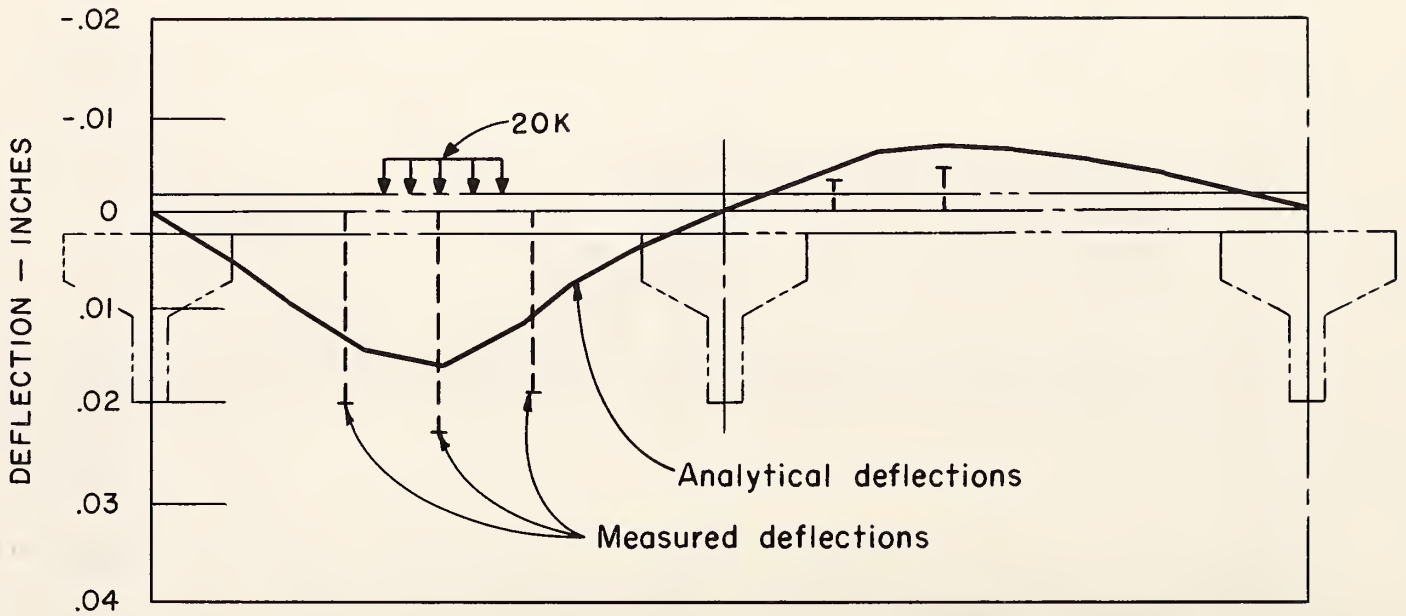

Figure 48. Plot of analytical and measured displacements on panel No. 8, 20 kip load at position 4.

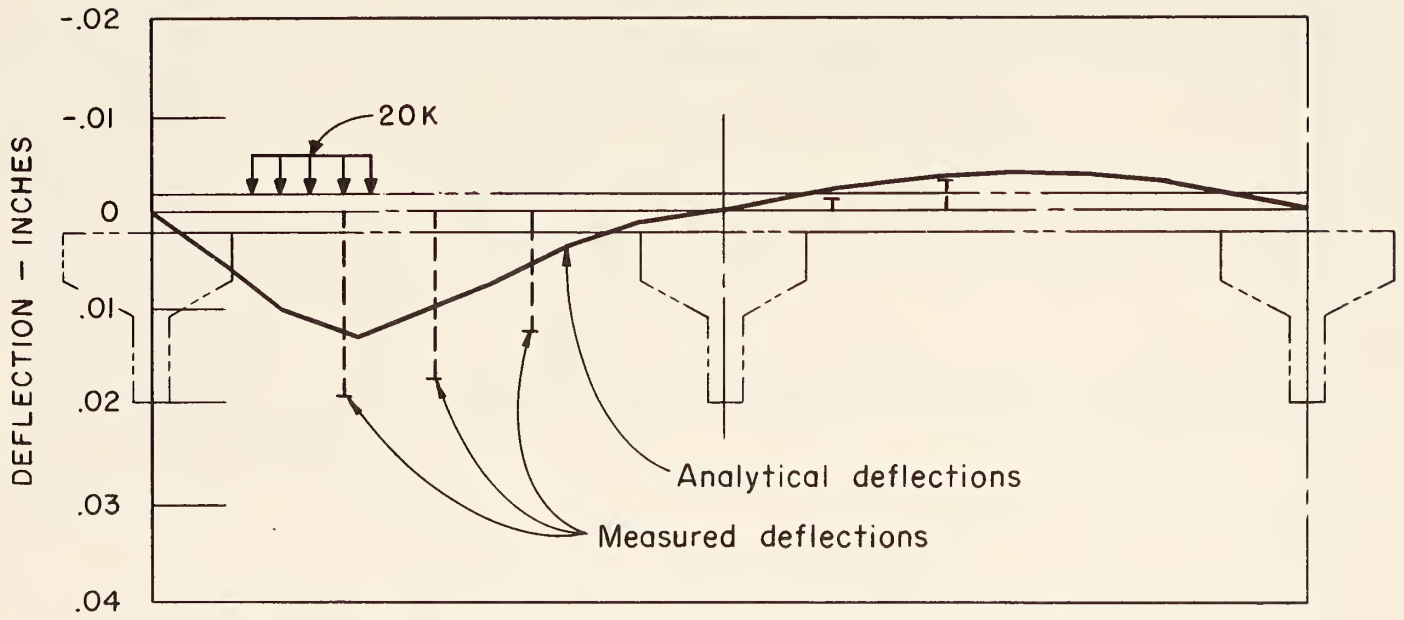

Figure 49. Plot of analytical and measured displacements on panel No. 8, 20 kip load at position 8.

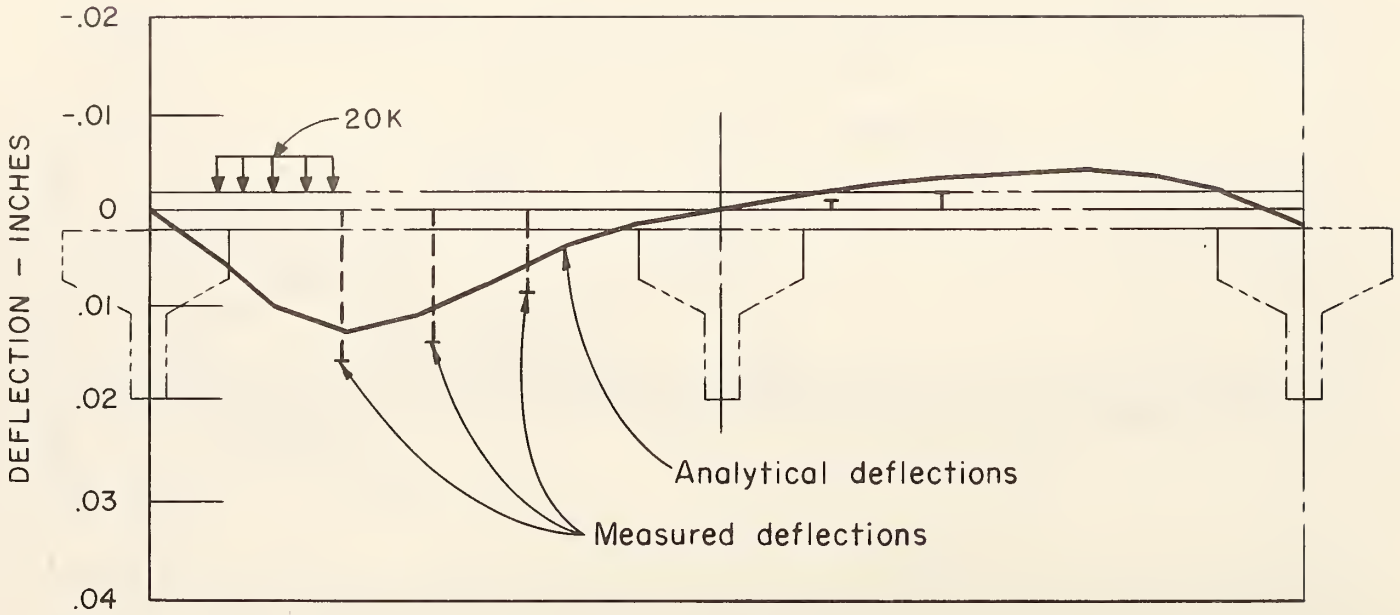

Figure 50. Plot of analytical and measured displacements on panel No. 8, 20 kip load at position 12.

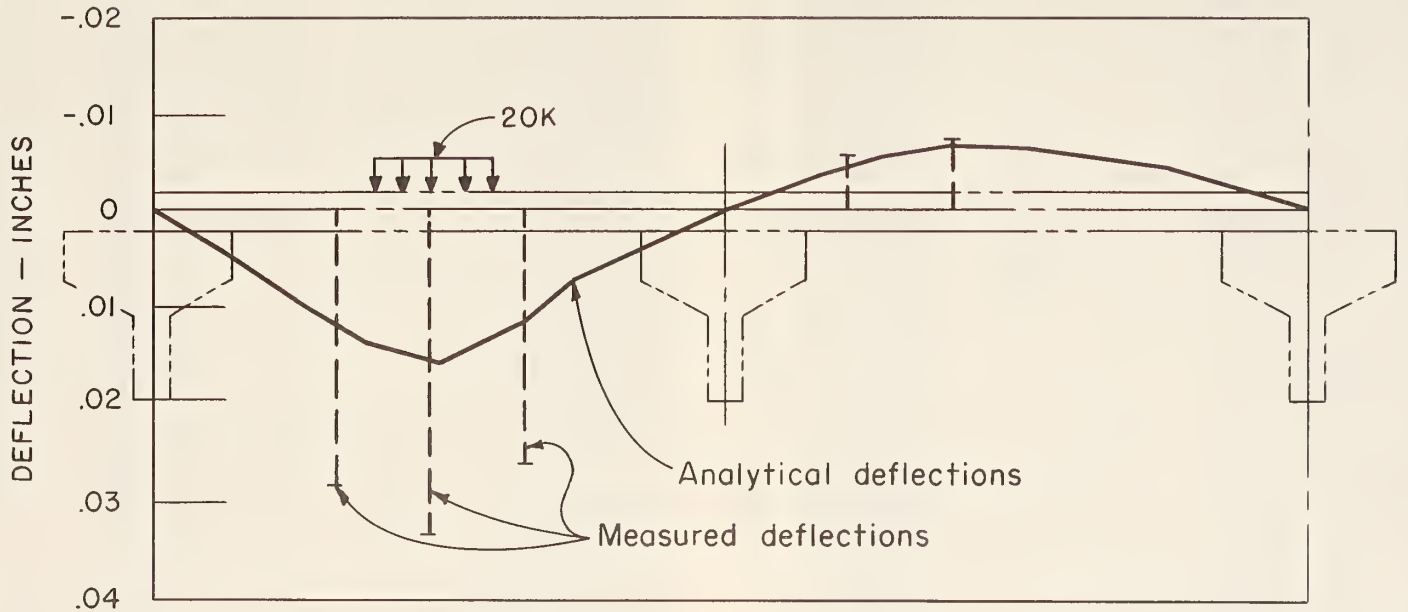

Figure 51. Plot of analytical and measured displacements on panel No. 2, 20 kip load at position 4.

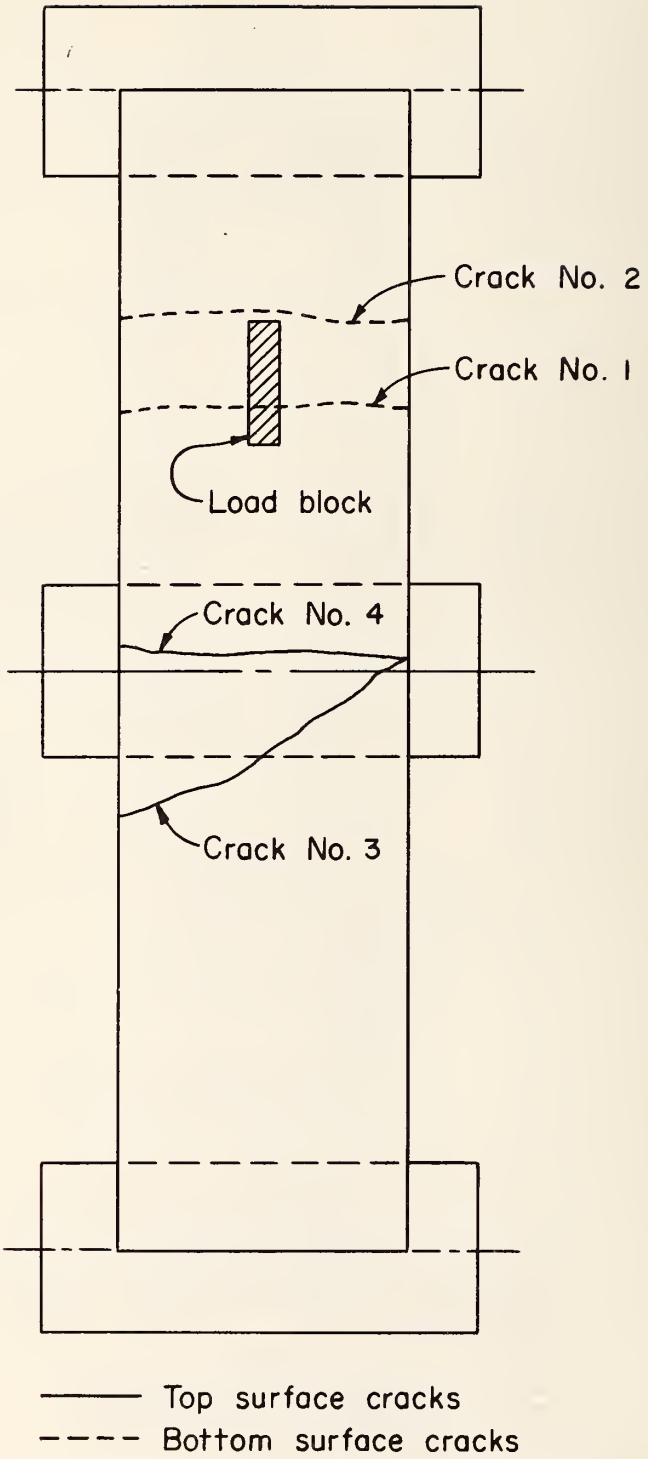

Figure 52. Crack pattern in panel No. 8 after ultimate load of 95 kips in load position 4.

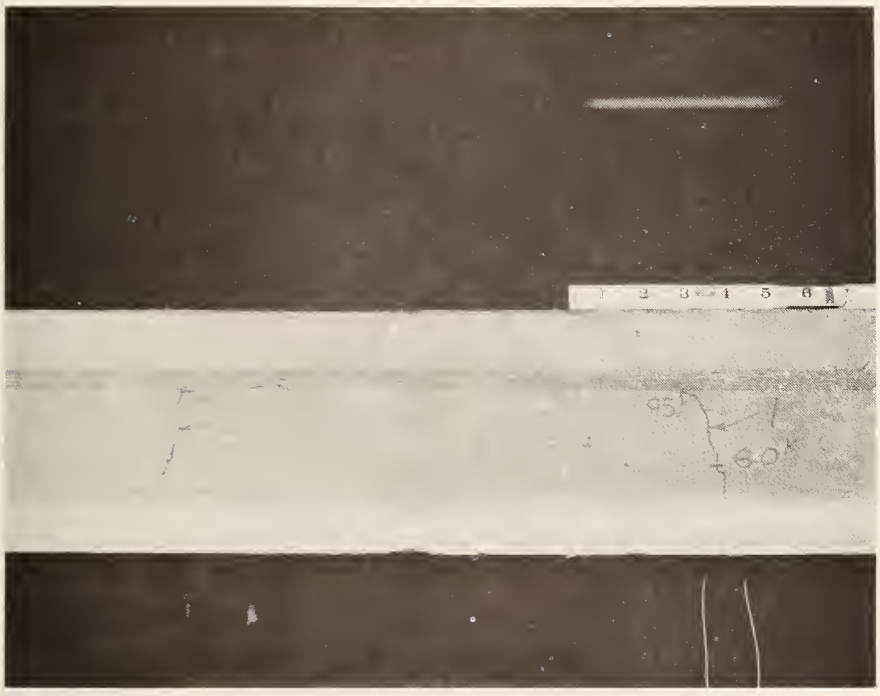

Figure 53. Positive moment cracks in panel No. 8 during single-panel static test; end of rule is midspan.

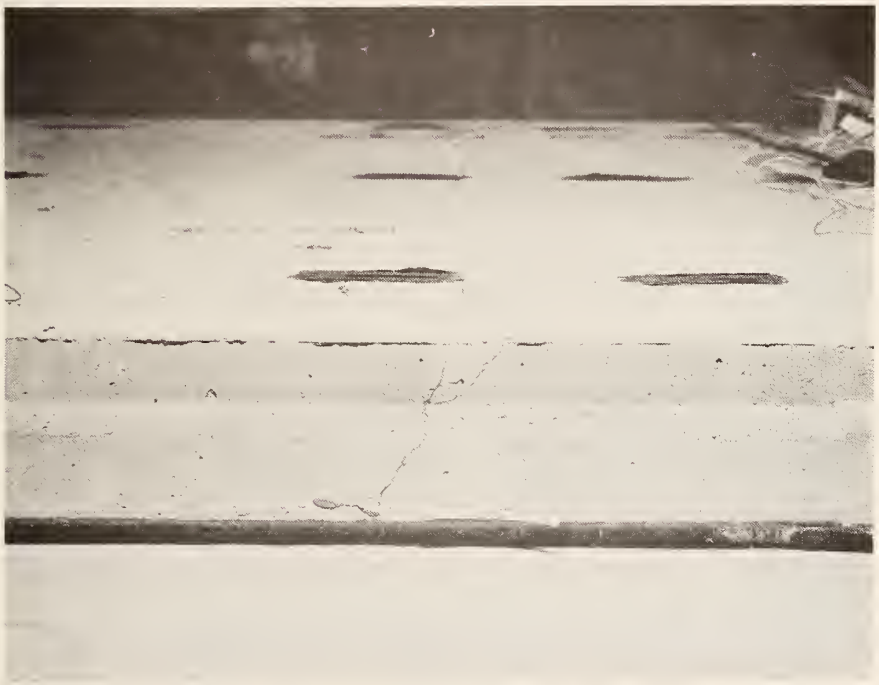

Figure 54. Intersection of cracks No. 3 and No. 4 over center girder support in panel No. 8 at ultimate load of 95 kips.

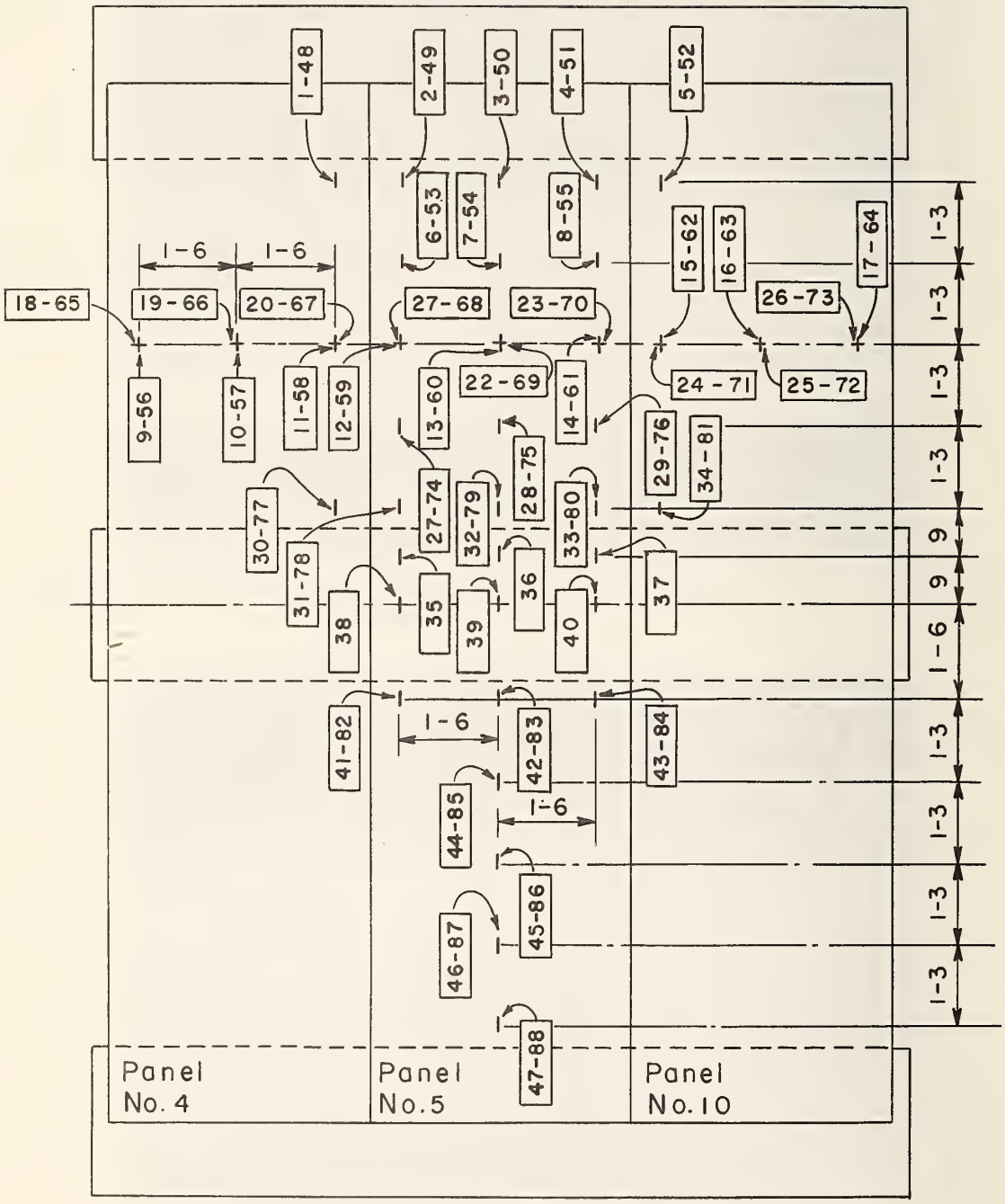

Note Single numbers-gage on top surface only.

X-Y X is on top surface, Y is on bottom surface.

Figure 55. Strain gage locations and identifications for first three-panel static test.

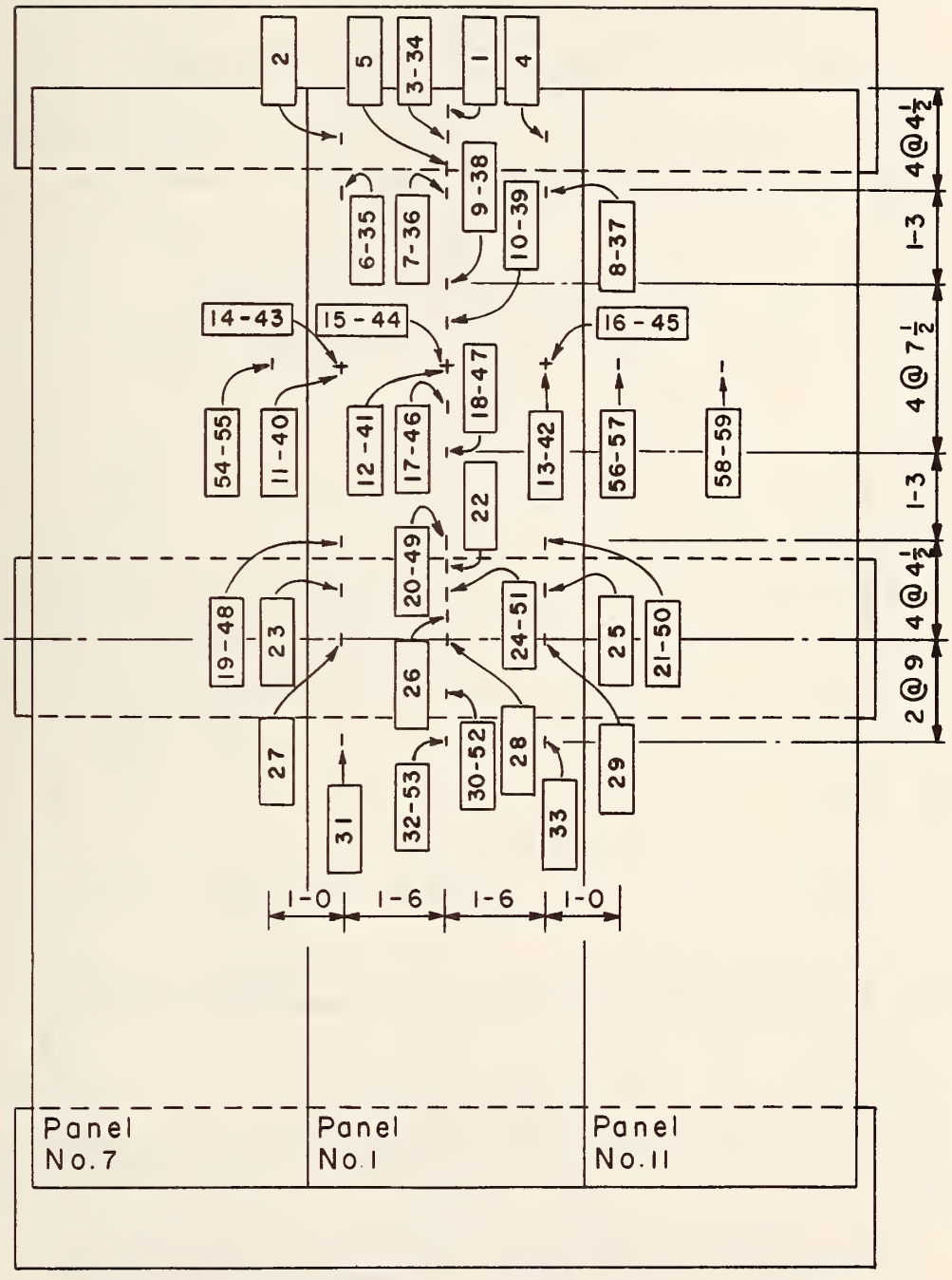

Note Single numbers-gage on top surface only.

[X-Y] X is on top surface, Y is on bottom surface.

Figure 56. Strain gage locations and identifications for second three-panel static test.

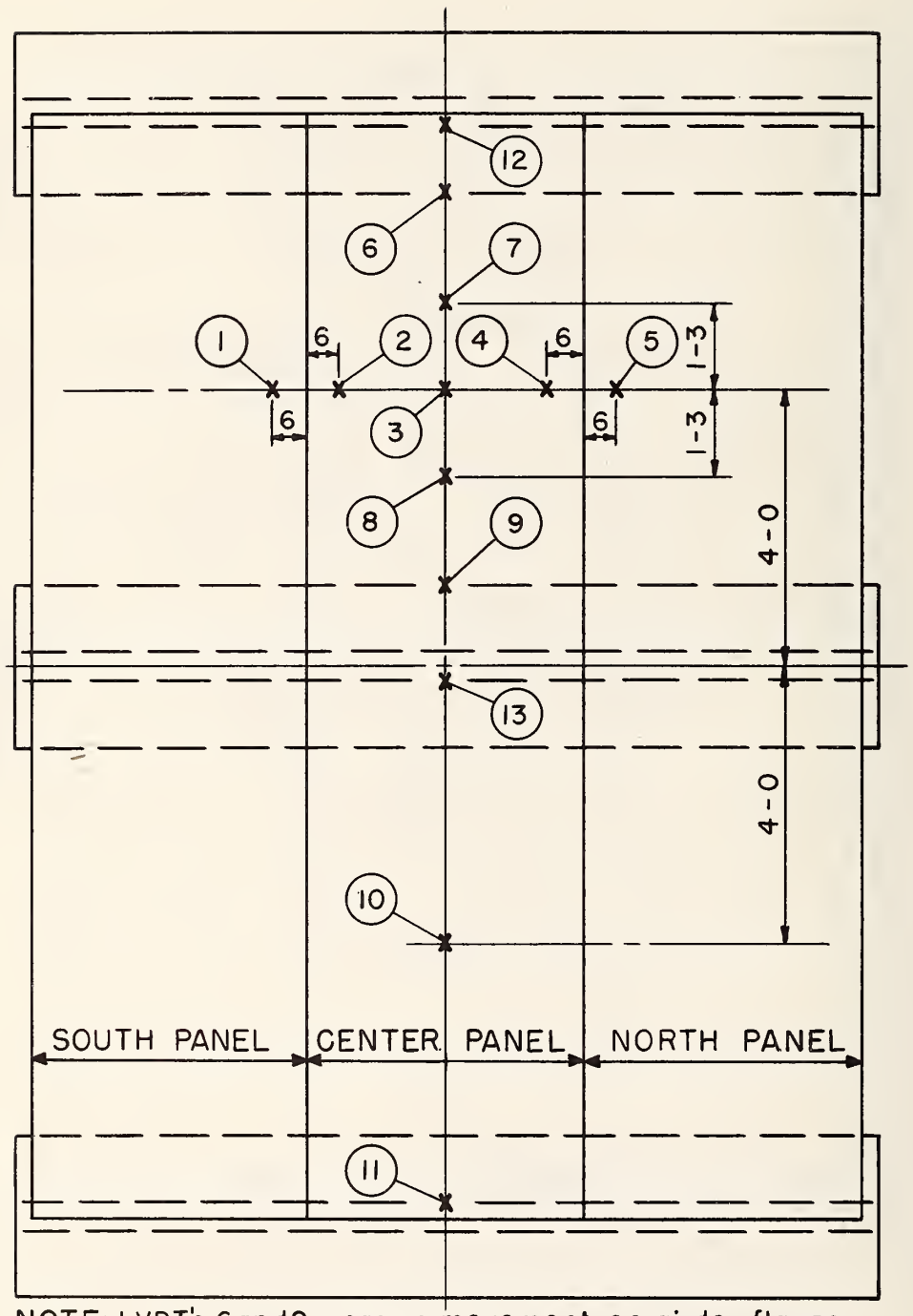

NOTE: LVDT's 6 and 9 measure movement on girder flange. Nos. 11, 12 and 13 measure movement at bottom of girder stem. All others measure vertical movement of the bottom panel surfaces.

Figure 57. LVDT locations and identifications for the three-panel tests.

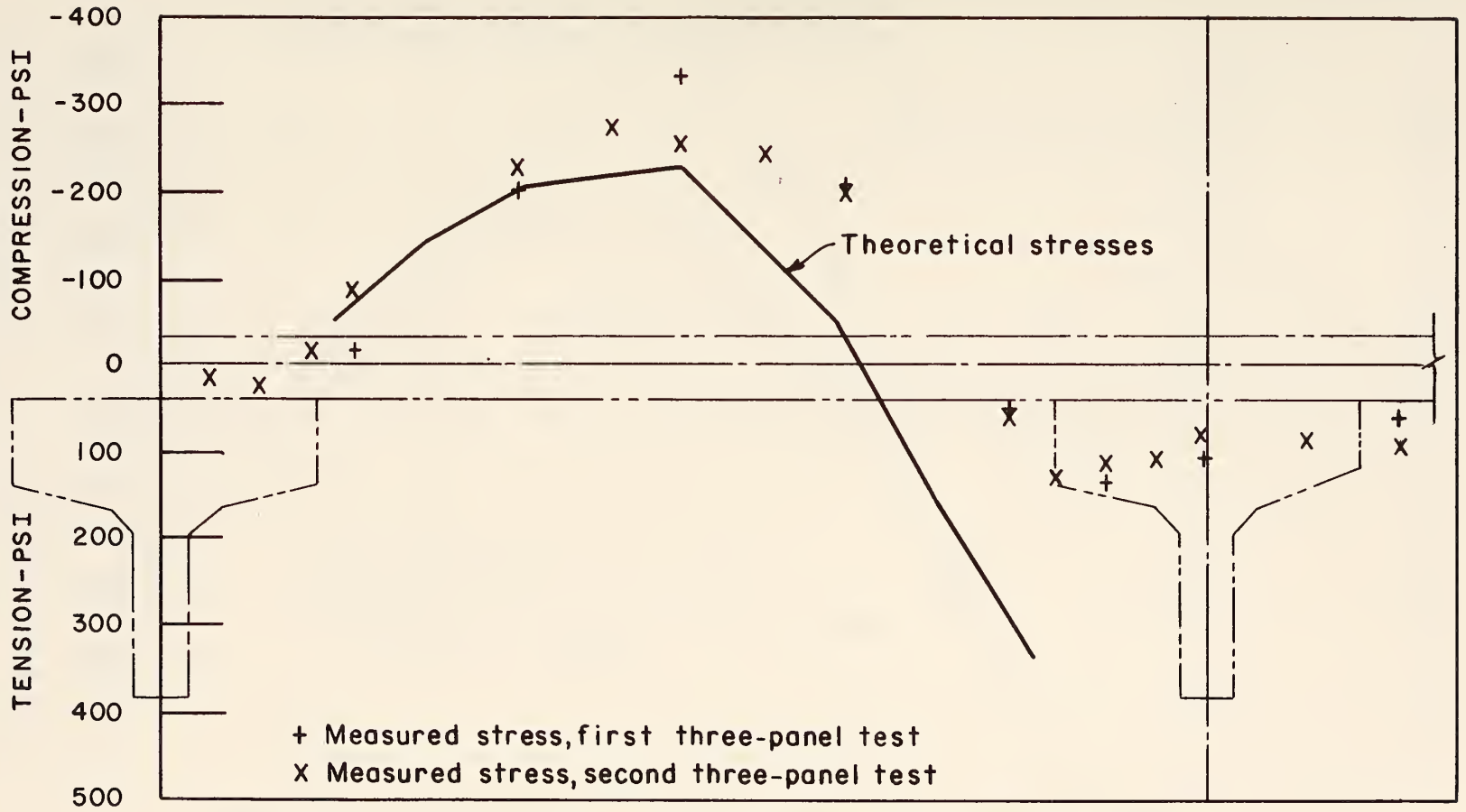

Figure 58. Plot of top theoretical and measured transverse stresses along the centerline of the center panel in three-panel tests for 20 kip load in position 1.

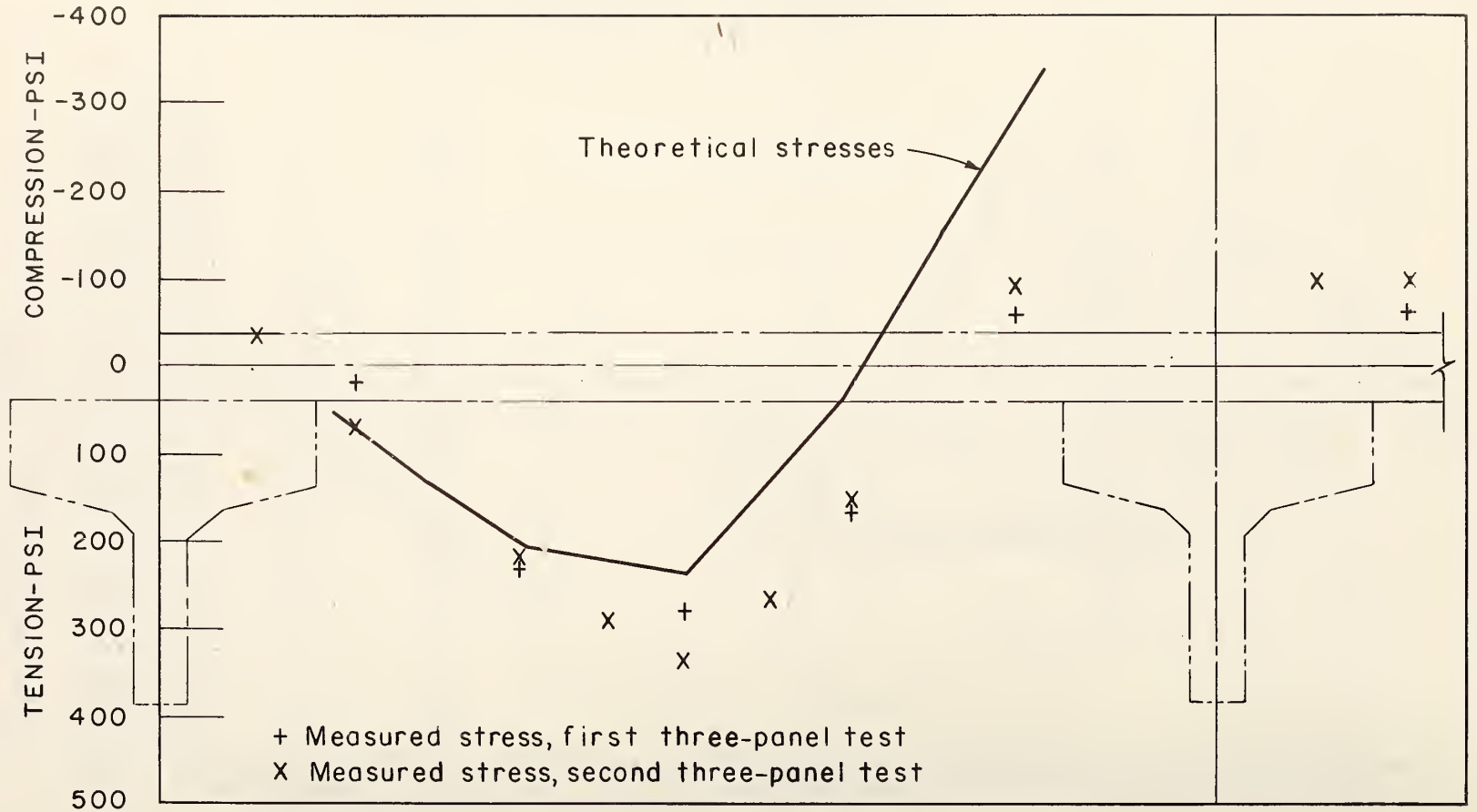

Figure 59. Plot of bottom theoretical and measured transverse stresses along the centerline of the center panel in three-panel tests for 20 kip load in position 1.

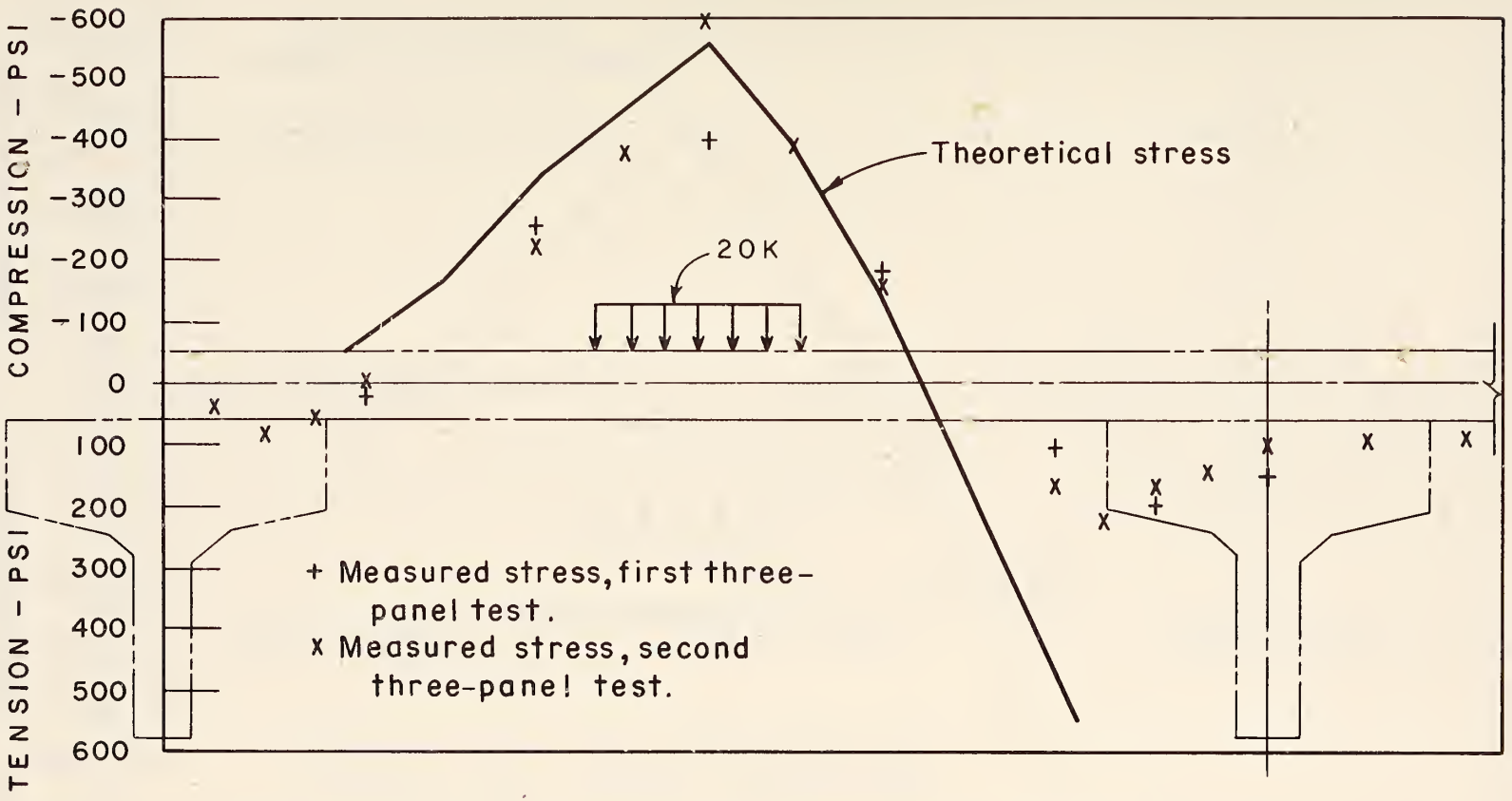

Figure 60. Plot of top theoretical and measured transverse stresses along the centerline of the center panel in three-panel tests for 20 kip load in position 4.

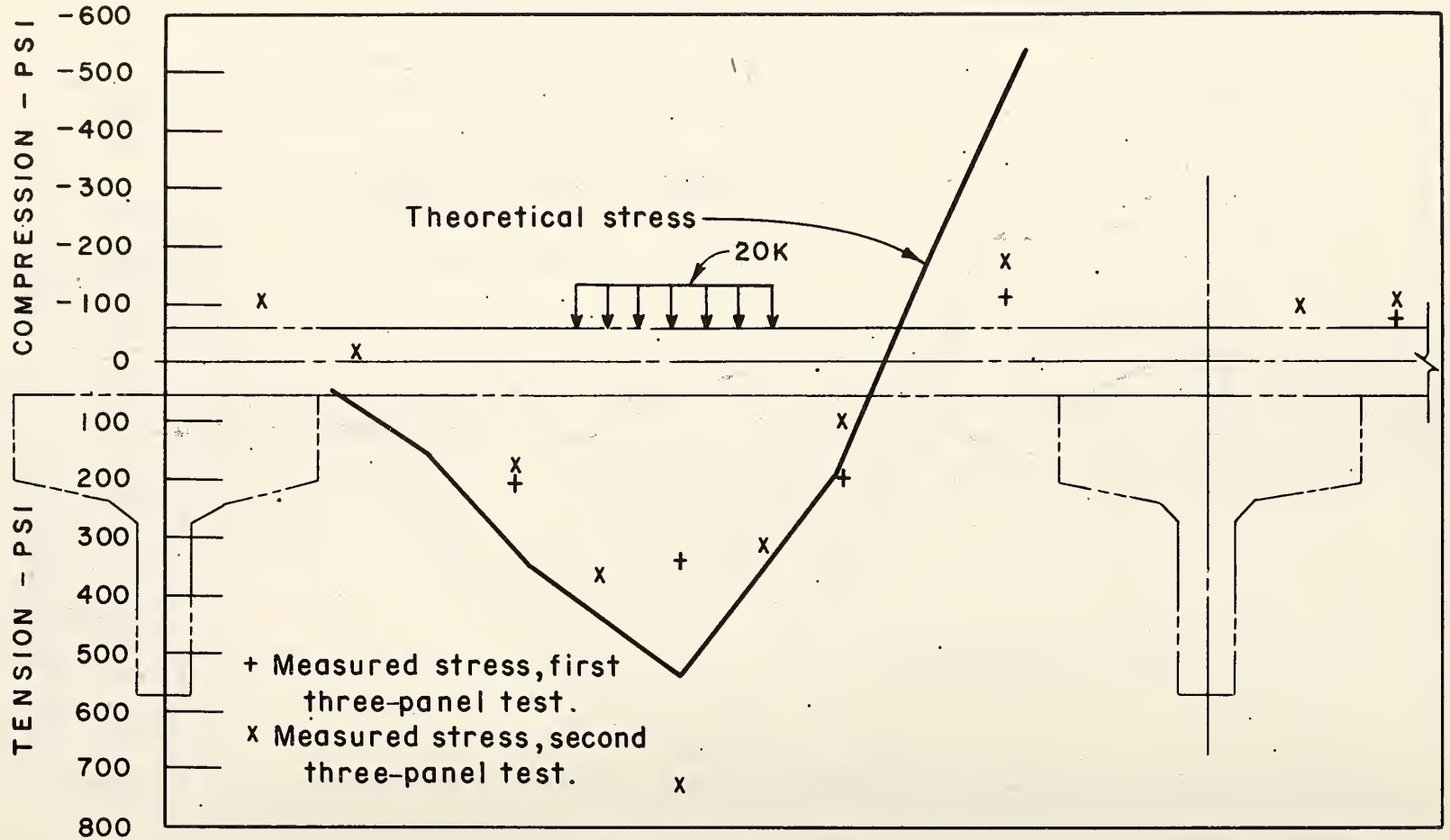

Figure 61. Plot of bottom theoretical and measured transverse stresses along the centerline of the center panel in three-panel tests for 20 kip load in position 4.

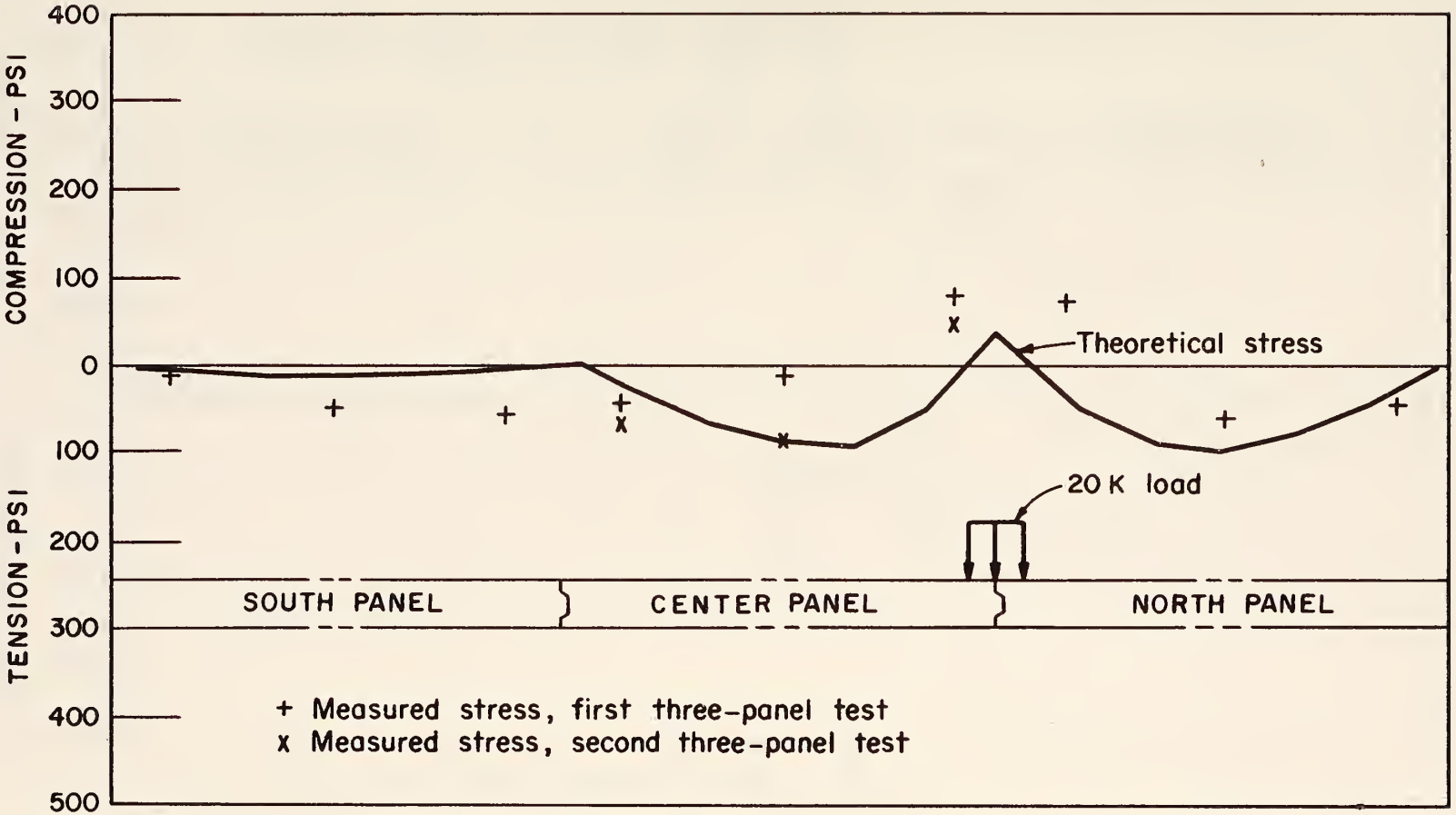

Figure 62. Plot of top theoretical and measured longitudinal stresses along the midspan section of three-panel tests for 20 kip load in position 1.

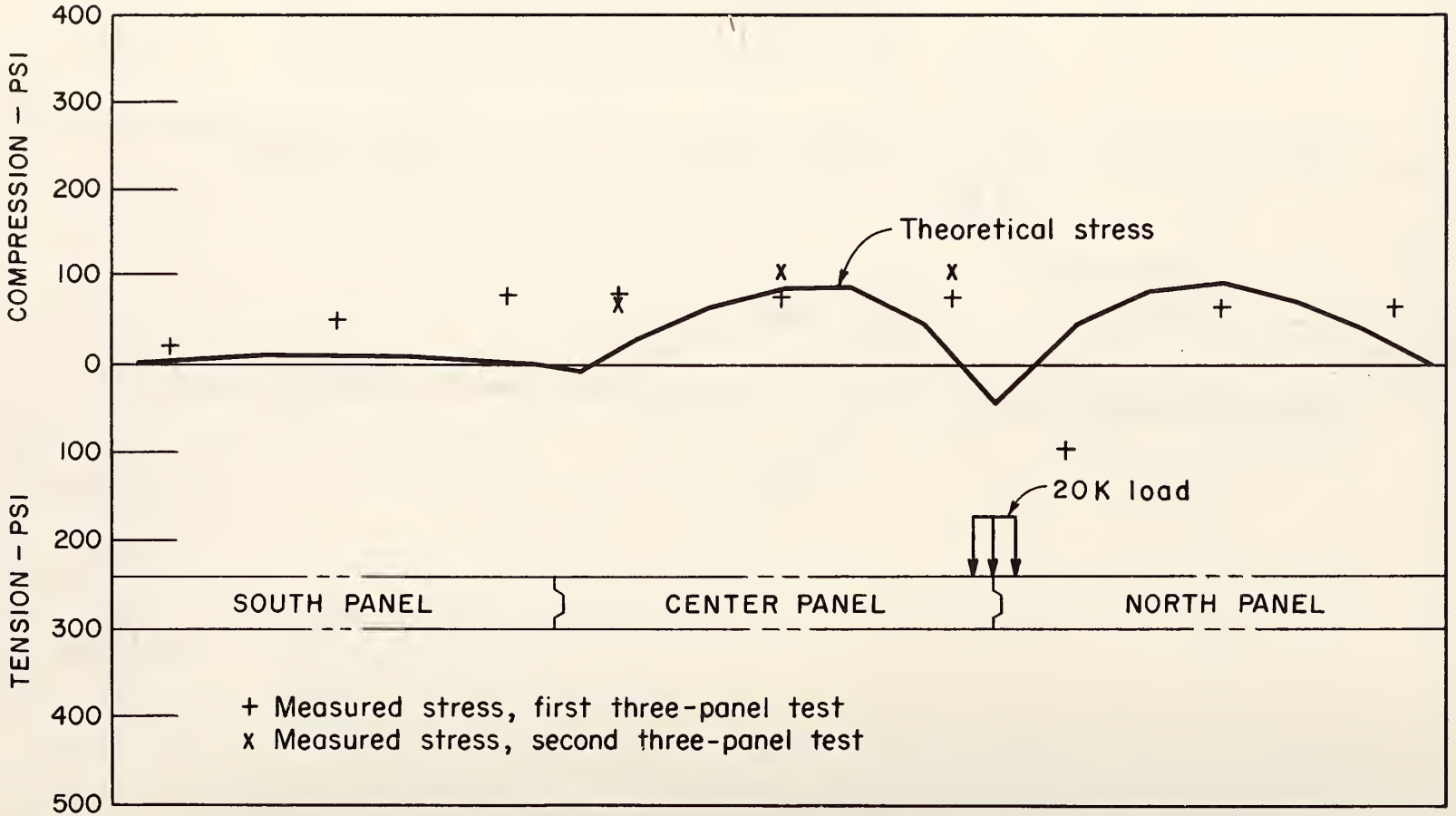

Figure 63. Plot of bottom theoretical and measured longitudinal stresses along the midspan section of three-panel tests for 20 kip load in position 1.

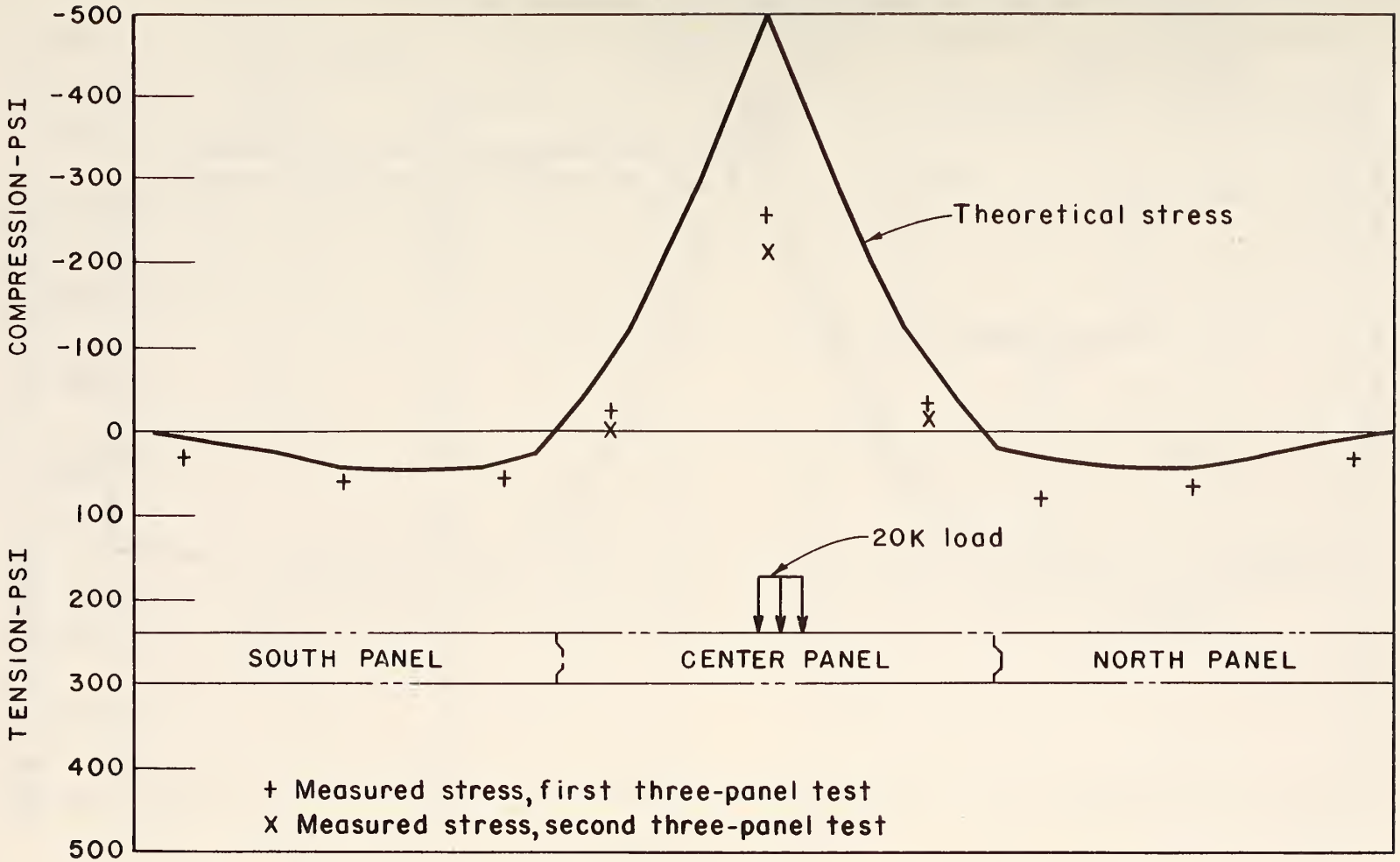

Figure 64. Plot of top theoretical and measured longitudinal stresses along the midspan section of three-panel tests for 20 kip load in position 4.

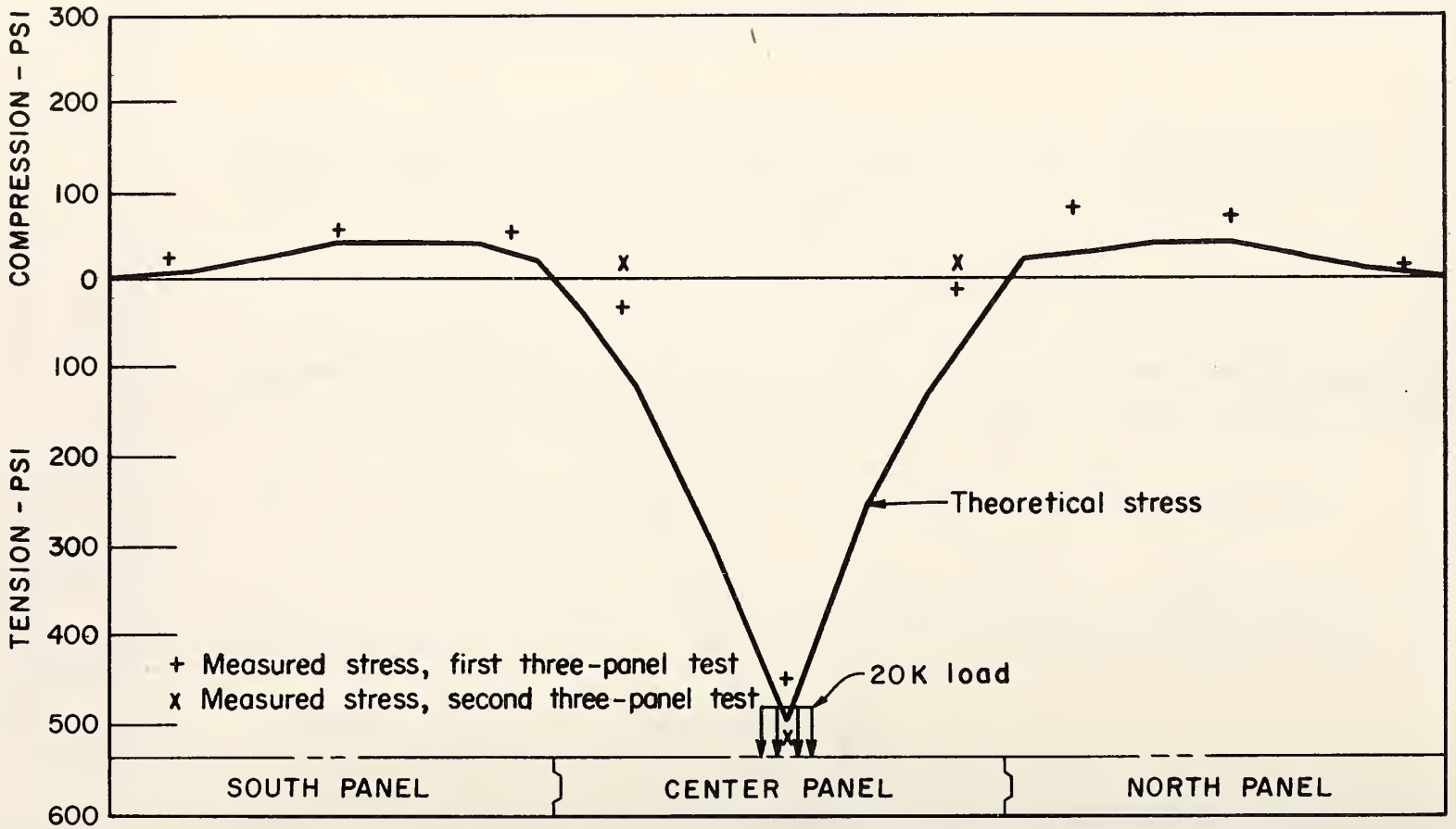

Figure 65. Plot of bottom theoretical and measured longitudinal stresses along the midspan section of three-panel tests for 20 kip load in position 4.

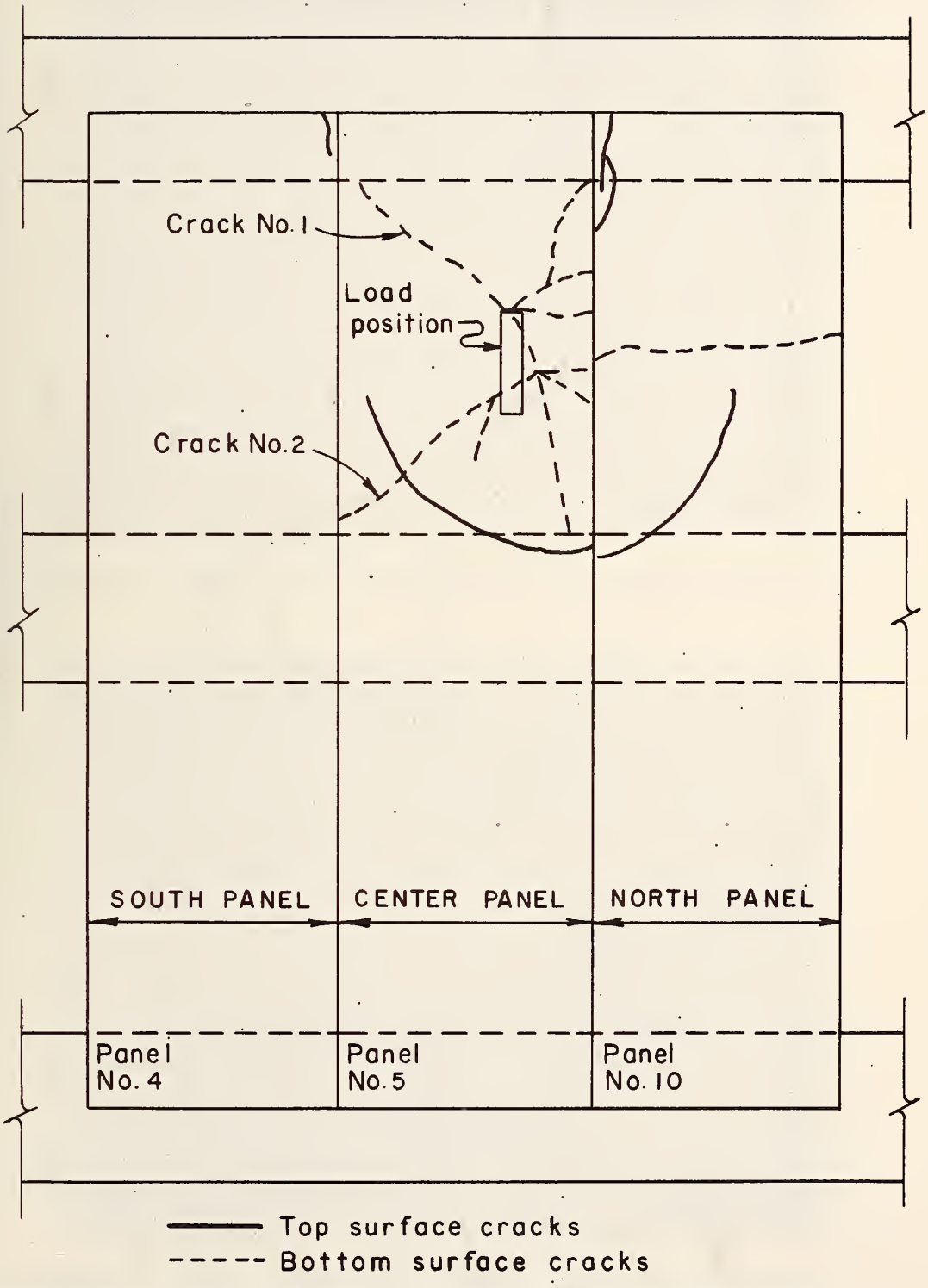

Figure 66. Crack pattern in first three-panel test after ultimate load of 160 kips in load position 3.

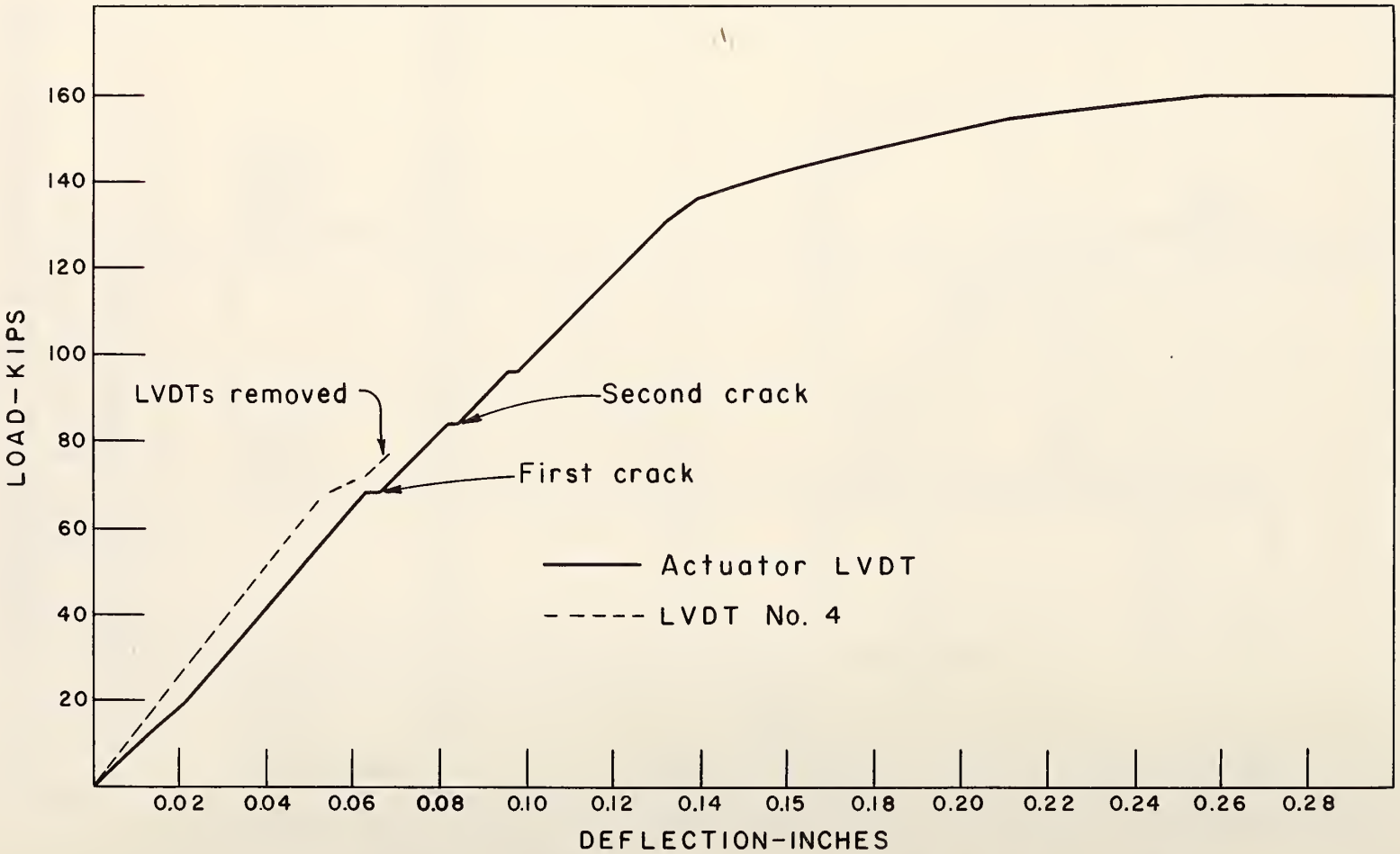

Figure 67. Plot of load versus deflection from the failure loading on the first three-panel test with load in position 3.

Figure 68. Shear crack between south and center panels at the transverse joint, south panel is on the right.

Figure 69. Shear crack between center and north panels at the transverse joint, center panel is on the right.

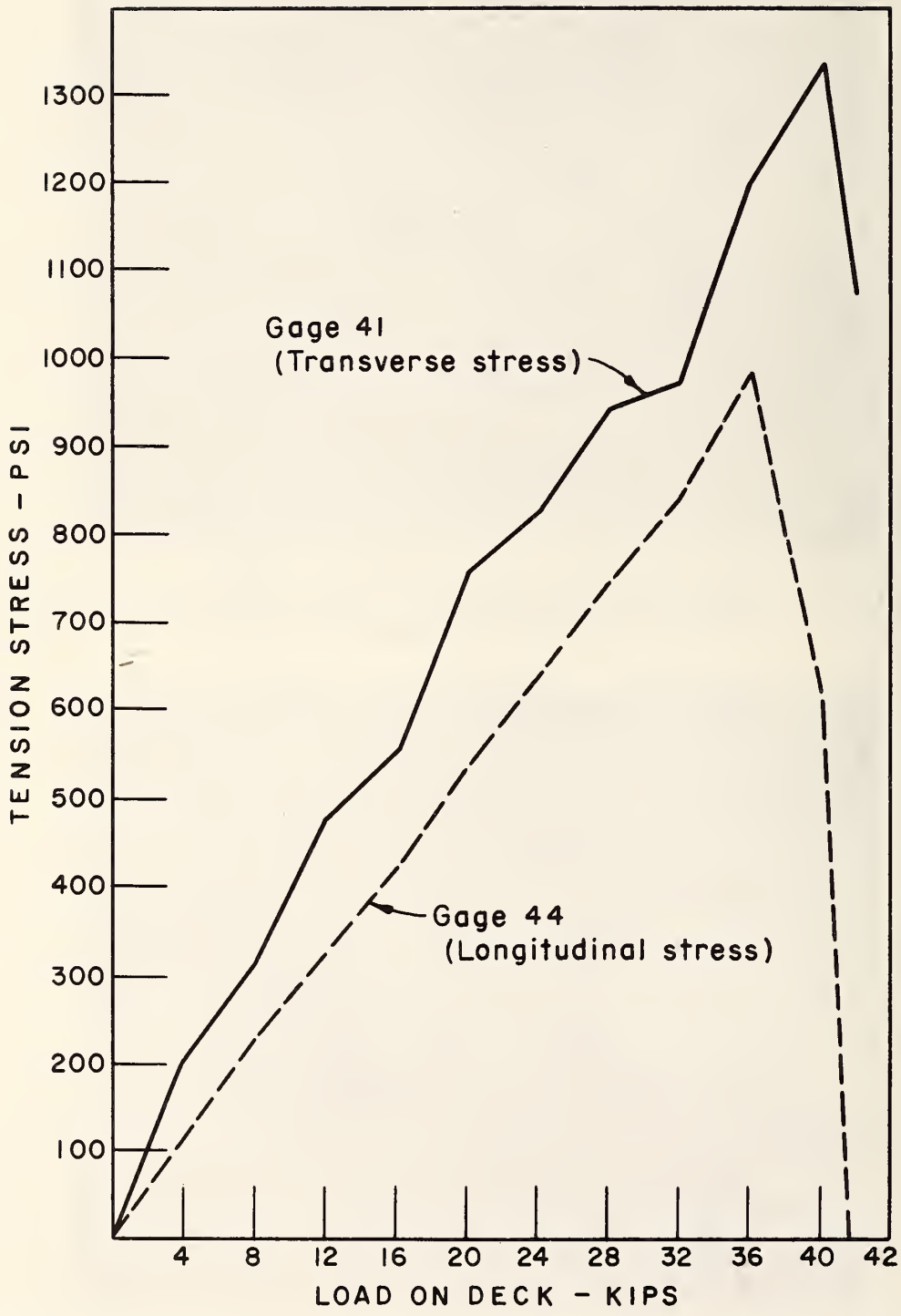

Figure 70. Plots of transverse and longitudinal stresses versus load obtained during static preloading of second three-panel test, load in position 4.

Figure 71. Failure of bottom prestress strand after fatigue loading for 300,000 cycles with load of 5 to 42 kips in load position 4.

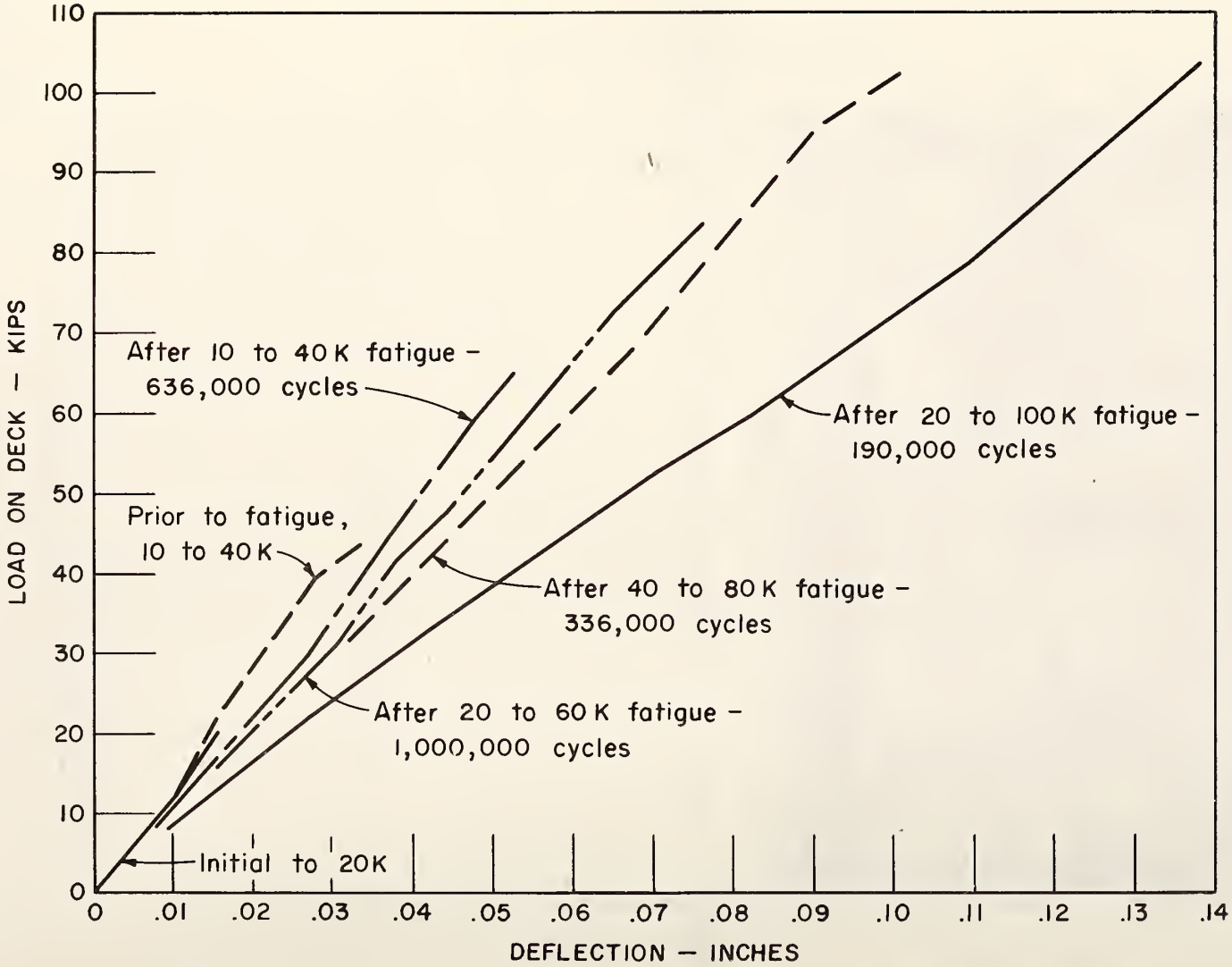

Figure 72. Plot of deflection versus load before and after cyclic load of the three-panel fatigue test.

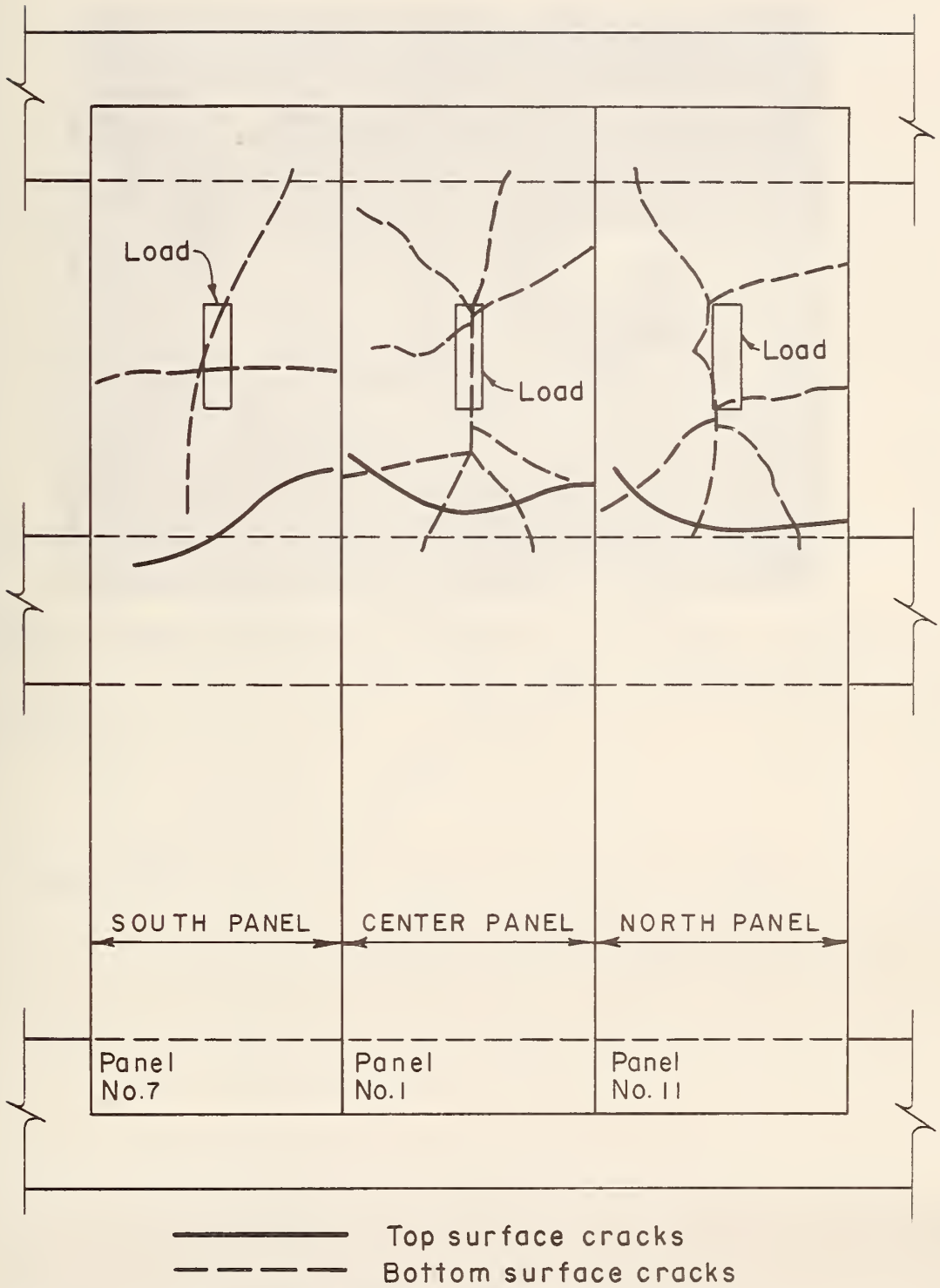

Figure 73. Crack patterns resulting from static failure loading on each of the three panels in the second three-panel test following 2.1 million cycles of fatigue loading.

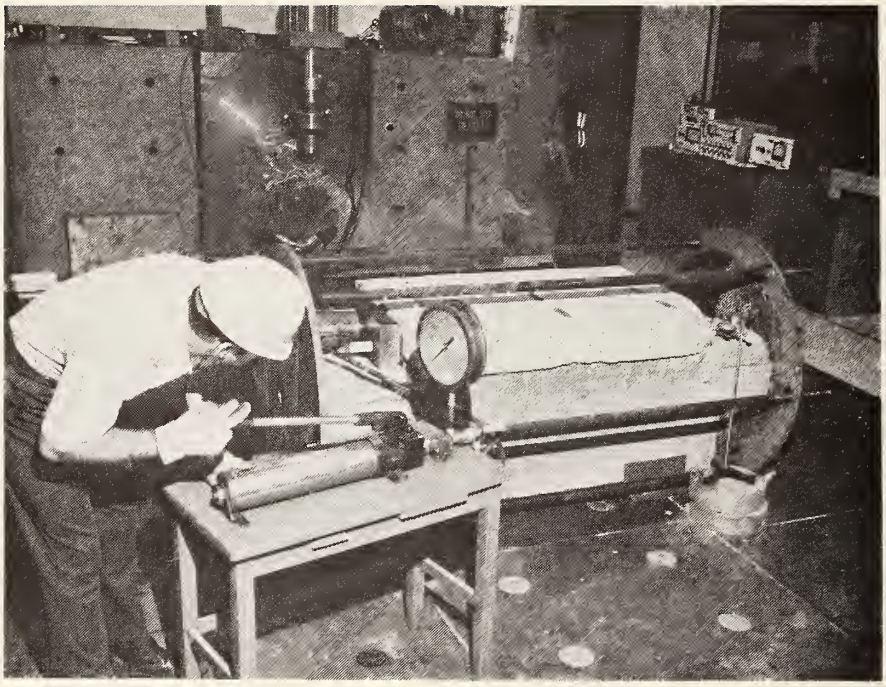

Figure 74. Shear test to evaluate the horizontal shear capacity between a panel and center girder support.

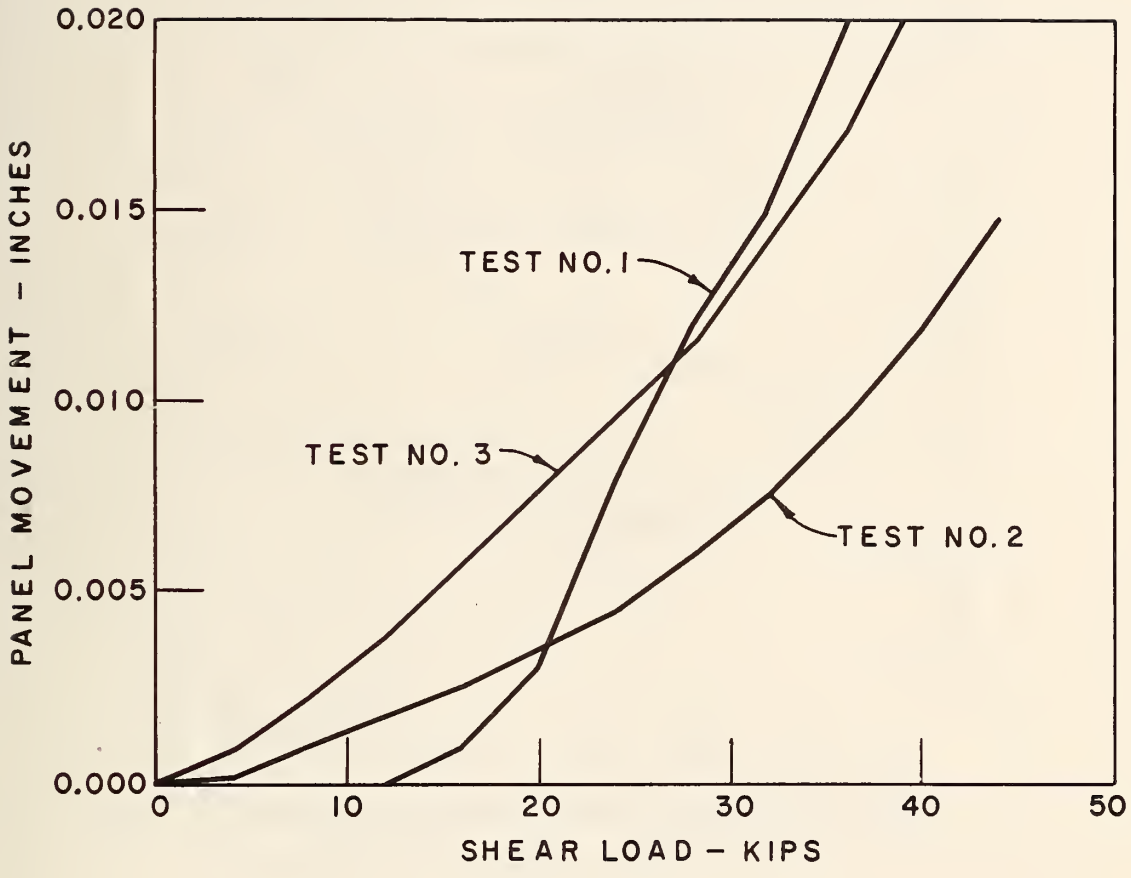

Figure 75. Panel movement versus shear load from tests of panel to girder connections.

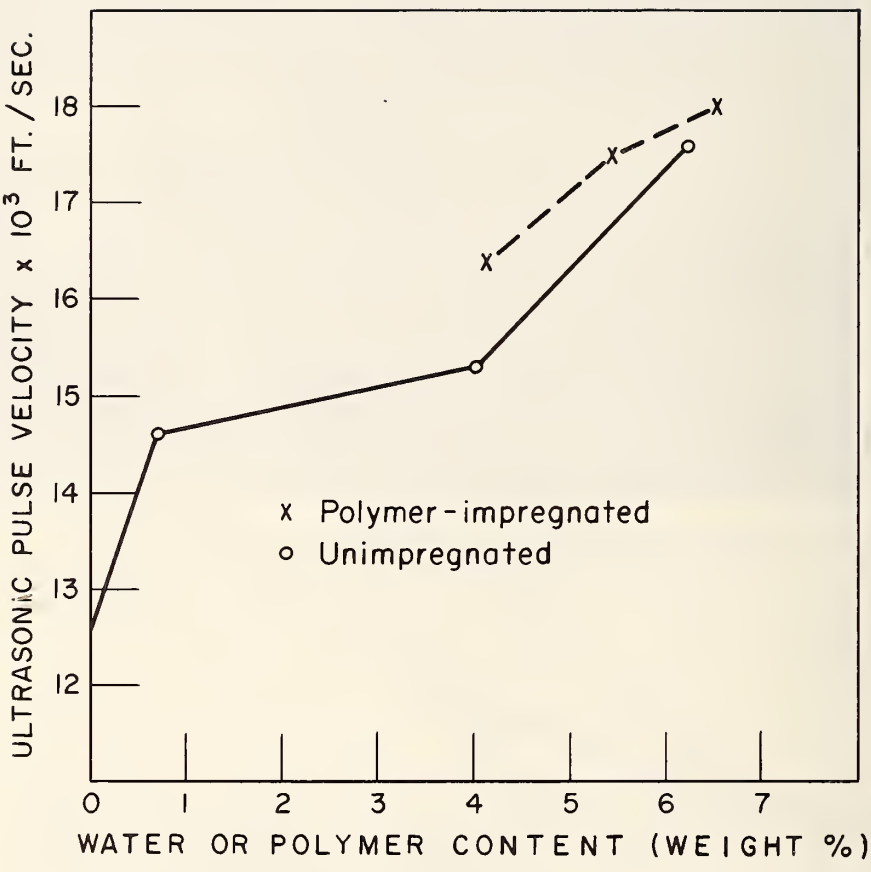

Figure 76. Ultrasonic pulse velocity of unimpregnated and PIC 3-by 6-inch cylinders.

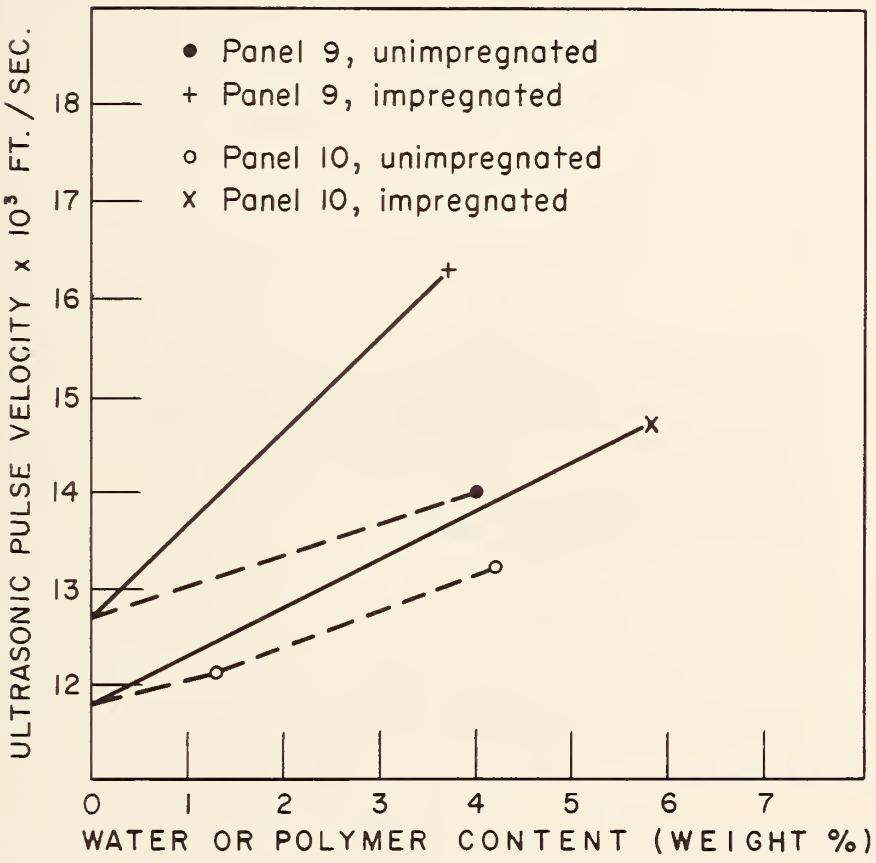

Figure 77. Ultrasonic pulse velocity of prestressed concrete bridge deck panels before and after impregnation.

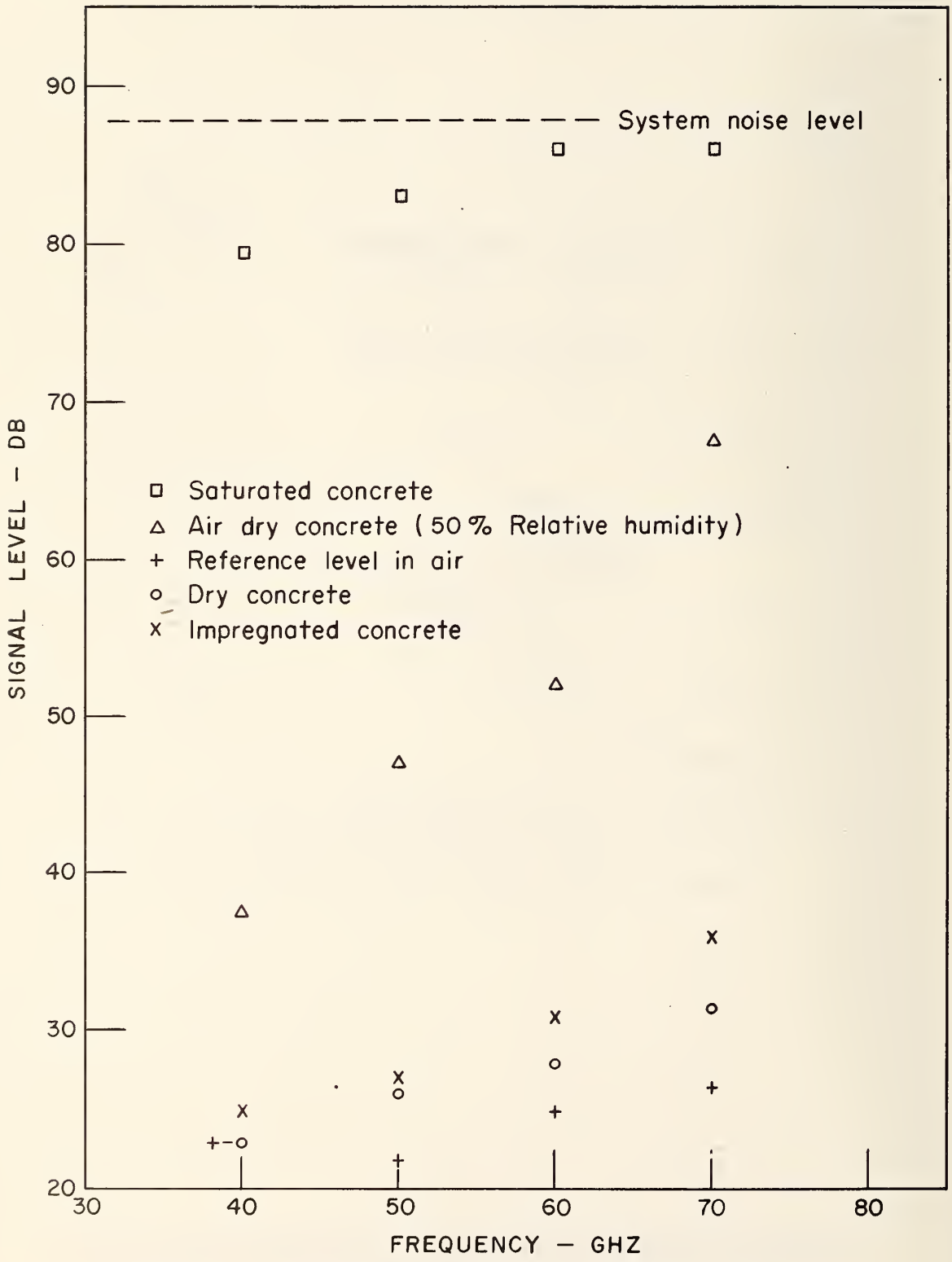

Figure 78. Microwave test of 6-by 12-inch cylinders.

APPENDIX A

PANEL DESIGN SUMMARY

DESIGN PROPERTIES FOR PANEL DESIGN.

Initial concrete prior to treatment

$f'_c = 5,500$ lb/in^2

$f'_{ci} = 4,000$ lb/in^2

$E = 3,000,000$ lb/in^2

Density $= 145$ lb/ft^3

Polymer-impregnated concrete

$f'_c = 15,000$ lb/in^2

$E = 6,000,000$ lb/in^2

$f_r = 1,300$ lb/in^2

$v_c = 750$ lb/in^2

Poisson's Ratio $= 0.20$

Note: The above properties of PIC are based on tests conducted in research programs prior to this study.

DETERMINE THICKNESS OF PIC PANEL

The thickness of PIC panel is to be such as to have the same dynamic response as a 7.5-inch thick conventional concrete slab.

$$\omega_{n\,PIC} = \omega_{n\,cc}$$

General Euler Equation for a Beam

$$\omega_n = n^2 \sqrt{\frac{gEI}{w}}$$

where: n is a constant which is dependent upon boundary conditions.

E = modulus of elasticity

I = moment of inertia $= \frac{bt^3}{12}$

w = weight per foot $= bt\gamma$

$$\frac{E_{PIC}\, t_{PIC}^3}{t_{PIC}\, \gamma_{PIC}} = \frac{E_{cc}\, t_{cc}^3}{t_{cc}\, \gamma_{cc}}$$

assume: $E_{PIC} = 2E_{cc}$

$$\gamma_{PIC} = 1.05\, \gamma_{cc}$$

$$\frac{2\, t_{PIC}^2}{1.05} = t_{cc}^2$$

$$t_{PIC} = t_{cc} \sqrt{\frac{1.05}{2}}$$

$t_{cc} = 7.5$ inch

$$t_{PIC} = 5.4 \text{ inches.}$$

Say $t_{PIC} = 6$ inches because E_{PIC} might not be exactly 2 times E_{cc}

LOADING CONDITIONS

Maximum live load is HS20-44

Maximum wheel load, P = 16,000 lbs.

Determine contact area for wheel load, based on Section 1.3.4 AASHTO

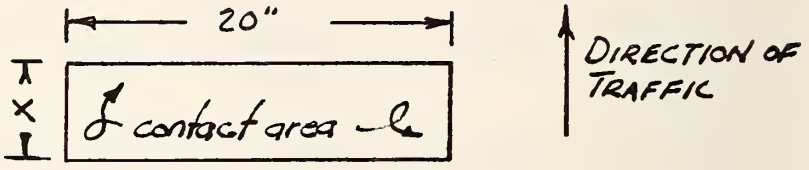

assume tire pressure = 150 lb/in²

$$20 \times (150) = 16{,}000$$
$$x = 5.33 \text{ in}$$

Use 5" x 20" contact area for appling load on top of panel
or
Use 11" x 26" contact area for appling load at center of panel

Axial load for HS20-44

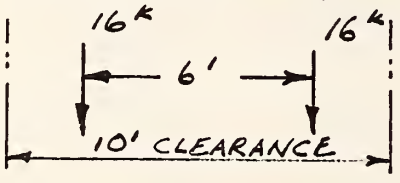

Span length of panel = clear span + depth of panel
(ACI 318-71 Section 8.5.2.1)
assume: girder flange width = 2'-4"

$$L = (8.0 - 2.33) + 0.5 = 6.17 \text{ ft}$$

Impact (Section 1.2.12 (c) AASHTO)

$$I = \frac{50}{6+125} = 0.38 > 0.30 \therefore I = 0.30$$

DESIGN OF PANEL USING AASHTO

Determine Live Load Moment
(Section 1.3.2 (c) AASHTO)

$$M_{LL} = \frac{(S+2)}{32} P_{20} \qquad S = 6.17' \quad P_{20} = 16{,}000\ lb$$

$$= \frac{(6.17+2)}{32}(16{,}000)$$

$$= 4{,}085 \text{ ft-lbs/ft}$$

Determine Dead Load Moment based on simple span

$$M_{DL} = \frac{wL^2}{8} = \frac{75(6.17)^2}{8}$$

$$= 357 \text{ ft-lbs/ft}$$

Impact Moment

$$M_I = 0.3(4{,}085) = 1{,}225 \text{ ft-lbs/ft}$$

Service Moment

$$M_T = M_{DL} + M_{LL} + M_I$$

$$= 5{,}667 \text{ ft-lbs/ft}$$

Section Properties of 1' width of slab

$$A_c = 6(12) = 72 in^2$$

$$I = \frac{12(6)^3}{12} = 216 in^4$$

Allowable Service Load Stresses.
(Section 1.5.26 (A) AASHTO)

Extreme fiber stress in comp. $= 0.4 f'_c$
Extreme fiber stress in tension $= 0.21 f_r$

DESIGN OF PANEL USING AASHTO, cont.

$f_c = 0.4(15{,}000) = 6{,}000 \text{ lb/in}^2$

$f_t = 0.21(1{,}300) = 273 \text{ lb/in}^2$

Determine amount of prestressing required / ft

assume: prestress loss of 20%
3/8 seven wire strand, $f_{pu} = 270$ ksi

$$\sigma = \frac{P}{A} \pm \frac{Mc}{I} \qquad P = 0.8(0.7 f_{pu} A_s) N = 12.88 N \text{ (kips)}$$

$$.273 = -\frac{12.88N}{72} + \frac{5.667(12)(3)}{216}$$

$N = 3.75$ or Say 4 strands / foot

If the panels were continuous over three or more girders than a continuity factor of 0.8 can be applied to moments

$M_{LL} = 4{,}085(0.8) = 3{,}268$ ft-lbs/ft

Service moment

$M_T = 357 + 3{,}268 + 0.3(3{,}268)$

$= 4{,}605$ ft-lbs/ft

Determine amount of prestress

$$.273 = -\frac{12.88N}{72} + \frac{4.605(12)(3)}{216}$$

$N = 2.76$ or Say 3 strands/foot

Check of stresses in panel prior to treatment.

$f'_{ci} = 4{,}000 \text{ lb/in}^2$

DESIGN OF PANEL USING AASHTO, cont.

Stresses at release using 4 3/8 in. strands per foot.

assume: concentric pattern-no dead load.

$$f_c = \frac{4(0.7 f_{pu} A_s)}{A_c}$$

$$= \frac{4(16.1)}{72} = .894 \text{ ksi}$$

or $894 \text{ lb/in}^2 < 0.60 f'_{ci} = 2400 \text{ lb/in}^2$

Stresses during handling

assume: pick up points 16 ft apart

$$M = \frac{wL^2}{8} = \frac{75(16)^2}{8} = 2400 \text{ ft-lb/ft}$$

$$f_H = \pm \frac{Mc}{I} = \frac{2.4(12)(3)}{216}$$

$$= \pm .40 \text{ ksi}$$

bottom fiber stress at lifting from prestressing bed.

assume 5% due elastic shortening

$$f_b = 0.95(894) - 400$$

$$= 450 \text{ lb/in}^2 \text{ (comp.)}$$

Stresses at release using 3 3/8 in. strands per foot.

assume: concentric pattern - no dead load

$$f_c = \frac{3(16.1)}{72} = .670 \text{ ksi}$$

DESIGN OF PANEL USING AASHTO, cont.

or $670\ lb/in^2 < 0.60 f'_{ci} = 2{,}400\ lb/in^2$

Stresses during handling

same assumption as previous

$$f_b = 0.95(670) - 400$$

$$= 236\ lb/in^2 \text{ (comp.)}$$

According to Section 1.3.2 (F) slabs designed in this method bond and shear are considered satisfactory.

However, this applies to cast-in-place concrete slabs and not a precast system of slabs.

From AASHO Specs. 10TH Edition 1969 Section 1.6.11, minimom percent of high-tensile-strength strand for bond anchorage is 0.3 percent.

$$\text{Minimom } A_s = 0.003(12)(6) = 0.216\ in^2/ft$$

If 3/8-inch strand is used.

No. of strands minimom /ft = 2.54

Say - 3 strands / ft.

Based on Section 1.6.11 AASHTO - Using 4 3/8 strands /ft

$$f^*_{su} = f'_s\left(1 - 0.5\frac{\rho^* f'_s}{f'_c}\right) \qquad \rho^* = \frac{4(0.085)}{12(3)}$$

$$= 270\left(1 - 0.5\frac{(0.009)(270)}{15}\right) \qquad = 0.009$$

$$= 248\ ksi \qquad \text{(Note: } d = 3\text{")}$$

No nonprestressed reinf.

$$\frac{\rho^* f^*_{su}}{f'_c} = \frac{0.009(248)}{15} = 0.149 < 0.3 \text{ O.K.}$$

DESIGN OF PANEL USING AASHTO, cont.

Check Ultimate Flexural Strength Section 1.6.9(A) AASHTO

For 4 3/8 strands/ft. $p^* = 0.009$

$$M_u = A^*_s f^*_{su} d \left(1 - 0.6 \frac{p^* f^*_{su}}{f'_c}\right)$$

$$= 0.34(248)(0.25)\left[1 - 0.6\frac{(0.009)(248)}{15}\right]$$

$$= 19.20 \text{ ft-k/ft}$$

or $M_u = 19{,}200$ ft-lb/ft

Service Moment without continuity factor

$M_T = 5{,}667$ ft-lb/ft Hence design looks good.

For 3 3/8 strands/ft $p^* = \frac{3(0.085)}{12(3)}$

$$= 0.007$$

$$f^*_{su} = f'_s\left(1 - 0.5\frac{p^* f'_s}{f'_c}\right)$$

$$= 270\left(1 - 0.5\frac{(0.007)270}{15}\right)$$

$$= 253 \text{ ksi}$$

$$M_u = 0.26(253)(0.25)\left[1 - 0.6\frac{(0.007)(253)}{15}\right]$$

$$= 15.28 \text{ ft-k/ft}$$

or $M_u = 15{,}280$ ft-lb/ft

Service Moment with 0.8 continuity factor

$M_T = 4{,}605$ ft-lb/ft Hence design looks good.

DESIGN OF PANEL USING AASHTO, cont.

Determine ultimate moment capacity required Section 1.6.5 AASHTO

$$M_{UR} = \frac{1.30}{\phi}[D + 2.2(L+I)]$$

$\phi = 1.0$ because panels will be factory produced.

Without 0.8 continuity factor.

$$M_{UR} = 1.30[357 + 2.2(4,085 + 1,225)]$$

$$= 15,650 \text{ ft-lb/ft}$$

With 0.8 continuity factor

$$M_{UR} = 1.30[357 + 2.2(3,268 + 980)]$$

$$= 12,610 \text{ ft-lb/ft}$$

Summary of Design

Without 0.8 continuity factor

Service moment, $M_T = 5,667$ ft-lb/ft

requires 4 3/8-in strand/ft, $f_{su} = 270$ ksi, concentric

Ultimate moment, $M_u = 19,200$ ft-lb/ft

Ultimate moment required,

$M_{UR} = 15,650$ ft-lb/ft

With 0.8 continuity factor

Service moment, $M_T = 4,605$ ft-lb/ft

requires 3 3/8-in strand/ft, $f_{su} = 270$ksi, concentric

DESIGN OF PANEL USING AASHTO, cont.

Summary of Design, cont.

Ultimate moment, M_u = 15,280 ft-lb/ft

Ultimate moment required,

M_{UR} = 12,610 ft-lb/ft

Without 0.8 continuity factor panel could be continuous over 2 girders and 8-foot center-to-center girders Max. L = 24 ft.

With 0.8 continuity factor panel could be continuous over 3 or more girders
Max. L = Bridge width

CHECK OF AASHTO DESIGN METHOD FOR PANELS

Since the design of the panel using AASHTO considers the panels to act as a slab it was decided to determine an effective width of the panel.

Take a simply supported beam 12" wide and determine max. moment due to live load and impact.

HS20-44 Wheel load = 16,000 lb.
Impact = 30 %.

Length of load = 20"

$$w = \frac{16{,}000 + 0.3(16{,}000)}{1.67}$$

$$= 12{,}500 \text{ lb/ft}$$

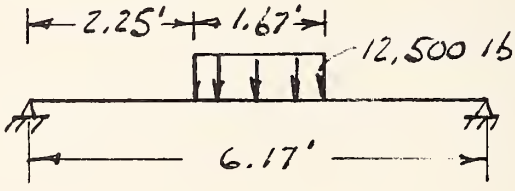

$$M_{max} = 10.44\left(\frac{6.17}{2}\right) - 12.5\left(\frac{0.935}{2}\right)^2$$

$$= 27.35 \text{ ft-k}$$

Using no continuity factor from AASHTO Design. or Dead Load

$$M' = 4.095 + 0.3(4.095) = 5.31 \text{ ft-k/ft}$$

$$be = \frac{M_{max}}{M'} = \frac{27.35}{5.31} = 5.24 \text{ ft}$$

Since panel width of 4-feet was selected and the possible discontinuity at the transverse joint the use of AASHTO is questionable.

DESIGN OF PANEL USING ELASTIC ANALYSIS

Portion of bridge deck to be analyzed (performed by USBR)

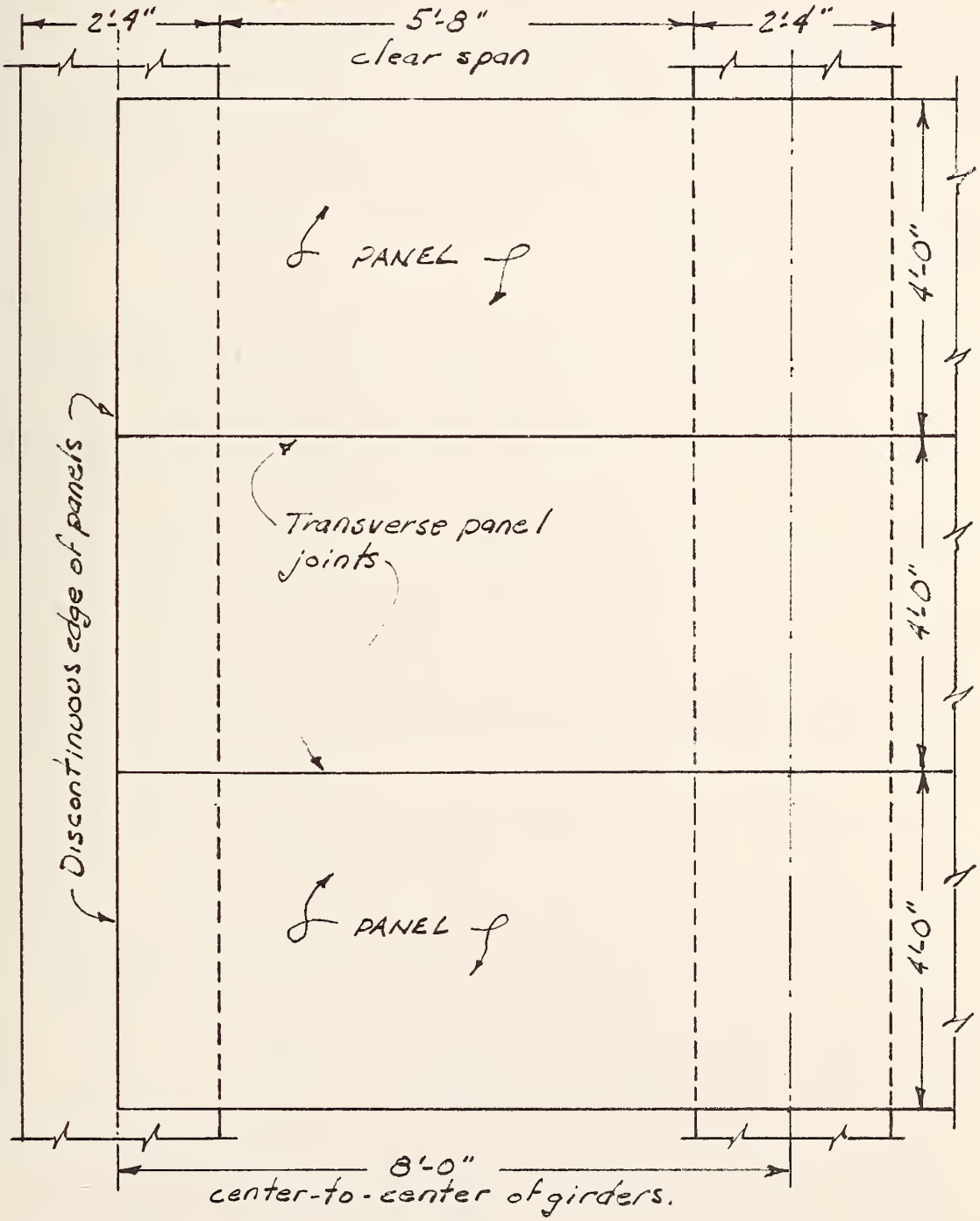

DESIGN OF PANEL USING ELASTIC ANALYSIS, cont.

Analytical model of portion of bridge deck using plate bending elements.

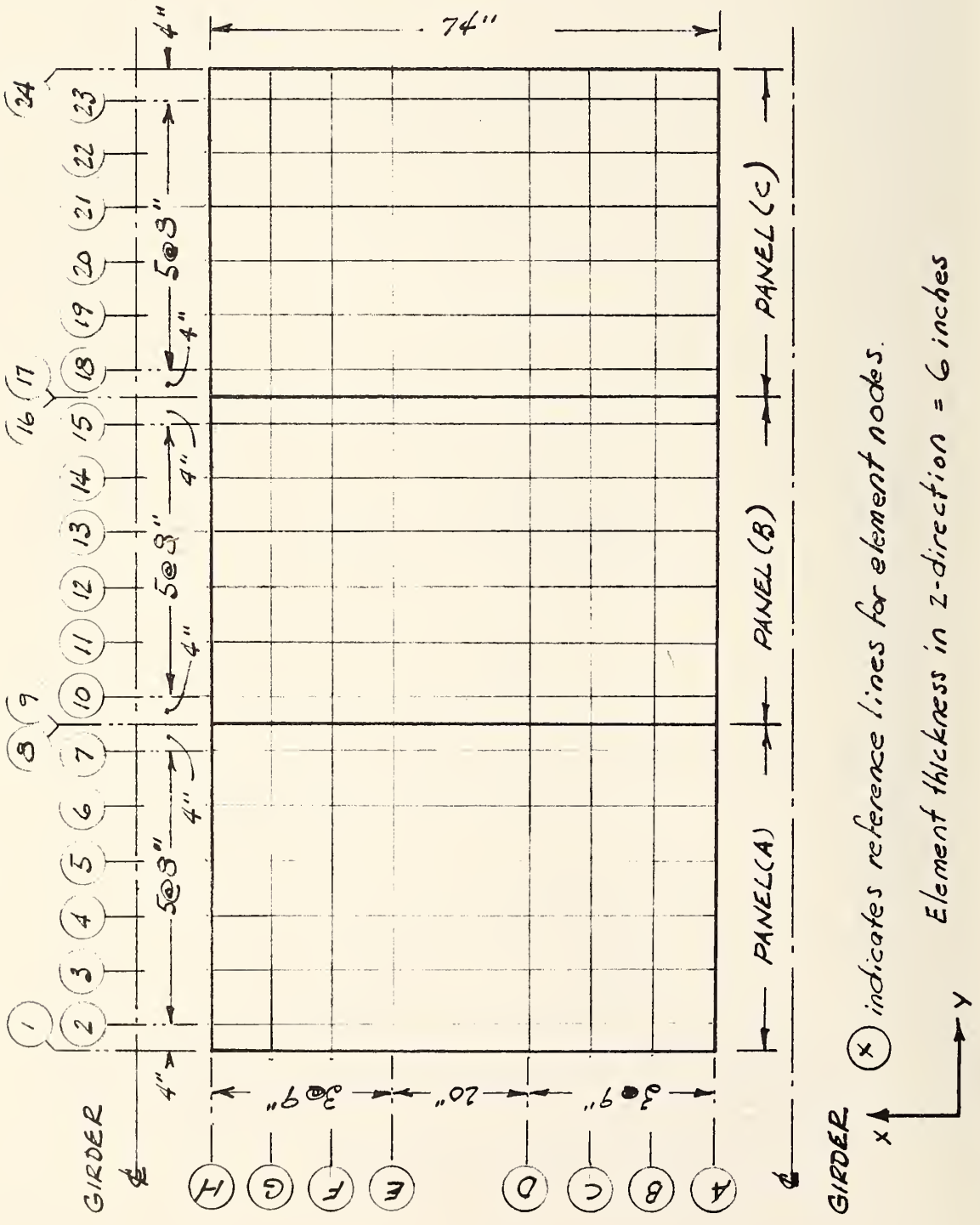

DESIGN OF PANEL USING ELASTIC ANALYSIS, cont.

To perform analysis the USBR's Indeterminate Structural Analysis Program (STR5) was used.

Element were defined by A1-B1/A2-B2, B1-C1/B2-C2, C1-D1/C2-D2, etc.

(A) dimension is parallel to x-axis
(B) dimension is paralkel to y-axis

Panel material was given: $E = 6{,}000{,}000$ lb/in^2
PR (Poisson's ratio) = 0.20
DENSITY = 150 lb/ft^3

Analysis made use of substructuring and common nodes were at the transverse panel joints.

Only displacements in the z-direction at common nodes were used to represent shear transfer.

Reference line (A) represents continuous panel over girder and was assumed as fixed

Reference line (H) represents the discontinuous edge of panels and was fixed for displacement in z-direction, but allow to rotate about x and y axes.

All other nodes were allowed rotate about x and y axes and displace in z axis.

To simulate various positions of wheel loads the following elements were loaded with 130 lb/in^2 uniform load.

LOAD 1: D15 - E15/D16 - E16
& D17 - E17/D18 - E18

LOAD 2: D14 - E14/D15 - E15

LOAD 3: D13 - E13/D14 - E14

DESIGN OF PANEL USING ELASTIC ANALYSIS, cont.

LOAD 4 : D12 - E12 / D13 - E13

Since above elements that are loaded have an area of 160 in² the total load = 20,800 lbs for each load condition.

This represents live load plus impact of 30 percent or

Total load = 16,000 + 0.3(16,000)

= 20,800 lbs.

Moments about y-axis at center of elements between reference lines (D) & (E) for various loads.
+ Moment indicates tension in bottom surface of panel. Moment in ft-k/ft

LOAD 1.

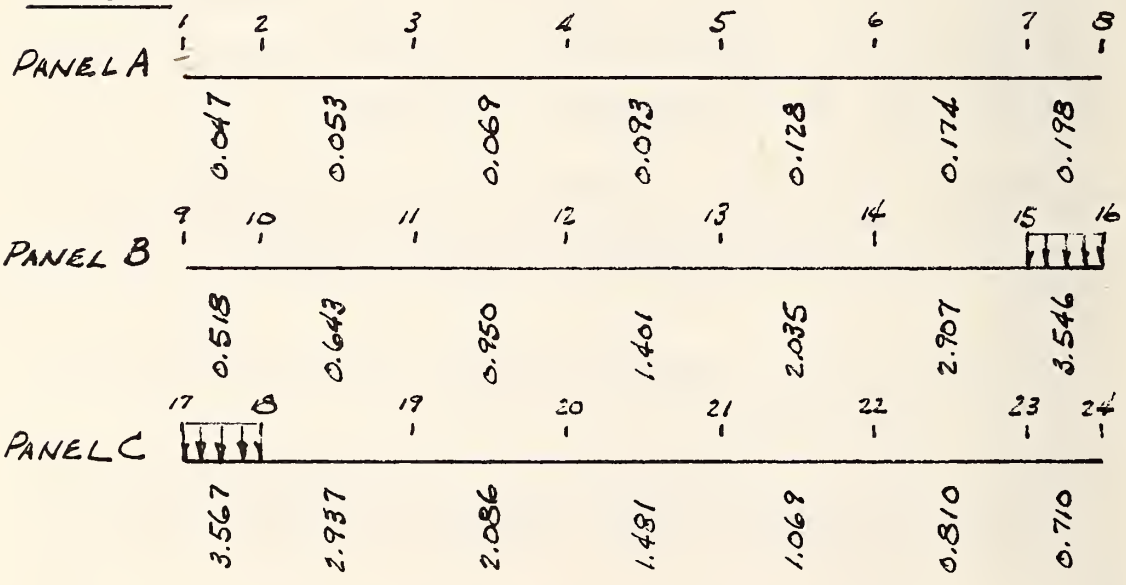

NOTE: Moments about y-axis (ft-k/ft)

DESIGN OF PANEL USING ELASTIC ANALYSIS, cont.

LOAD 2.

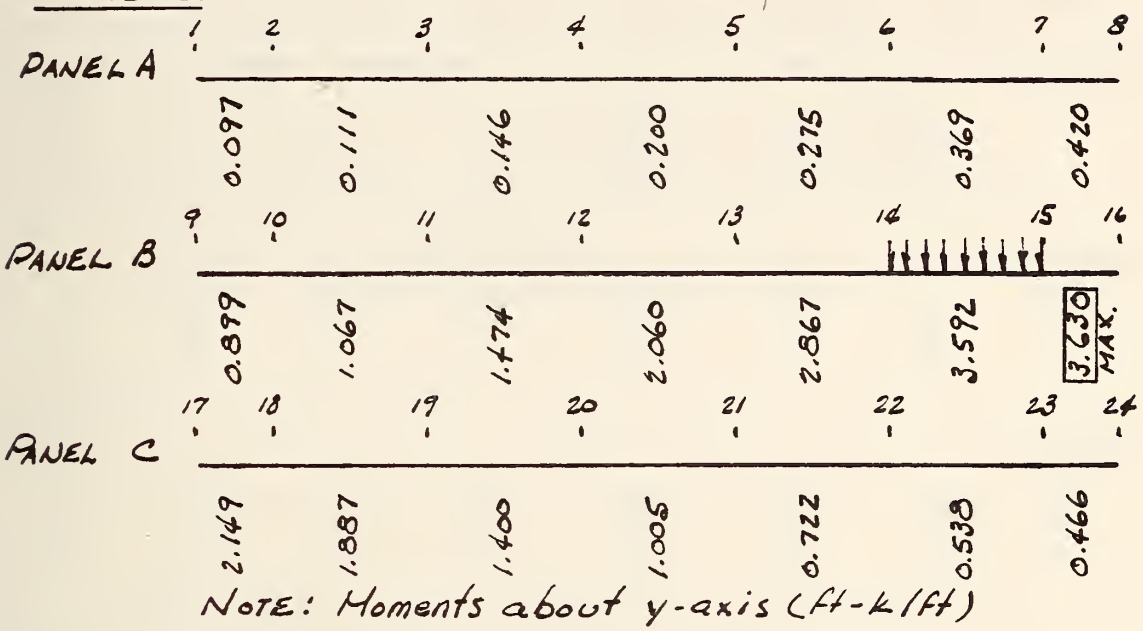

NOTE: Moments about y-axis (ft-k/ft)

LOAD 3.

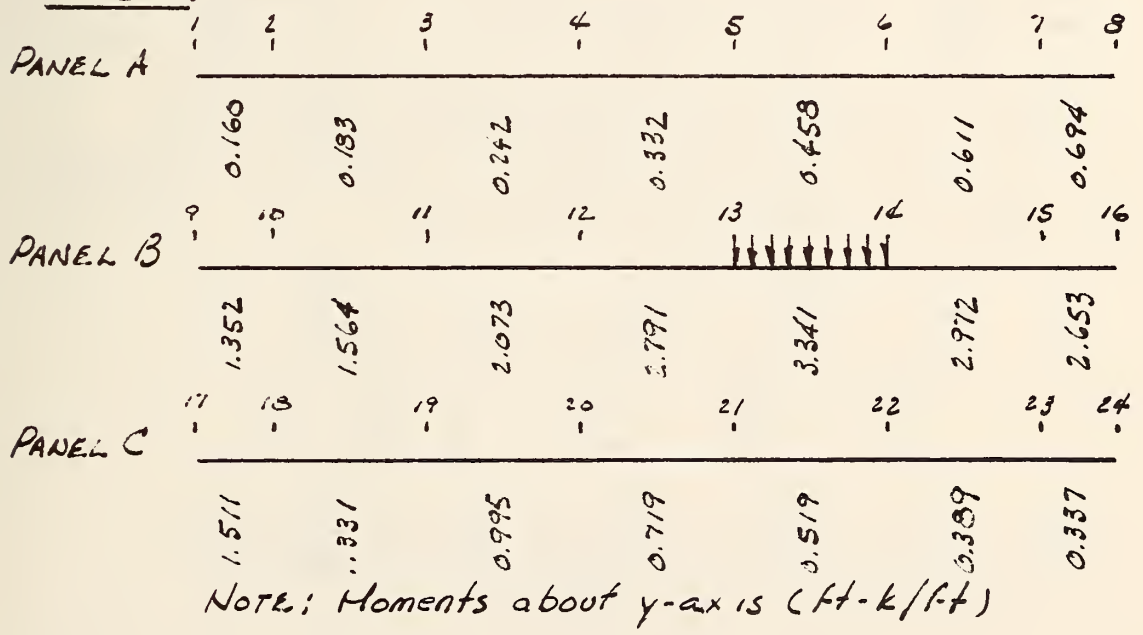

NOTE: Moments about y-axis (ft-k/ft)

LOAD 4.

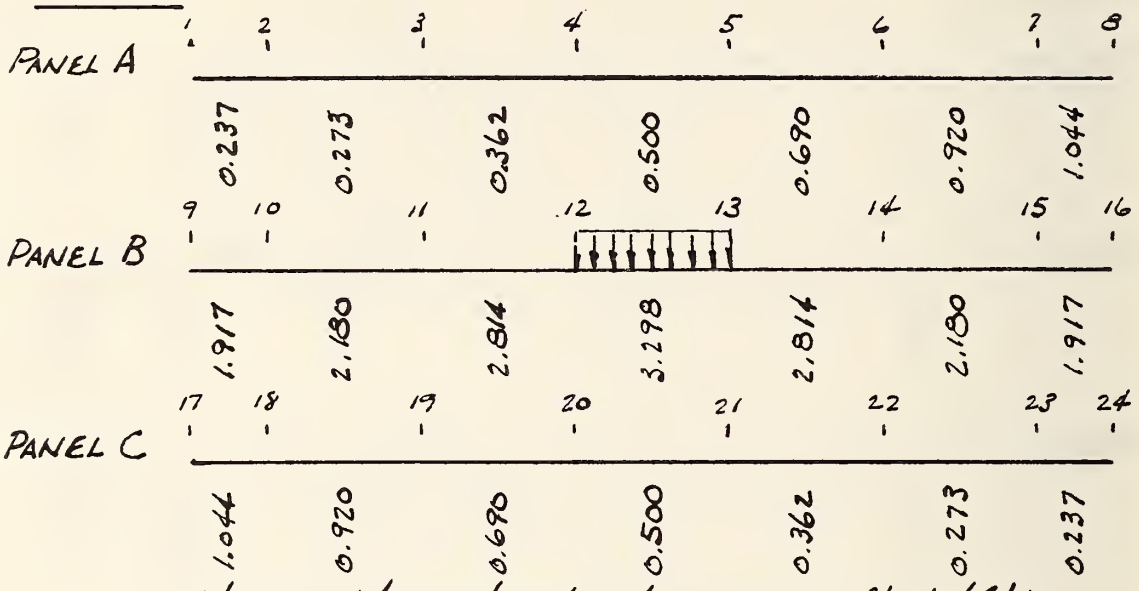

NOTE: Moments about y-axis (ft-k/ft)

Maximum My = 3.630 ft-k/ft from LOAD 2 in element D15-E15/D16-E16.

Moments about y-axis at center of elements between reference lines (15) & (16) for LOAD 2.
+ Moment indicates tension in bottom surface of panel Moment in ft-k/ft.

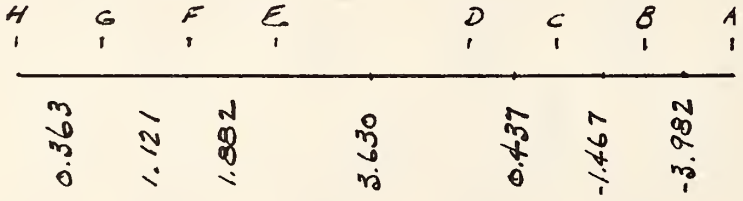

Also, Moments about y-axis at center of elements between reference lines (14) & (15) for LOAD 2.

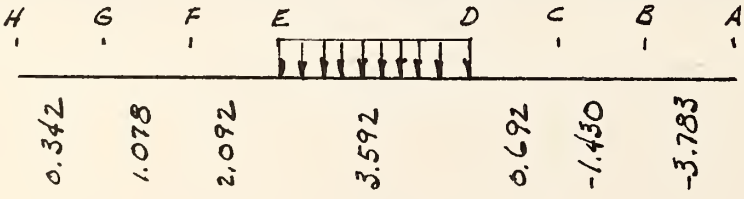

DESIGN OF PANEL USING ELASTIC ANALYSIS, cont.

Since the negative moment at reference line (A) elements is greater than positive moments it might control design.

Moments about y-axis at center of elements between reference lines (A) & (B) for various loads for PANELS B & C

+ Moment indicates tension in bottom surface of panel. Moment in ft-k/ft.

LOAD 1.

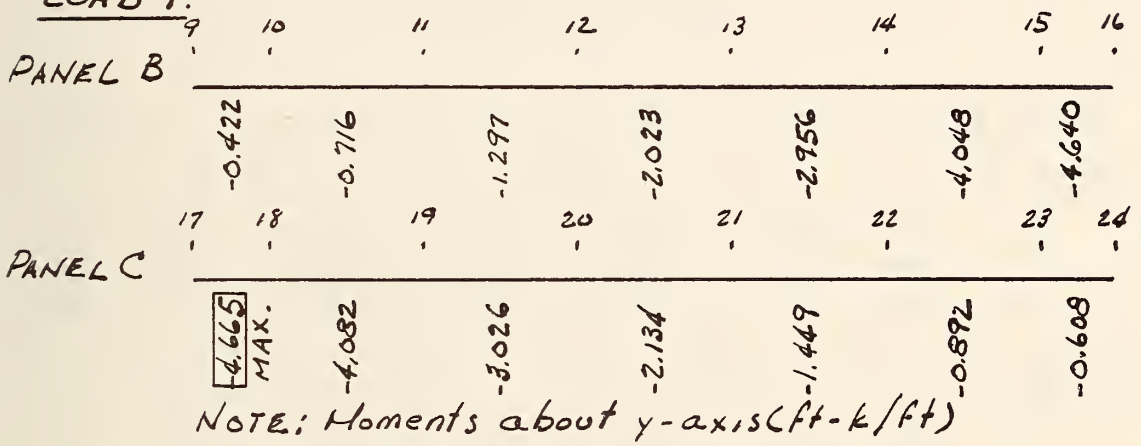

NOTE: Moments about y-axis (ft-k/ft)

LOAD 2.

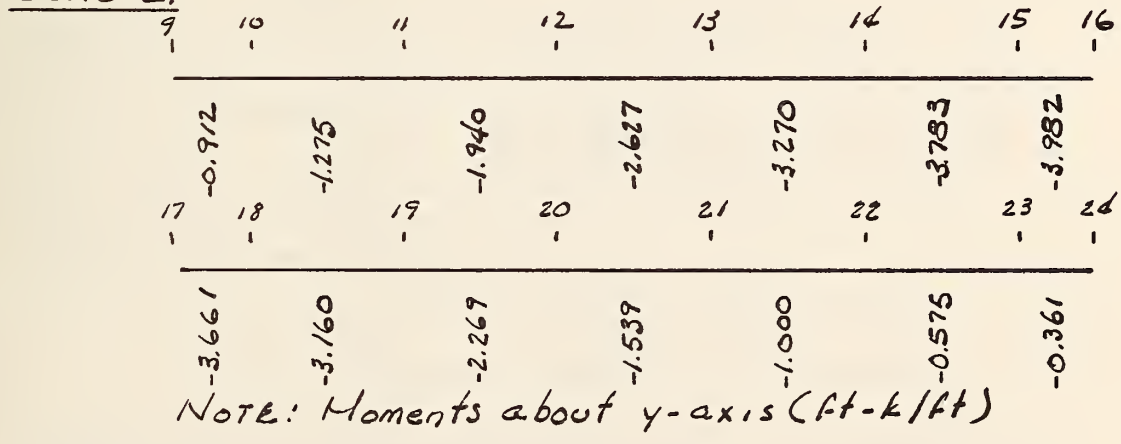

NOTE: Moments about y-axis (ft-k/ft)

DESIGN OF PANEL USING ELASTIC ANALYSIS, cont.

LOAD 3.

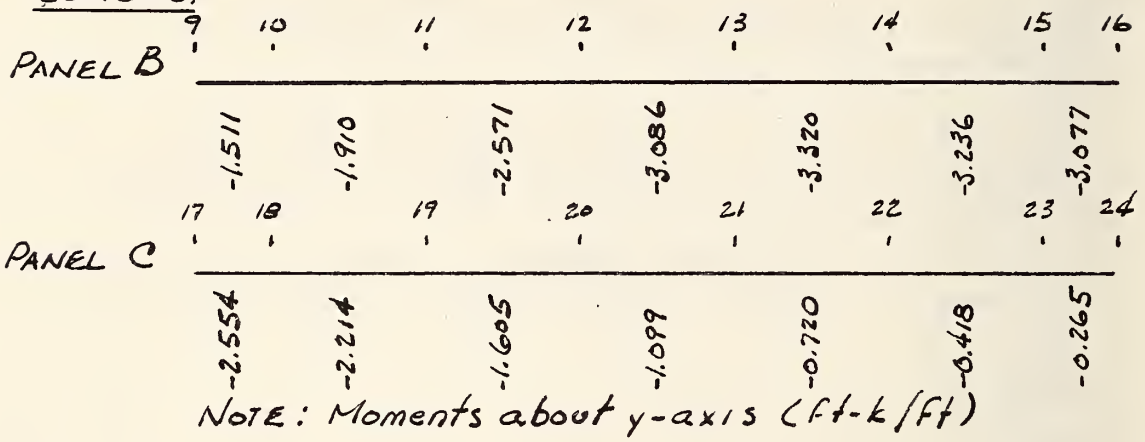

NOTE: Moments about y-axis (ft-k/ft)

LOAD 4.

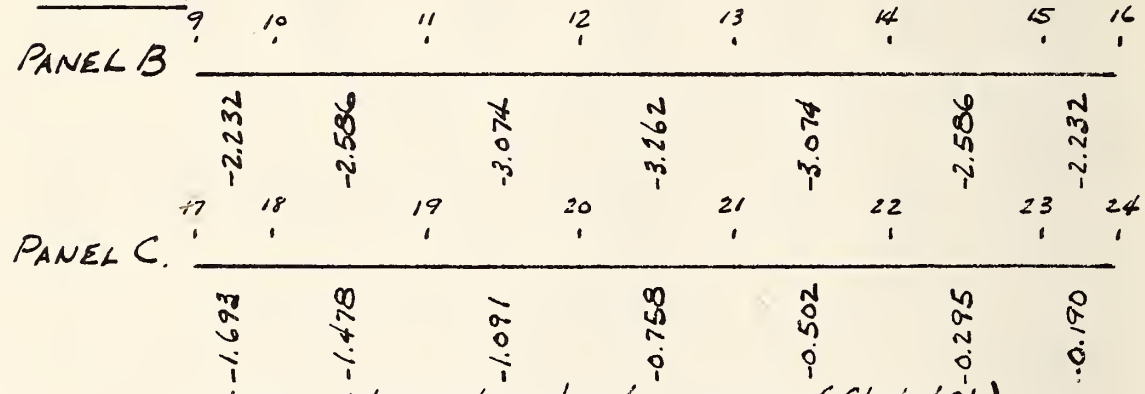

NOTE: Moments about y-axis (ft-k/ft)

Maximum (-) My = -4.665 ft-k/ft from LOAD 1 in element A17-B17/A18-B18.

Reaction moments at A15, A16, A17 & A18 LOAD 1.

My @ A15 = -3.115 ft-k

My @ A16 = -1.120 ft-k

My @ A17 = -1.121 ft-k

My @ A18 = -3.125 ft-k.

DESIGN OF PANEL USING ELASTIC ANALYSIS, cont.

Negative edge moments for various loads.- PANEL (B)
(moments in ft-k/ft)

	-9	-10	-11	-12	-13	-14	-15	-16
LOAD 1								
	-0.204	-0.440	-1.135	-1.988	-3.096	-4.455	-6.230	-6.720
	-9	-10	-11	-12	-13	-14	-15	-16
LOAD 2								
	-0.816	-1.132	-2.009	-2.975	-3.901	-4.781	-5.374	-5.514
	-9	-10	-11	-12	-13	-14	-15	-16
LOAD 3								
	-1.620	-1.986	-2.976	-3.862	-4.409	-4.506	-4.162	-3.978
	-9	-10	-11	-12	-13	-14	-15	-16
LOAD 4								
	-2.664	-3.006	-3.865	-4.400	-4.400	-3.865	-3.006	-2.664

In actual bridge the continuous edge of the panel would not be fixed because the flange of the girder can bend and girder would also displace and rotate about its longitudinal axis. Hence above neg. moments are assumed to be reduced by 75% to account for not complete fixity.

Dead Load moment

$$M_{DL} = \frac{wL^2}{8} = \frac{0.075(6.17)^2}{8} = 0.357 \text{ ft-k/ft}$$

Check shear - max. shear due to LL + I was at A16 from LOAD 1

$V_{max} = 7.560$ k/ft

$$v = \frac{7,560}{(12)(6)} = 105 \text{ lb/in}^2$$

DESIGN OF PANEL USING ELASTIC ANALYSIS, cont.

Average maximum moment for edge of panel

$$M_{y(EDGE)} = \frac{1}{3}(-6.720 - 6.230 - 4.655)$$

$$= -5.868 \text{ ft-k/ft}$$

Average maximum moment for middle of panel

$$M_{y(MIDDLE)} = -4.400 \text{ ft-k/ft}$$

Maximum total moment for edge & middle of panel

$$M_{T(EDGE)} = 0.75(-0.357 - 5.868)$$

$$= \underline{-4.669 \text{ ft-k/ft}}$$

$$M_{T(MIDDLE)} = 0.75(-0.357 - 4.400)$$

$$= \underline{-3.568 \text{ ft-k/ft}}$$

A check of the USBR's elastic analysis method was made by comparing it to the elastic analysis performed by Prestressed Concrete of Colorado, Inc. (PCC).

PCC's elastic analysis

PCC's analysis of the panel was performed by using A. Pucher's influence surfaces to compute the bending moments in slabs under moving loads. These influence surfaces are shown in "Einfluss felder Elastischer Platten", Springer Verlag, Berlin.

Using Charts No. 86 & 84 from A. Pucher, which are plates with b/a = 0.667 fixed on (a) dimension and free on (b) dimension, moments were obtained for a wheel load at the center of span on the free edge and at the center of the panel, respectively.

DESIGN OF PANEL USING ELASTIC ANALYSIS, cont.

PCC's elastic analysis, cont.

Plan view of panel indicating load positions A & B.

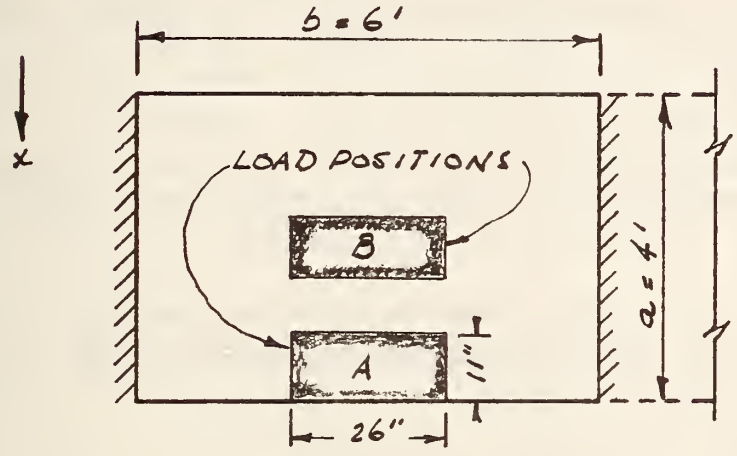

30% impact

LIVE LOAD AT POSITION A (Use Pucher chart #86)

Positive moment $\bar{m}_x = \frac{11.7(16)}{8\pi} = 7.45$ ft-k/ft

Corrections:

1. Because slab is continuous over 3 supports, decrease above value by 20% (allowed by AASHTO Section 1.3.2 (c)).

2. Due to shear transfer at transverse joint, assume adjacent unloaded slab picks up 60% of load.

Corrected m_x with impact

$m_x = 0.80(0.60)(7.45)(1.30)$

$= 4.65$ ft-k/ft

NOTE: Comparison from finite element analysis (LOAD 2 - PANEL B) My = 3.630 ft-k/ft, assume increase of 25% because not completely fixed

My = 3.630(1.25) = 4.537 ft-k/ft.

DESIGN OF PANEL USING ELASTIC ANALYSIS, cont.

PCC's elastic analysis, cont.

LIVE LOAD AT POSITION B (Use Pucharchart # 84)

$$\text{Positive moment } \bar{m}_x = \frac{8.2(16)}{8\pi} = 5.22 \text{ ft-k/ft}$$

Corrections:

1. Because slab is continuous over 3 supports, decrease above value by 20% (allowed by AASHTO section 1.3.2(C))

2. Due to shear transfer at transverse joints, assume adjacent slabs pick up 30% of load.

Corrected m_x with impact

$$m_x = 0.80(0.70)(5.22)(1.30)$$

$$= 3.80 \text{ ft-k/ft}$$

NOTE: Comparison from finite element analysis (LOAD 4 - PANEL B) $M_y = 3.298$ ft-k/ft, assume increase of 25% because not completely fixed.

$$M_y = 3.298(1.25) = 4.122 \text{ ft-k/ft}$$

PCC concluded that moments at support should be of the same order of magnitude as determined above by Pucher's charts because no real fixity at the panel edges which attach to the girders can be assumed.

Further check on corrections were made by PCC assuming a 36-inch wide contact area of the transverse joint about the midspan was engaged for shear transfer.

DESIGN OF PANEL USING ELASTIC ANALYSIS, cont.

PCC's elastic analysis, cont.

Through a trial and error procedure of assuming a shear, substracting the shear influence from the load, and determining new slab moments it was determined a final bending moment at the edge for the load in Position A from Puchar would be 3.92 ft-k/ft. This compares to a value of 4.41 ft-k/ft as originally determined by assuming the 60% shear transfer to adjacent panel.

Final design from PCC for L.L. + I assuming the 20% reduction due to slab continuity.

$$M_{LL} + M_I = 0.8(1.30)(3.92)$$

$$M_T = 4.08 \text{ ft-k/ft}$$

Panel moment from differential deflections.

Since differential deflections of the bridge girders can cause moment in the deck slab PCC performed an analysis to determine the slab moments. (performed by PCC)

Analytical model of bridge.

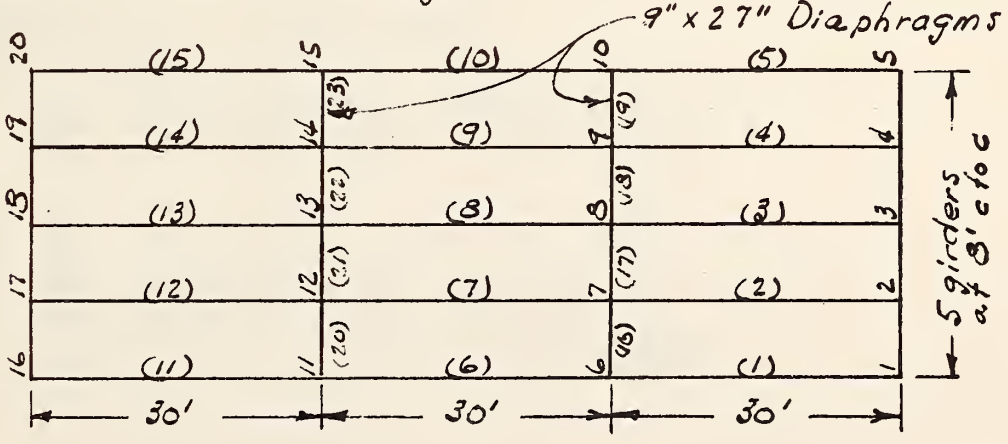

DESIGN OF PANEL USING ELASTIC ANALYSIS, cont.

Panel moment from differential deflections, cont.

Cross-section of bridge girder

$E_{SLAB} = 6{,}000$ ksi

$E_c = 4{,}000$ ksi

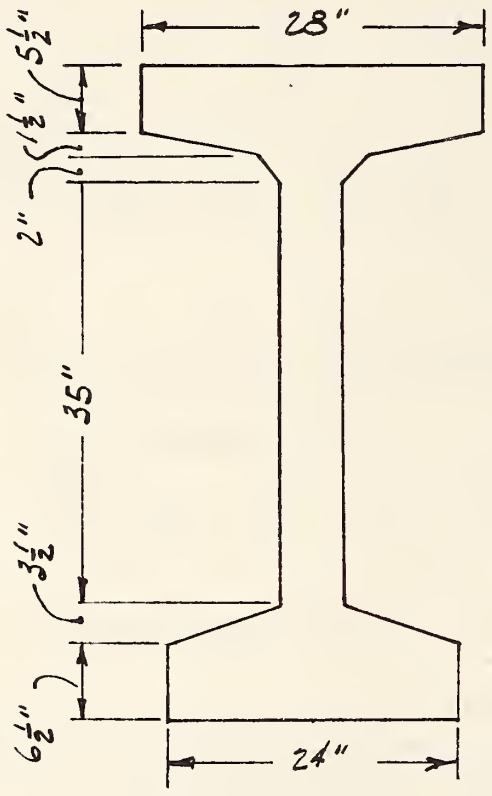

Colorado G-54 girder

$I_{girder} \cong 500{,}000$ in^4

Torisonal constant (incl. slab)

$J \cong 11{,}000$ in^4

I diaphragm + slab $\cong 19{,}120$ in^4

J diaphragm + slab $\cong 5170$ in^4

I diaphragm = $14{,}800$ in^4

Loading positions on model.

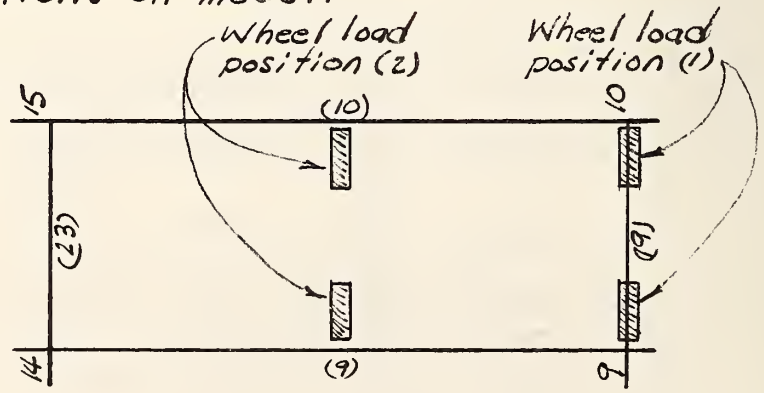

DESIGN OF PANEL USING ELASTIC ANALYSIS, cont.

Panel moment from differential deflections, cont.

Slope-deflection equation where no load is present on span, is:

$$M_{AB} = \frac{2EI}{L}(2\theta_A + \theta_B - 3\psi)$$

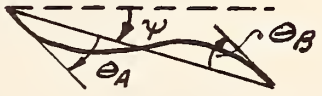

The slab nearest to member 18, which is a diaphragm, will have same displacements and rotations as member 18. $I_{(SLAB)} = \frac{48(6)^3}{12} = 648\ in^4$

Thus: $$\frac{m_{ab(SLAB)}}{M_{AB(DIAPH)}} = \frac{EI_{(SLAB)}\ L_{(DIAPH)}}{EI_{(DIAPH)}\ L_{(SLAB)}}$$

From analysis of analytical model $M_{AB(DIAPH)} = 443\ in\text{-}k$

$$m_{ab(SLAB)} = \frac{443(6{,}000)(648)(91)}{(4{,}000)(14{,}800)(74)}$$

$$= 36.0\ in\text{-}k \quad \text{or } 3.0\ ft\text{-}k$$

Convert to ft-k/ft.

$$m_{ab(SLAB)} = 0.8\ ft\text{-}k/ft$$

or to include impact of 30%

$$m_{ab(SLAB)} = 1.3(0.8)$$

$$= 1.0\ ft\text{-}k/ft$$

DESIGN OF PANEL USING ELASTIC ANALYSIS, cont.

Summary of Panel Moments about Longitudinal Axis

(1) USBR Analysis

Since the negative moment in the panel at the girder was found to be the most critical, the moment from the differential deflection of the girders was added to the moment determine from the finite element analysis.

$$M_{F(EDGE)} = m_{ab(SLAB)} + M_{T(EDGE)}$$

$$= 1.00 + 4.669 = \underline{5.67 \text{ ft-k/ft}}$$

$$M_{F(MIDDLE)} = m_{ab(SLAB)} + M_{T(MIDDLE)}$$

$$= 1.00 + 3.568 = \underline{4.57 \text{ ft-k/ft}}$$

(2) PCC Analysis

Positive moment was taken as the most critical However, PCC concluded as the positive and negative moments in the panel system would be equal.

$$M_F = M_{DL} + M_T + m_{ab(SLAB)}$$

$$M_{DL} = \frac{wL^2}{10} = \frac{0.075(6.17)^2}{10} = 0.28 \text{ ft-k/ft}$$

$$M_F = 0.28 + 4.08 + 1.0 = \underline{5.36 \text{ ft-k/ft}}$$

DESIGN OF PANEL USING ELASTIC ANALYSIS, cont.

Design of Prestress for Panel.

Two design approaches may be taken:

(1) Use allowable service load stress and M_{FS} as shown in the summary of panel moments, or

(2) Use a factor of safety to increase moments to an ultimate condition and use ultimate design stresses.

Allowable service load design

Extreme fiber stress can be the following either

$f_T = 0.21 f_r$ or $f_T = 3\sqrt{f'_c}$

since $f_r = 1{,}300$ lb/in² for PIC

$f_T = 273$ lb/in²

since $f'_c = 15{,}000$ lb/in² for PIC

$f_T = 367$ lb/in²

assume: 21% prestress loss

(3/8-inch) 270ksi strand

$P/\text{strand} = 0.79(0.7) f_{pu} A_s$

$= 12.72$ k

Determine no. of strands (N) using $f_T = 273$ lb/in²

$$0.273 = -\frac{12.72(N)}{72} + \frac{5.67(12)(3)}{216}$$

$N =$ 3.80 strands/ft at edge (USBR)

$$0.273 = -\frac{12.72(N)}{72} + \frac{4.57(12)(3)}{216}$$

$N =$ 2.77 strands/ft at middle (USBR)

DESIGN OF PANEL USING ELASTIC ANALYSIS, cont.

Design of Prestress for Panel, cont.

$$0.273 = -\frac{12.72(N)}{72} + \frac{5.36(12)(3)}{216}$$

$N =$ 3.51 strands/ft (PCC)

Determine no. of strands (N) using $f_T = 367$ lb/in²

$$0.367 = -\frac{12.72(N)}{72} + 0.945$$

$N =$ 3.27 strands/ft at edge (USBR)

$$0.367 = -\frac{12.72(N)}{72} + 0.762$$

$N =$ 2.24 strands/ft at middle (USBR)

$$0.367 = -\frac{12.72(N)}{72} + 0.893$$

$N =$ 2.98 strands/ft (PCC)

To compute strands/panel for USBR design take 2 N(edge) + 2 N(middle) for PCC design 4 N, for both round to nearest higher even number so a concentric prestress pattern can be obtained.

Using $f_T = 273$ lb/in²

N/panel = 14 strands (USBR)

N/panel = 14 strands (PCC)

Using $f_T = 367$ lb/in²

N/panel = 12 strands (USBR)

N/panel = 12 strands (PCC)

DESIGN OF PANEL USING ELASTIC ANALYSIS, cont.

Design of Prestress for Panel, cont.

Load factor design.

From Section 1.6.5 AASHTO

$$\text{Load factor (Group I)} = \frac{1.30}{\phi}\left[D + \frac{5}{3}(LL+I)\right]$$

From analysis Dead Load (D) is the following percentage of L.L. + I. and slab moment due to differential girder displacement:

(1) PCC $\quad D = 0.06(LL + I + M_{ab})$

(2) USBR $\quad D = 0.08(LL + I + M_{ab})$

use average

Hence, $\quad L.F. = \frac{1.30}{\phi}\left(0.07 + \frac{5}{3}(1.0)\right)$

ϕ = 1.0 for factory produced prestressed concrete members.

$$\underline{L.F. = 2.3} \quad \text{(AASHTO)}$$

From ACI 318-71 Section 9.3.1

$$\text{Load factor for flexure} = \frac{1}{\phi}(1.4D + 1.7L)$$

$\phi = 0.9$ flexure.

$$L.F. = \frac{1}{0.9}\left(1.4(0.07) + 1.7(1.0)\right)$$

$$\underline{L.F. = 2.0} \quad \text{(ACI)}$$

AASHTO L.F. is limited mainly to girders and other members, so it would be probably to conservative. Hence for load factor design of deck panels L.F. = 2.0 based on ACI.

DESIGN OF PANEL USING ELASTIC ANALYSIS, cont.

Load factor design, cont.

Determine no. of strands (N) using $f_t = 1{,}300$ lb/in²

$$1.3 = -\frac{12.72(N)}{72} + 2.0(0.945)$$

$$N = \underline{3.34 \text{ strands/ft}} \text{ at edge (USBR)}$$

$$1.3 = -\frac{12.72(N)}{72} + 2.0(0.762)$$

$$N = \underline{1.27 \text{ strands/ft}} \text{ at middle (USBR)}$$

$$1.3 = -\frac{12.72(N)}{72} + 2.0(0.893)$$

$$N = \underline{2.75 \text{ strands/ft}} \text{ (PCC)}$$

No. of strands per panel, round to nearest higher even number so a concentric prestress pattern can be obtained

N/panel = 10 strands (USBR)

N/panel = 12 strands (PCC)

Use 12 strands/panel

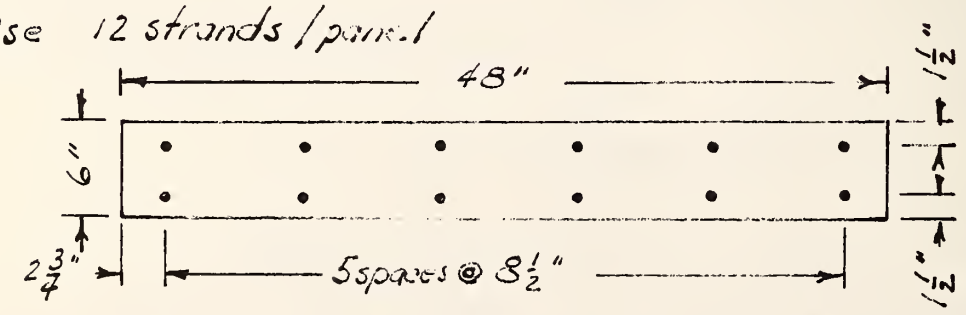

DESIGN OF PANEL USING ELASTIC ANALYSIS, cont.

Check of stress at release

$$f_c = 0.6\, f'_{ci} = 0.6(4{,}000) = 2{,}400 \text{ lb/in}^2$$

$$\sigma = \frac{0.7\, f_{pu}\, A_s\, N}{(6)(48)}$$

$$= \frac{0.7(270{,}000)0.085(12)}{6(48)}$$

$$= 670 \text{ lb/in}^2 < 2{,}400 \text{ lb/in}^2 \quad \text{O.K.}$$

Based on computations under AASHTO design portion of these computations 12 3/8-inch diameter strands are adequate percentage of prestress steel.

Determine ultimate Moment

assume top layer of strands is below N.A.
& $c = 1.22$ in.

strain capacity in bottom steel $E_s = 29{,}000 \text{ k/in}^2$

$$\varepsilon_{cup.} = \frac{270\,(1 - 0.79(0.7))}{29{,}000} = 0.0042 \text{ in/in.}$$

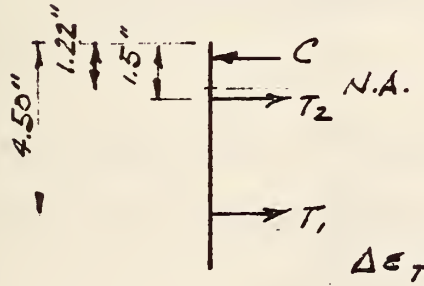

$$C = 0.85\, a\, b\, f'_c$$

$$c = \frac{a}{k_1} \qquad k_1 = 0.85 - (0.05)(11) = 0.30$$

$$\Delta\varepsilon_{T2} = \frac{0.0042(0.29)}{3.28} = 0.0004$$

$$T_1 = 270(0.085)(6) = 137.70 \text{ k}$$

$$T_2 = [149.4 + 0.0004(29{,}000)](0.085)(6)$$

$$= 82.11 \text{ k.}$$

DESIGN OF PANEL USING ELASTIC ANALYSIS, cont.

Determine Ultimate Moment, cont.

$$C = T_1 + T_2 = 137.70 + 82.11$$

$$= 219.81^{k}$$

$$a = \frac{219.81}{0.85(48)(15)} = 0.359$$

$$c = \frac{0.359}{0.3} = 1.20 \text{ close enough to } 1.22$$

$$M_u = T_1\left(d_1 - \frac{a}{2}\right) + T_2\left(d_2 - \frac{a}{2}\right)$$

$$= 137.70(4.50 - 0.18) + 82.11(1.50 - 0.18)$$

$$= \underline{\underline{703.2 \text{ in-k}}}$$

$$\text{OR} = 14.6 \text{ ft-k/ft}$$

Compare with initial AASHTO design.

$$M_u = 15.28 \text{ ft-k/ft}$$

Determine Ultimate Moment of Unimpregnated Panel

assume: $c = 1.26$ $\quad k_1 = 0.85 - (0.05)(1.5) = 0.775$

$$\Delta\varepsilon_{T2} = \frac{0.0042(0.24)}{3.24} = 0.0003 \qquad f'_c = 5{,}500 \text{ psi}$$

$$T_2 = [149.4 + 0.0003(29{,}000)](0.085)(6) = 80.63^{k}$$

$$C = 137.70 + 80.63 = 218.33^{k}$$

$$a = \frac{218.33}{0.85(48)(5.5)} = 0.972 \qquad c = \frac{0.972}{0.775} = 1.25$$

$$M_u = 137.70(4.50 - 0.486) + 80.63(4.50 - 0.486)$$

$$= \underline{\underline{634.5 \text{ in-k.}}}$$

DESIGN OF PANEL USING ELASTIC ANALYSIS, cont.

Check of bending about transverse axis

Moments about x-axis at center of elements between reference lines (D) & (E) for various loads. - PANEL (8)
+ Moment indicates tension in bottom surface of panel. Moment in ft-k/ft.

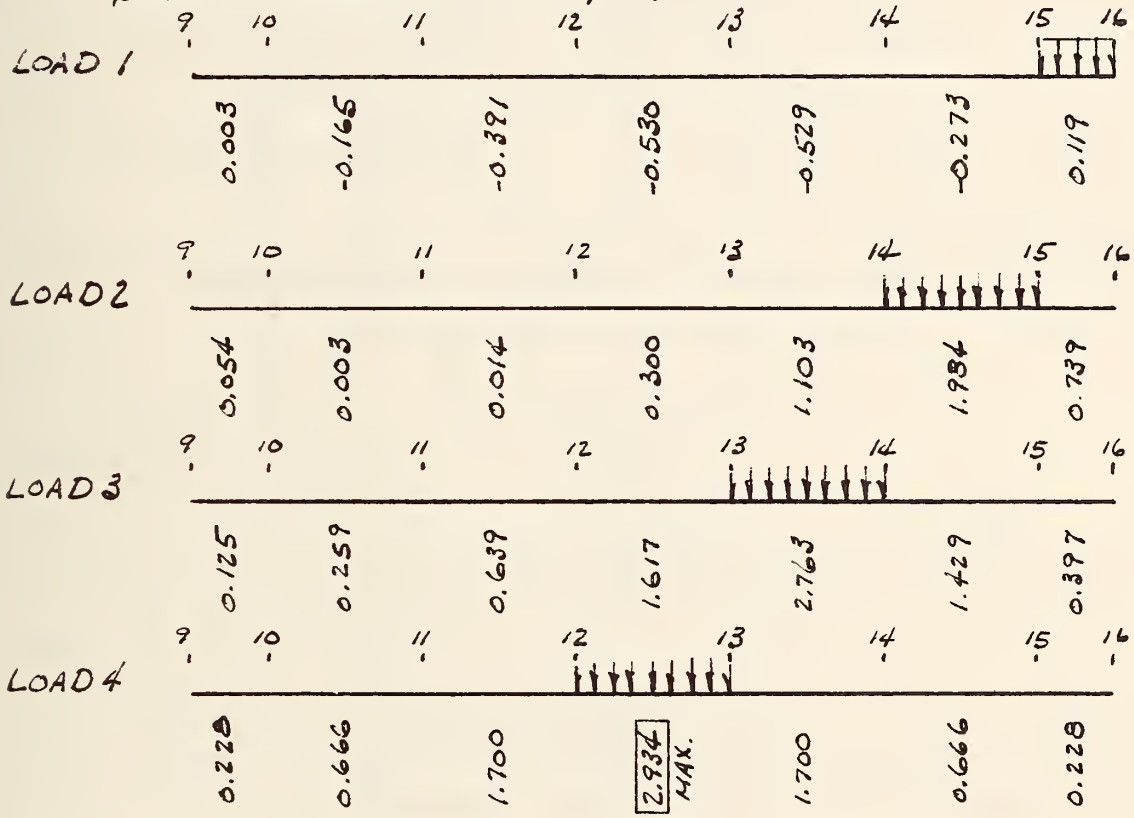

Dead Load moment

$$M_{DL} = \frac{wL^2}{8} = \frac{0.075}{8}(4)^2 = 0.150 \text{ ft-k/ft}$$

Service load moment.

$$M_T = M_{DL} + M_{LL+I}.$$

$$= 0.150 + 2.934 = 3.084 \text{ ft-k/ft}$$

DESIGN OF PANEL USING ELASTIC ANALYSIS, cont.

Check of bending about transverse axis, cont.

Compute service load stress

$$\sigma = \frac{Mc}{I} = 3.084\frac{(12)(3)}{216} = .514 \text{ k/in}^2$$

or $\sigma = 514 \text{ lb/in}^2$ greater than $3\sqrt{f'_c}$ (367 lb/in^2)

Since crack will occur in bottom of the panel it will not affect deck durability and conventional reinforcement or longitudinal post-tensioning of the panel system can be used.

Check above with Load Factor design.

$$\sigma = 2.0\frac{(3.084)(12)(3)}{.216} = 1.028 \text{ k/in}^2$$

or $\sigma = 1,028 \text{ lb/in} < f_T = 1,300 \text{ lb/in}^2$

Based on Load Factor design PIC panel can withstand moment about transverse axis

Also, finite element analysis assumed no moment about the transverse axis would be transferred across transverse panel joint. If transverse joint is an epoxy joint some moment transfer will occur.

Check of shear stress along transverse joint.

Following are shear / ft along transverse joint between PANEL B & C +Shear in kips is upward on PANEL B

	A	B	C	D	E	F	G	H
LOAD 1	0.029	0.022	0.016		-0.025	-0.013	-0.012	

Above should be zero but analytical model was not symmetrical about transverse joint.

DESIGN OF PANEL USING ELASTIC ANALYSIS, cont.

Check of shear stress along transverse joint, cont.

	A	B	C	D	E	F	G	H
LOAD 2		-0.441	-0.056	-3.255	-3.323 MAX.	-0.352	-0.088	
LOAD 3	A	B	C	D	E	F	G	H
		-0.603	-0.085	-2.172	-2.297	-0.625	-0.312	
LOAD 4	A	B	C	D	E	F	G	H
		-0.691	0.089	1.453	1.610	0.572	0.361	

Dead Load Shear

$$V_{DL} = \frac{wL}{2} = \frac{0.075(4)}{2} = 0.150 \text{ k/ft.}$$

Service Load Shear

$$V_T = V_{DL} + V_{LL+I}$$

$$= 0.150 + 3.323 = 3.473 \text{ k/ft}$$

From Section 1.5.26 AASHTO, shear in slabs

$$v_c = 1.8\sqrt{f'_c} = 220 \text{ lb/in}^2 \text{ for PIC}$$
using $f'_c = 15{,}000 \text{ lb/in}^2$

assume minimum shear area on a tongue and grove type transverse joint is 1/3 total area.

$$A_v = \frac{1}{3}(12)(6) = 24 \text{ in}^2\text{/ft}$$

DESIGN OF PANEL USING ELASTIC ANALYSIS, cont.

Check of shear stress along transverse joint, cont.

$$v = \frac{3,473}{24} = 145 \text{ lb/in}^2 < 220 \text{ lb/in}^2 \text{ O.K.}$$

Use Load factor design check.

$$v = \frac{2(3,473)}{24} = 290 \text{ lb/in}^2 < 750 \text{ lb/in}^2$$

BOND DEVELOPMENT IN ENDS OF PANEL.

From finite bending element analysis the following elements were loaded with 143 lb/in² uniform load:

LOAD 5 : E15-F15/E16-F16
F15-G15/F16-G16
E17-F17/E18-F18
F17-G17/F18-G18

LOAD 6 : E14-F14/E15-F15
F14-G14/F15-G15

LOAD 7 : E13-F13/E14-F14
F13-G13/F14-G14

LOAD 8 : E12-F12/E13-F13
F12-G12/F13-G13

LOAD 9 : F15-G15/F16-G16
G15-H15/G16-H16
F17-G17/F18-G18
G17-H17/G18-H18

LOAD 10 : F14-G14/F15-G15
G14-H14/G15-H15

LOAD 11 : F13-G13/F14-G14
G13-H13/G14-H14

LOAD 12 : F12-G12/F13-G13
G12-H12/G13-H13

Moments about y-axis at center of elements between (15) & (16) LOAD 5 +M (tension in bottom) ft-k/ft

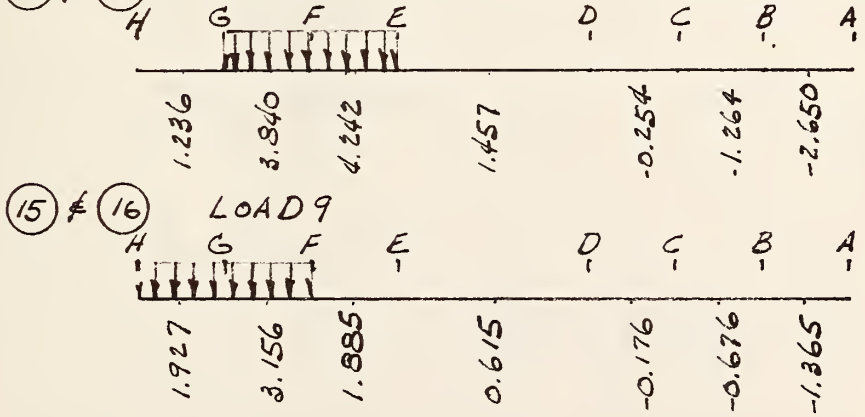

(15) & (16) LOAD 9

BOND DEVELOPMENT IN ENDS OF PANEL, cont.

Moments about y-axis at center of elements between

(14) & (15) LOAD 6

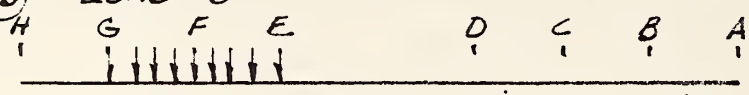

1.145 3.577 3.871 1.378 -0.237 -1.094 -2.185

(14) & (15) LOAD 10

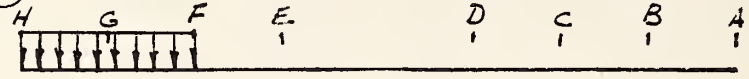

1.335 2.973 1.702 0.562 -0.144 -0.583 -1.129

(13) & (14) LOAD 7

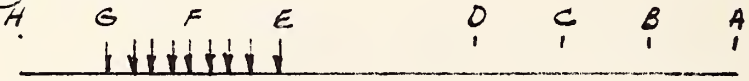

1.105 3.427 3.702 1.316 -0.223 -0.970 -1.863

(13) & (14) LOAD 11

1.767 2.364 1.622 0.534 -0.145 -0.514 -0.756

LOAD 8 & LOAD 12 are not shown because moments continue to decrease as load moves toward center of panel in elements that are loaded.

Maximum Moments about y-axis for various load positions can be drawn as follows:

1.927 (LOAD 9) 3.840 (LOAD 5) 4.242 (LOAD 5) 3.630 (LOAD 2)

NOTE: Moments about y-axis (ft-k/ft)

BOND DEVELOPMENT IN ENDS OF PANEL, cont.

Dead Load at corresponding points.

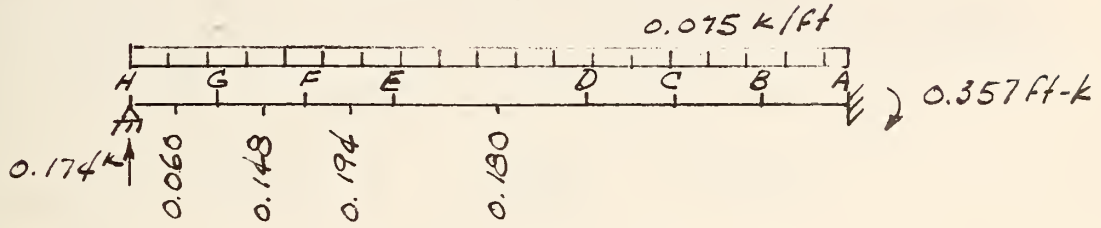

Assume max. moments and dead load moment are uniform over width of panel which is a very severe assumption

Moments below are in (in-k)

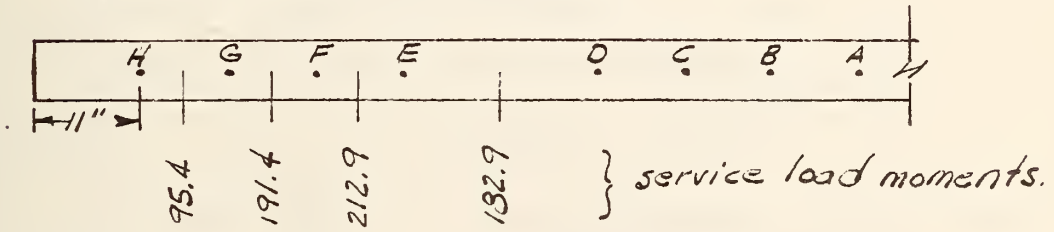

For required ultimate moment just multiply service load moments by Load Factor or Factor of safety which equals 2.0.

Compute panel section cracking moment based on f_r (modulus of rupture) = 1,300 lb/in²

Concrete stress after losses = 530 lb/in²

$$\frac{M_{cr}}{Z} = 1300 + 530 = 1830 \text{ lb/in}^2$$

$$M_{cr} = 527 \text{ in-k}$$

Distance of N.A. from top fiber. (c_T)

$$c_T = \frac{(1830 + 530)(6)}{(1830 + 530 + 1300)}$$

$$= 3.93 \text{ in.}$$

BOND DEVELOPMENT IN ENDS OF PANEL, cont.

Determine bottom steel stress at cracking moment using strain compatibility.

bottom concrete strain - $\varepsilon_{c\,BOT}$

$$\varepsilon_{c\,BOT} = \frac{1,300}{6,000,000} = 0.0002$$

bottom steel strain which is 4.5 inches from top. - $\varepsilon_{s\,BOT}$

$$\varepsilon_{s\,BOT} = \frac{0.0002\,(4.5 - 3.93)}{(6.0 - 3.93)} = 0.000,05$$

$$f_{s\,CR} = 0.79\,(0.7)(270) + 0.000,05\,(29,000)$$

$$= 150.76\ k/in^2$$

Bond Length based on Section 1.6.18 AASHTO or ACI 12.11.1

$$L_{CR} = \left(f_{s\,CR} - \frac{2}{3} f_{se}\right) d$$

where d = nominal dia. of strand.

$$L_{CR} = \left(150.76 - \frac{(2)(149.3)}{(3)}\right) 0.375$$

$$= 19.2\ in.$$

Bond Length for Ultimate Moment

$$L_u = \left(f^*_{su} - \frac{2}{3} f_{se}\right) d$$

$$= \left(270 - \frac{(2)(149.3)}{(3)}\right) 0.375$$

$$= 63.9\ in.$$

Maximum transfer length as specified in ACI 11.5.3

$L = 50d$

$= 18.75$ for 3/8" strand

$= 25.00$ for 1/2" strand

BOND DEVELOPMENT IN ENDS OF PANEL, cont.

Taking bond lengths required from AASHTO for Cracking Moment and Ultimate Moment, and service load moments and load factor moments the following diagram can be made:

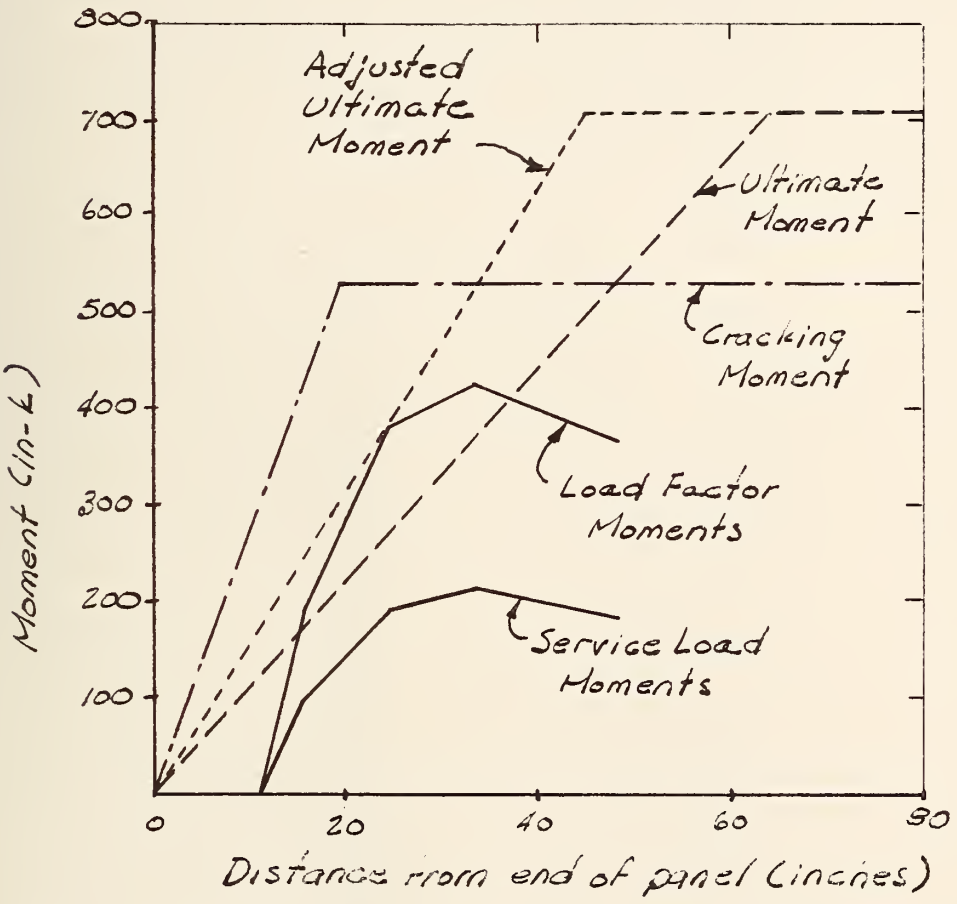

From above it can be seen that the bond development for Ultimate Moment does not satisfy the Load Factor Moments. It was determined since the panel were PIC that the bond required for Ultimate Moment could be reduced by 30 percent which gives Adjusted Ultimate Moment.

☆U.S. GOVERNMENT PRINTING OFFICE: 1977—240-897:83

TE662
.A3
no.FHWA-RD-
75-121
BORROWE
Form DOT F 1720.2
FORMERLY FORM DOT F 1

DOT LIBRARY
00054664